UNDERWATER ACOUSTIC COMMUNICATION

by

LIXUE WU
B.Sc., East China Normal University, 1982

A THESIS SUBMITTED IN PARTIAL FULFILLMENT
OF THE REQUIREMENTS FOR THE DEGREE OF
MASTER OF APPLIED SCIENCE
in the Department of
Electrical and Computer Engineering

We accept this thesis as conforming
to the required standard

[redacted]

Supervisor Dr. A. Zielinski

[redacted]

Dr. N. J. Dimopoulos

[redacted]

Dr. R. L. Kirlin

[redacted]

Dr. R. E. Horita

[redacted]

Dr. S. Waddell

UNIVERSITY OF VICTORIA

Supervisor: Dr. A. Zielinski

ABSTRACT

Underwater acoustic communication has been developed since it was recognized that the ocean could support sound wave propagation. Requirements for commercial applications have been rapidly growing. In this thesis the theoretical work serves to develop the realistic acoustic communication systems which operate in shallow water environment.

Methods of reduction of multipath interference in a shallow water channel are discussed. It is suggested that a vertically suspended linear array is a useful configuration for middle range acoustic communications and its performance is superior to that of a planar array with the same number of elements.

The system aspects of a narrowbeam acoustic communication system are presented. The practical upper limit of system performance has been obtained. It has been shown that a communication channel with a relatively broad bandwidth is possible using a narrowbeam receiver. A higher transmission rate can be achieved using frequency and beam diversity.

Based on these results, the high data rate acoustic communication system using VLSI technique has been proposed. It has been shown that an acoustic communication link suitable for transmitting data from bottom instrumentation to the surface receiver is feasible using a fixed, broad transmitting beam and a steerable, narrow receiving beam. A vertically suspended linear array is suggested to generate an umbrella-type narrow beam which offers superior performance in rejecting multipath interference. Because of a high directivity index associated with such an array, a longer transmission range is possible in comparison with broadbeam systems with the same transmitted powers. Such an array can be conveniently utilized to estimate the angular direction (elevation) of the arriving signals needed for proper positioning of the beam. A high data transmission rate acoustic communication system can be relatively easily implemented using a multi-transmitted-beam and a broad band receiving array. A noncoherent BFSK data transmission scheme is postulated and a FFT algorithm is suggested to implement both direction finding and demodulation algorithms. The system can be used to derive information from sea bottom in shallow water environment.

In order to achieve high data transmission rate, dealing with broadband signal in shallow water environment has been addressed. A method of broadband direction finding applicable to broadband acoustic communication, navigation and remote sensing is proposed. Problems associated with shading function approximation, multipath interference and ambient noise are addressed and their effects on system performance are analysed. The possible solutions to improve the performance are suggested.

Examiners:

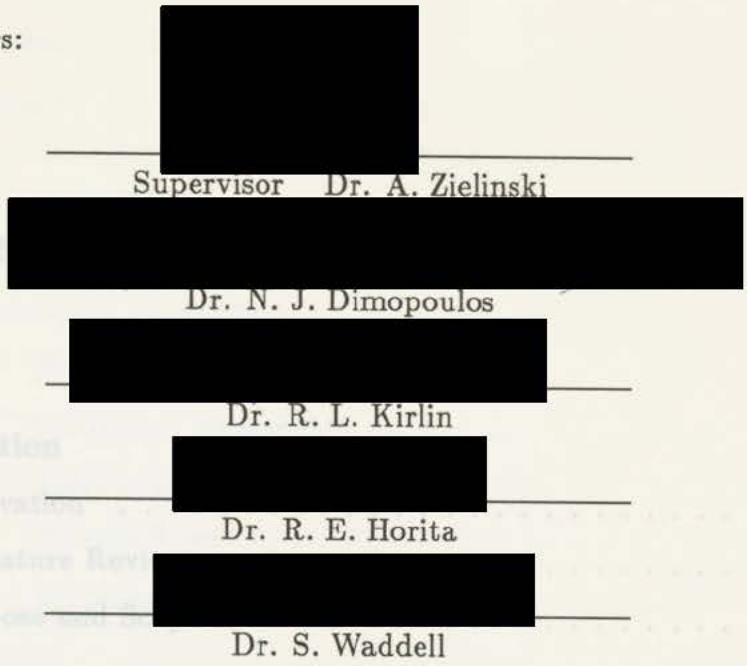

Supervisor Dr. A. Zielinski

Dr. N. J. Dimopoulos

Dr. R. L. Kirlin

Dr. R. E. Horita

Dr. S. Waddell

Contents

List of Tables

List of Figures

Acknowledgements

I would like to thank my supervisor, Dr. A. Zielinski of the Department of Electrical and Computer Engineering, for his encouragement, patience, and advice, for many interesting and helpful discussions, and for his help in the preparation of this document. Financial assistance received from Dr. A. Zielinski (through NSERC), and from the University of Victoria, as well as from B.C. Advanced Systems Institution, is also gratefully acknowledged.

To my parents

Chapter 1

Introduction

1.1 Motivation

Underwater acoustic communication has been developed since it was recognized that the ocean could support sound wave propagation. In 1490, two years before Columbus discovered America, Leonardo da Vinci wrote [1]: "If you cause your ship to stop, and place the head of a long tube in the water and place the outer extremity to your ear, you will hear ships at a great distance from you." Since that time essentially no improvement or application was made in the science of underwater sound until, at the turn of this century, a submarine ball and a fog horn were simultaneously sounded to determine distance offshore by measuring the interval between their airborne and waterborne arrivals [2]. The underwater telephone, developed in 1954 by the Naval Underwater Sound Laboratory (now Naval Underwater Systems Center, NUSC), was the first application of underwater voice communications. The underwater telephone was developed to communicate with submerged submarines and employed the upper sideband of an

8.3 kHz suppressed carrier. From this first operational system, military underwater acoustic communications have moved toward lower frequencies that permit transmission over longer ranges.

In the past, most of the attention has come from Navy needs associated with submarines. Recently, requirements for commercial applications have been rapidly growing. Offshore structures are being installed at ever increasing depths where deploying divers is extremely hazardous and expensive. As a result, unmanned submersibles are being used or proposed to be used for a variety of work tasks. In the deep sea, submersibles are the only means of operation; however, they are severely limited if they require tethering for surface support. A transmission link is required for diverse underwater operations such as communication with submersibles, telemetry and remote control of subsea oil production units, blow out preventers, releases, remote operated vehicles, transmission of voice and/or TV pictures, transmission of measurements from underwater sensors, and others. Acoustic transmission is often the only viable communication link for these purposes and several experimental and commercial systems have been developed [3,4,7,74].

High data rates are desirable for many applications. The limitations of the underwater communication links result from several transmission problems associated with underwater acoustic channel such as attenuation and absorption, ambient noise, Doppler shifts, refraction, scattering and multipath. The multipath effect is particularly severe in shallow water transmission where strong surface and bottom reflections are encountered. Unfortunately, the ocean is a difficult propagation medium. High data rate transmission requires either wide bandwidths or a very clean channel, but

the available bandwidth is limited by both the absorption of high frequency acoustic energy and the physical size of receiving (transmitting) elements, and the ocean is a notoriously reverberant channel with both time and frequency spreading [8,9].

Over the years, various forms of acoustic communication systems have been developed. These include direct AM and SSB for underwater telephones, FM for sensor data, FSK and DPSK for digital data, and parametric sonars for narrow beam systems. Most high data rate acoustic communication systems attempt to operate with coherent signaling since this leads to better performance. This is done by tracking the receiving beam and careful attention to reducing multipath influences. For example, deep-ocean near-vertical-path acoustic communication system operate in this way [10].

The complexities of the acoustic channel demand its careful exploitation. Fortunately, the availability of VLSI technique and higher density power supplies has opened up many possibilities for implementations of acoustic communication systems. The recent proliferation of specialized signal processing hardware and introduction of new piezoelectric polymetric films, suitable for acoustic array makes construction of such a system feasible within the limits of a reasonable budget and size.

1.2 Literature Review

The literature surrounding the subject of underwater acoustic communications is, in some respects, surprisingly scant. This is particularly the case if one concentrates only on that material directly concerned with actual underwater communication systems. Therefore, in this section we have

deliberately chosen to take a broader view of underwater communications, to include consideration of the acoustic channel.

Two decades ago, a general review by Anderson [12] sets the scene in underwater communications, and discusses the major difficulties which revolve around the problems of reverberation and multipath transmission and high attenuation at high acoustic frequencies. Quazi and Conrad [13] also contribute an interesting historical insight and make the suggestion that parametric transmission, because of its ability to establish pencil-beam transmission at relatively low frequencies, might have particular advantage in avoiding surface and sea-floor reflections and thus minimizing the effects of multipath. On a more selective basis of acoustic telemetry, an excellent review is provided by Baggeroer [14]. A useful collection of references for those who wish to pursue further subject of underwater acoustic communications is provided by Coates and Willison [15].

In dealing with the nature of the acoustic channel, a computer model is the Generic Sonar Model [16,17]. The papers by Hummels [18], Kwon and Birdsall [19], and Rowlands and Quinn [20] investigate the channel capacity from the information theory point of view. A sequence of papers by Gulin et al. are concerned with signals reflected from randomly rough surfaces [21,22,23,24,25,26,27]. The channel stability is discussed by Jobst and Dominijanni [28] and by Veenkant [29]. The subject of noise is considered by many authors. Dunbar [30] considers the under-resourced area of acoustic noise in the vicinity of oil extraction platforms. The book "Ambient noise in the sea" by Urick [31] provides a broad account of this topic with an extensive bibliography. Several papers were written on multipath modeling

and identification. Papers by Fjell [32] and by Hassab [33,34] explain how to acquire the information via the cepstrum analysis technique. Two further papers provide actual multipath investigation in the Atlantic [35] and Pacific [36] Oceans, and follow this with papers on anti-multipath strategies [37,38].

Over the years, various forms of acoustic communication systems have been developed. The submarine underwater telephone system is typically a single sideband modulated system [39]. Data communication from sensors in the deep ocean was demonstrated by the Woods Hole Oceanographic Institution and the Lamont-Doherty Geophysical Observatory using both continuous amplitude and frequency modulation systems [40]. A 4-channel time-division multiplexed system was created, where the pulse repetition frequency of a 40 kHz carrier is modulated to produce a form of FM signal [41]. The highest data rates reported to date have been obtained by using frequency shift keying and/or phase shift keying and a parametric sonar which generates very narrow beam [42]. Recently, multiple-frequency shift keying(MFSK) systems have been implemented for telemetry over reverberant channels. These have operated at low data rates, 40 bit/s, and with very low error probability, less than 10^{-6} [43,44]. MFSK systems have been used for short-range reverberant channels at data rates of 1200 bit/s [45,46]. The highest rates achieved using linear acoustic which have been documented employed phase shift encoding [7,47]. These rates have been achieved over the deep water bottom to surface channel paying particular attention to multipath reduction. Amplitude shift keying systems have also been reported which have data rates of 600 bit/s operating in a

lake [48,49]. In addition to these systems many theoretical analyses have been done [50,51,52,53,54,55]. Many of these studies applied communication theory concepts to the underwater channel, but much uncertainty still remains about communication in the underwater acoustic channel.

1.3 Purpose and Scope of Thesis

For shallow water environments, the acoustic link is best described as a highly reverberant, fading communication channel. The shallow water channel is substantially different from the deep ocean near vertical propagation channel for which a number of communication systems have resently been developed. It is unrealistic to expect that most of the systems developed for deep water will perform adequately over shallow water channel. High rates systems for shallow water channel have not been published in the literature. A main part of this work is to model the shallow water channel and to implement a high rate communication system in such environment.

The first 4 chapters present the principles involved in the underwater acoustic communication systems. Chapter 1 gives the motivation and literature review. This is followed by an definition of acoustic communication system (Chapter 2) and a discussion of the acoustic channel. Multipath rejection which is the most challenging aspect of the underwater acoustic channel is addressed in Chapter 3. Channel parameters are dealt with in Chapter 4, with emphasis on the transmission parameters. The final chapters of the thesis incorporate the results of the analytic work. Chapter 5 and 6 describe the applications of narrow beam acoustic communications. The broadband signal associated with high rate communication system are

given a detailed analysis in Chapter 7. A final chapter summaries the results of this work and makes recommendations for further areas of research.

The main contribution of this thesis has been to lay a firm theoretical foundation for the development of high rate acoustic communication systems. The theoretical work serves to develop the realistic acoustic communication system which can be used in shallow water environment. System design aspects, multipath suppression and broadband signals have been studied. Based on these results, the high data rate acoustic communication system using VLSI technique has been proposed.

Chapter 2

Acoustic Communication Systems

2.1 Introduction

Underwater acoustic communication systems may be described by the block diagram shown in Figure 2.1. The processing block at the transmitter conditions the data source for more efficient transmission. For example, in a digital system the processor might consist of a microprocessor that provides redundancy reduction of the source. It may also provide channel encoding so that error detection and correction can be used at the processing unit at receive site to reduce error caused by noise and multipath in the channel. To use the channel physically, it is necessary to modulate the incoming data onto a carrier wave(usually sinusoidal) with fixed frequency limits imposed by the channel. The purpose of the system is for the data source to send information to the data user at the maximum possible rate and the highest reliability over acoustic channel. The acoustic channel has a finite bandwidth and introduces attenuation, noise, and distortions. These lead

to a fundamental tradeoff between the data rate and reliability. Here we discuss the potential data sources for acoustic communication systems, the underwater acoustic channel, the multipath transmission, and the various modulation methods that are available.

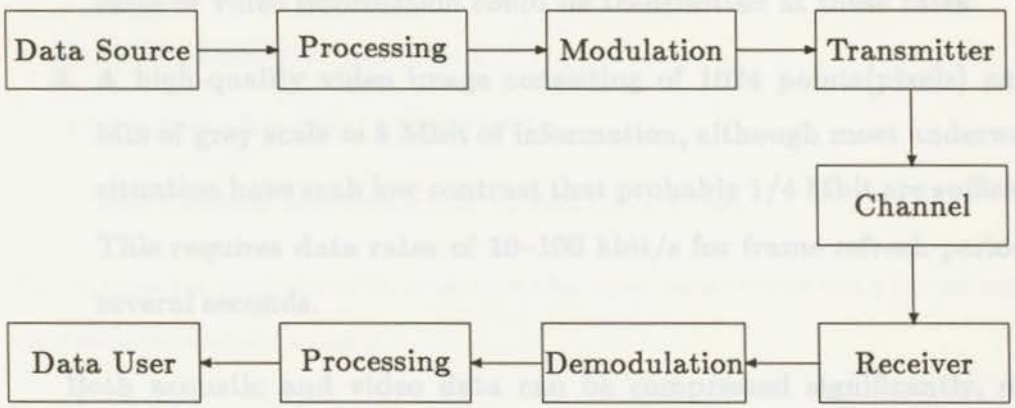

Figure 2.1: Representation of an acoustic communication system

2.2 Data Source

Three kinds of data are usually transmitted over an underwater communication system from a submerged data source:

1. Command/control data, such as navigation and equipment status, to a surface user is often necessary. The data rates required are low: $\approx$ 100-1000 bit/s; however, they must be transmitted with low error probability and high system reliability since the integrity of the entire

submerged system is involved. Several systems capable of these rates currently exist.

2. Acoustic instruments such as seismic profilers, sonars—both vertical and sidescan—ocean bottom seismometers, and hydrophones all require data rates of 1–10 kbit/s. In addition, very low picture frame rates of video information could be transmitted at these rates.

3. A high-quality video image consisting of 1024 points(pixels) and 8 bits of grey scale $\approx$ 8 Mbit of information, although most underwater situation have such low contrast that probably 1/4 Mbit are sufficient. This requires data rates of 10–100 kbit/s for frame refresh period of several seconds.

Both acoustic and video data can be compressed significantly, often with a minimal loss of fidelity. Several algorithms exist for speech and picture image compression, e.g., speech can be compressed to 900 bit/s and still be intelligible while pictures have been compressed to 2–3 bit/pixel with minimum loss in clarity [56,57]. (One of the algorithms commonly employed in speech compression, linear predictable encoding, when applied to seismic data, compressed the data to 1200 bit/s with a negligible loss in data fidelity.) The compression algorithms, however, require a modest computational capability at the site of the data source. Previously, this could not be done because the size and power requirements in even a small computer were prohibitive. The advent of microprocessors makes feasible the implementation of many of the algorithms developed for speech and image compression.

2.3 Acoustic Channel

The acoustic channel characteristics dominate the design of any acoustic communication system. There are four aspects that are of fundamental concern:

- transmission losses due to geometrical spreading and absorption,
- ambient noise,
- reverberation due to multipath,
- and Doppler spreading due to relative motion.

Each must be considered in selecting the appropriate signaling for an acoustic communication system.

2.3.1 Transmission Losses

The sea, together with its boundaries, forms a remarkably complex medium for the propagation of acoustic wave. It possesses an internal structure and a peculiar upper and lower surface which create many diverse effects upon the acoustic wave emitted from an underwater projector. In traveling through the sea, an acoustic signal becomes delayed, distorted, and weakened. Transmission loss expresses the magnitude of one of the many phenomena associated with acoustic wave propagation in the sea.

Transmission loss may be considered to be the sum of a loss due to spreading and a loss due to attenuation. Spreading loss is a geometrical effect representing the regular weakening of a acoustic signal as it spreads outward from the source. In most applications the primary transmission

path is direct, or line of sight, so a spherical spreading loss model, $20 \log R$ in decibels, is appropriate. Attenuation loss includes the effects of absorption, scattering, and leakage out of acoustic channels. The loss per unit of range α is a function of frequency as discussed in [2]. The total transmission loss $TL(f)$ is then

$$TL(f) = 20 \log R + \alpha(f) R \tag{2.1}$$

One can observe that the transmission losses determines either the maximum operating range of a system or the maximum usable frequency and hence bandwidth for a particular range. A useful set of criteria for determining when attenuation becomes significant is [14]

$$\alpha(f) R < 10\text{dB}. \tag{2.2}$$

In addition to these two principal kinds of loss, other losses not readily identified with range may occur; examples are the convergence gain in acoustic channels or its converse, refraction loss in shadow zones.

2.3.2 Ambient Noise

Ambient noise determines the signal-to-noise ratio at the receiver which ultimately limits the achievable data transmission rate. Ambient noise level decreases with frequency, and Figure 2.2 illustrates typical power density spectral distribution [2]. At the higher frequencies ($f \geq 100$kHz) the dominant source of ambient noise is isotropic thermal noise with one-sided power spectral density in $\mu\text{Pa}^2/\text{Hz}$ given by [2]

$$G_n(f) = 10^{-7.5} f^2 \tag{2.3}$$

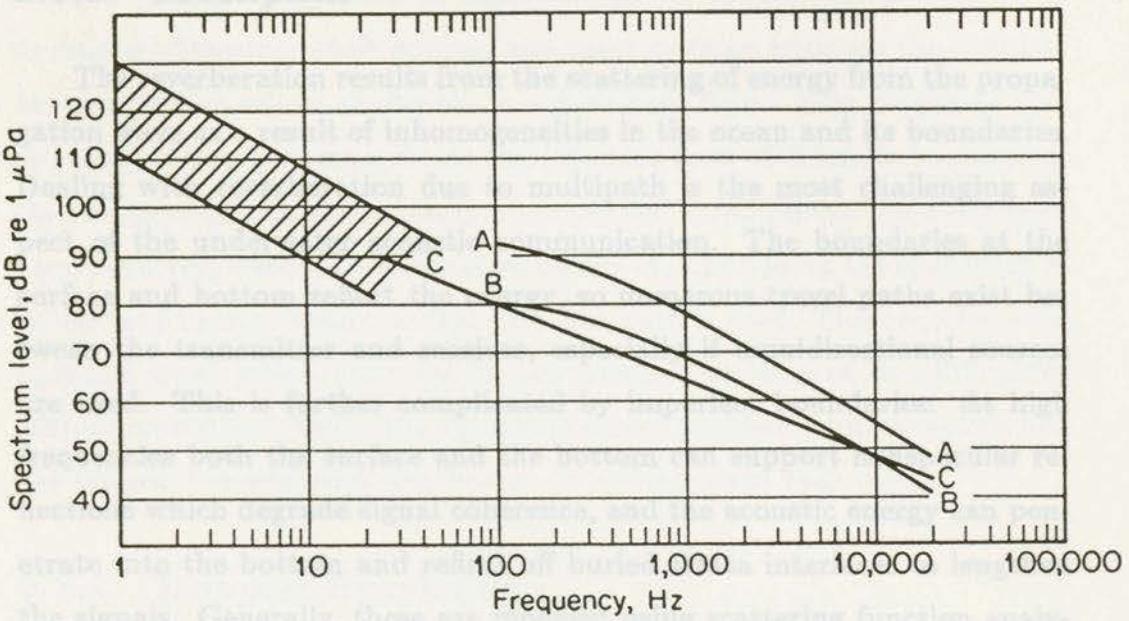

Figure 2.2: A summary of noise levels in bays and harbors. AA: A high noise location; entrance to New York Harbor in daytime. BB: An average noise lacation; upper Long Island Sound. CC: Average of many World War II measurements. Shaded area: Subsonic background measurements.

where f is frequency in Hz.

Noise levels are very site-dependent, especially in shallow water. Man-made noise due to activities associated with offshore platforms can increase noise levels dramatically. Generally, these man-made noises are concentrated at low frequencies and are localized, so it is desirable to use as high a frequency as possible consistent with transmission loss considerations. Moreover, narrower beams can be obtained conveniently at the higher frequencies which also lead to better suppression of localized noise sources.

2.3.3 Multipath

The reverberation results from the scattering of energy from the propagation wave as a result of inhomogeneities in the ocean and its boundaries. Dealing with reverberation due to multipath is the most challenging aspect of the underwater acoustic communication. The boundaries at the surface and bottom reflect the energy, so numerous travel paths exist between the transmitter and receiver, especially if omnidirectional sources are used. This is further complicated by imperfect boundaries. At high frequencies both the surface and the bottom can support nonspecular reflections which degrade signal coherence, and the acoustic energy can penetrate into the bottom and reflect off buried strata interfaces to lengthen the signals. Generally, these are modeled using scattering function analysis which was developed for similar multipath channel in electromagnetic communications [59]. One of the results for communication systems is that the convolution of channel scattering function and the ambiguity function of the transmitted signal set is a fundamental quantity in the detection process [60]. At frequencies below 10 kHz an impulsive signal can be time spread by multipath to hundreds of milliseconds in the shallow water and to several seconds in deep water. In many circumstances, however, the multipath is concentrated in packets, each of which is only locally spread by several milliseconds, so systematic signal design can be employed to take advantage of this. At high frequencies the total time spreading is less because of absorption at the boundaries and attenuation in the water. Spreading of 2-22 ms has been reported for a very shallow water channel (3-6 m) with the longer spreading occurring at the shorter ranges [14].

The principal approach to signal design for a time spread channel is to employ frequency shift keying, and most systems built for the acoustic communication where multipath is a dominant factor have employed this approach. Usually these systems employ some form of diversity to suppress the effects of fading, and recently more general spread spectrum techniques have been employed. An alternative means of suppressing the multipath is to use very narrow beams so that only one path is used. This requires wide aperture array which are large for low frequencies. One of the difficulties with narrow beam link is the "pointing error" problem which occurs when the transmitter and receiving beams do not intercept each other.

2.3.4 Doppler Spreading

Doppler spreading is introduced by relative motion between the transmitter and receiver or by water motion in the channel. The Doppler shift is 0.35 Hz/(kn · kHz) (one way) or 0.70 Hz/(kn · kHz) (two way) of relative motion. If the motion is slowly varying such as due to ship motion, such shifts can be compensated; however, random motion manifests itself by continuous frequency spreading. High-data-rate communication systems imply wide bandwidths which can only be obtained with high center frequencies. In addition to the high transmission losses, the high center frequencies lead to proportionally higher Doppler spreads, e.g., 17.5 Hz/kn at 50 kHz. Random motions in the water can be particularly important for frequency shift keying systems since some allowance for guard bands must be made. At frequencies below 1 kHz, several very careful experiments have demonstrated that the water itself has a very low Doppler spread on the

order of tens of millihertz, so one must conclude that most Doppler spreading is caused by transmitter/receiver relative motion. At high frequencies, few carefully controlled experiments have been done [61]. Signal design over Doppler spread channels leads to short pulses. To preserve signal-to-noise ratio, high-amplitude signals must be used which often implies a peak power problem because of the high voltage required to drive the acoustic sources.

Both multipath and Doppler spreading are important factors in the acoustic communication channel, and any design must recognize each. To avoid the effects of multipath one needs to have

$$1/W \gg L \tag{2.4}$$

where L is the multipath length and W the signal bandwidth; and to avoid Doppler spreading one needs to have

$$1/T \gg B \tag{2.5}$$

where T is the signal duration and B is Doppler spread [60]. A fundamental quantity for a channel is the product BL. If this quantity exceeds unity, the channel is said to be "overspread" and appropriate signal design must be employed to use the channel successfully.

Chapter 3

Multipath Rejection Using Narrowbeam Acoustic Link

The intent in this chapter is to discuss multipath suppression by using a narrowbeam link. We first compare two types of narrowbeam systems: umbrella-type beam produced by linear array and conical, searchlight-type beam produced by planar array. We then examine specular and non-specular reflections when the acoustic communication link is near the sea surface. It is shown that in both uses, a linear array offers better performance in rejecting multipath than the planar array with the same number of elements.

3.1 Introduction

The presence of multipath in underwater acoustic communication channels is the major limitation to reliable, high-rate data transmission needed in diverse applications.

The multipath conditions can vary significantly depending on sea state,

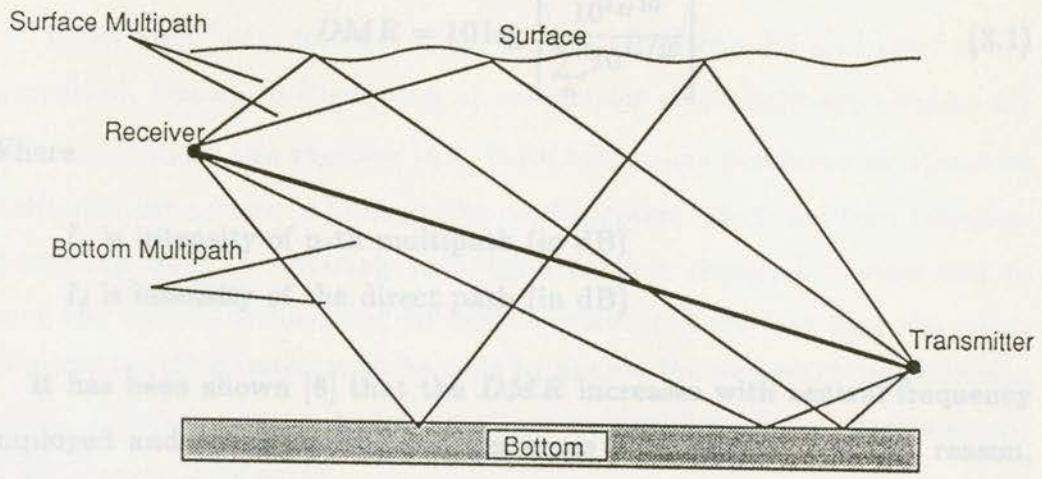

Figure 3.1: Multipath structure

ocean depth, type of bottom, sound velocity profile, transmitter-receiver configuration and their respective radiation patterns. Because of a relatively high frequency carrier used for acoustic communication the ray theory can be applied to determine the propagating paths linking a transmitter and a receiver. Shown in Figure 3.1 are primary possible paths linking transmitter and receiver in an isospeed acoustic channel. The intensity of a particular multipath can be calculated by taking into account the propagation distance, number of surface and bottom reflections and associated losses, and transmitting/receiving radiation patterns. The channel quality can be quantitatively characterized by the direct signal-to-multipath signal ratio. Assuming noncoherent multipath signals, this ratio (in dB) can be expressed as [8]:

$$DMR = 10 \log \left[\frac{10^{I_d/10}}{\sum_n 10^{I_n/10}} \right] \quad (3.1)$$

Where

I_n is intensity of n-th multipath (in dB)

I_d is intensity of the direct path (in dB)

It has been shown [8] that the DMR increases with central frequency employed and ocean depth, and decreases with range. For this reason, high frequencies, in near vertical transmission from deep ocean are least affected by multipath. For example, vertical transmission from a 200m depth encounters $DMR = 28dB$ at frequency $f = 100kHz$ which drops to $15dB$ at $f = 10kHz$. Omnidirectional transducers, smooth surfaces and a 5 Mrayls bottom acoustic impedance have been assumed. On the other hand, the DMR can drop as low as $5dB$ for very shallow water (50m) and a long propagation range (1000m).

Since multipath signals generally arrive from directions different from that of the direct path signal, they can be suppressed by utilizing suitable radiation patterns at the transmitter and the receiver. Such patterns will consist of a narrow mainlobe and small sidelobes. The transmitting/receiving beams should be kept aligned along the direct path. Suppression of some multipath can lead to a substantial increase in the DMR [8]. In order to ease the beam's alignment task, it is also possible to employ a broadbeam transmitter and a narrow beam receiver.

3.2 Multipath Suppression

Three basic beam configurations depicted in Figure 3.2 a), b) and c) are considered. Shown in Figure 3.2 a) are narrow searchlight-type beams for both transmitter and receiver [46]. Both beams are produced by steerable multi-element arrays. Although the configuration offers the best rejection of ambient noise, a relatively complex scheme is required to steer and to track the beams. Additional difficulties arise from the fact that the steerable transmitting beam must be able to handle the necessary transmission power. This necessitates a number of power amplifiers driving each element of the transmitting array.

The configuration shown in Figure 3.2 b) uses a relatively broad conical fixed transmitting beam while the steerable receiving beam is narrow [63]. The beam alignment for this configuration is less complicated. It will be demonstrated that the system performance is not critically dependent on a transmitting beamwidth.

Shown in Figure 3.2 c) is a steerable umbrella-type receiving beam, produced by a vertically suspended linear array. Beam alignment and tracking for this configuration is particularly simple. Subsequently it will be assumed that a fixed, relatively broad conical transmitting beam and steerable narrow (searchlight or umbrella-type) receiving beam are utilized.

The multipath signals can be admitted to the receiver through the main lobe beam or through the sidelobes of the radiation pattern. Sidelobe levels can be controlled by proper weighting coefficients applied to each element of the array. The Dolph-Chebyshev weights, for example, theoretically allow

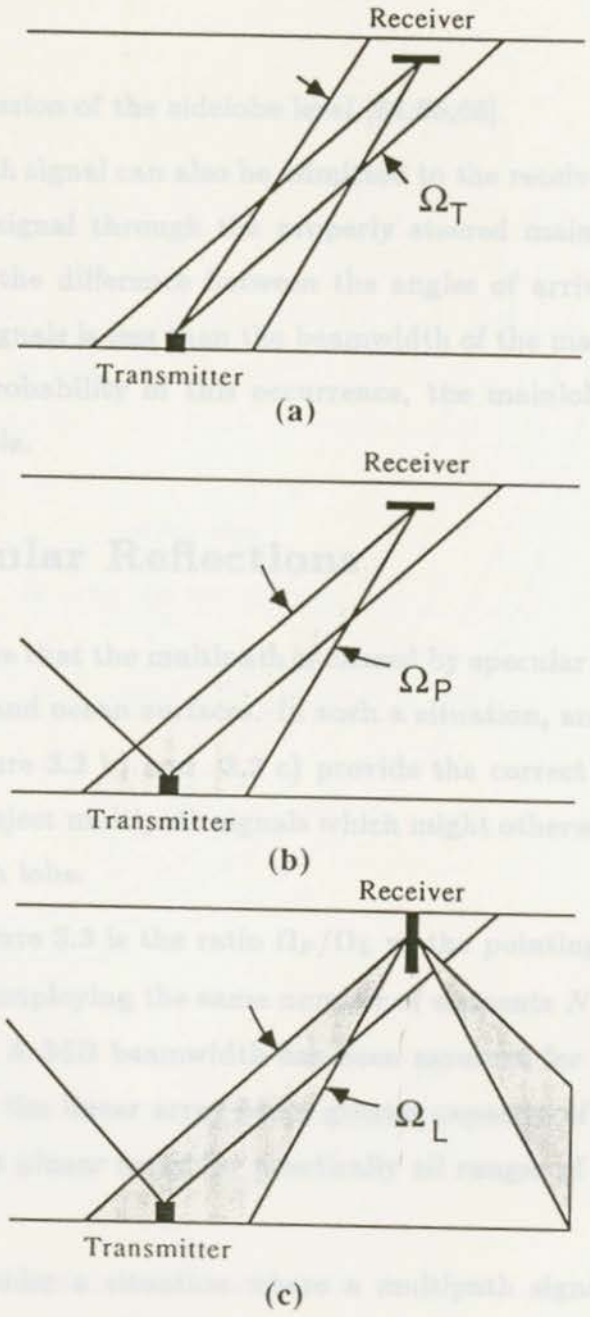

Figure 3.2: Configurations of acoustic beams

arbitrary suppression of the sidelobe level [64,65,66].

The multipath signal can also be admitted to the receiver together with the direct-path signal through the properly steered mainlobe. This will occur whenever the difference between the angles of arrival of the direct and multipath signals is less than the beamwidth of the mainlobe. In order to reduce the probability of this occurrence, the mainlobe should be as narrow as possible.

3.3 Specular Reflections

Let us assume that the multipath is caused by specular reflections from smooth bottom and ocean surfaces. In such a situation, angles Ω_P and Ω_L indicated in Figure 3.2 b) and 3.2 c) provide the correct measure of the array ability to reject multipath signals which might otherwise be admitted through the main lobe.

Shown in Figure 3.3 is the ratio Ω_P/Ω_L vs the pointing angle (off vertical) for arrays employing the same number of elements N separated by a half wavelength. A 3dB beamwidth has been assumed for calculations. It can be seen that the linear array has a greater capacity of multipath suppression than the planar array for practically all ranges of pointing angles and array sizes.

We now consider a situation where a multipath signal is caused by reflection from rough surfaces.

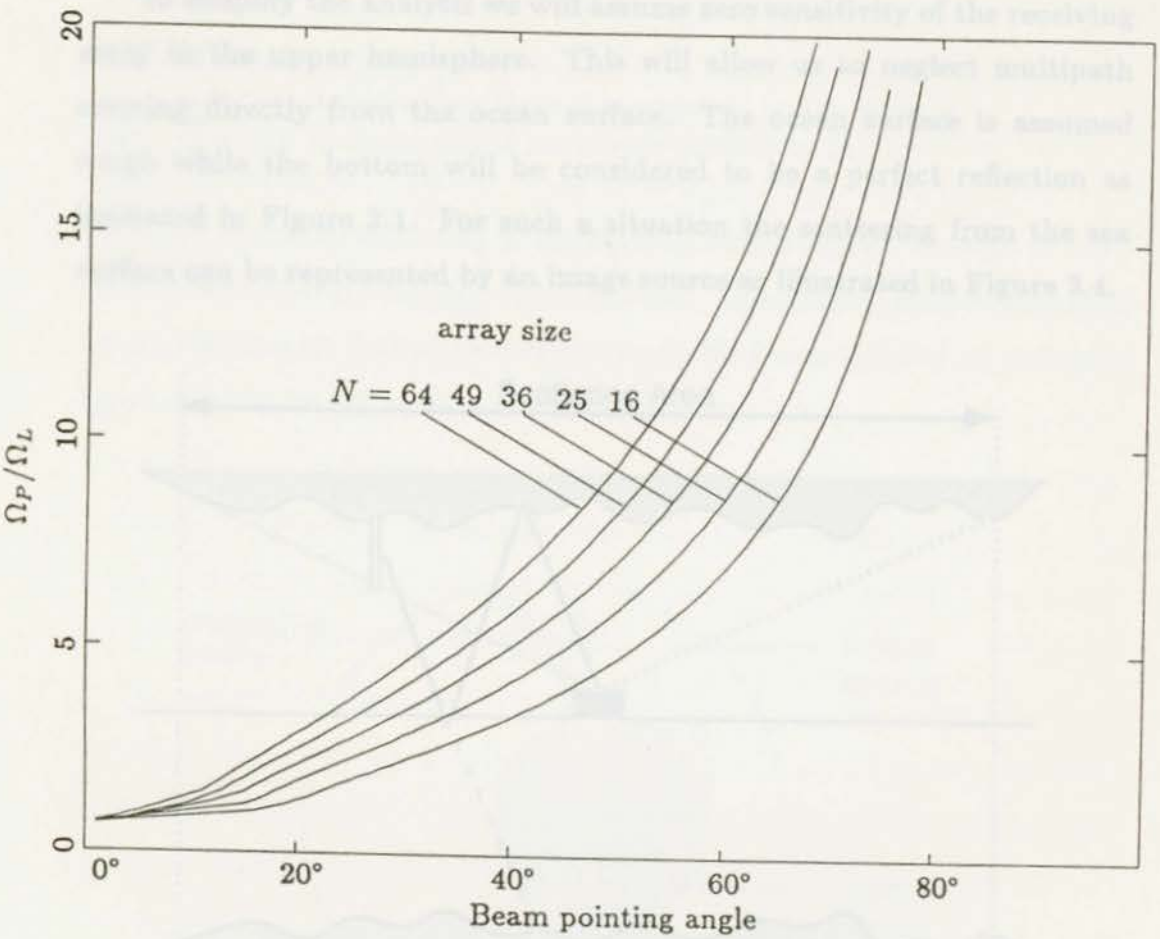

Figure 3.3: Comparison of beamwidths for planar and linear arrays

3.4 Nonspecular Reflections

To simplify the analysis we will assume zero sensitivity of the receiving array in the upper hemisphere. This will allow us to neglect multipath arriving directly from the ocean surface. The ocean surface is assumed rough while the bottom will be considered to be a perfect reflection as indicated in Figure 3.1. For such a situation the scattering from the sea surface can be represented by an image source as illustrated in Figure 3.4.

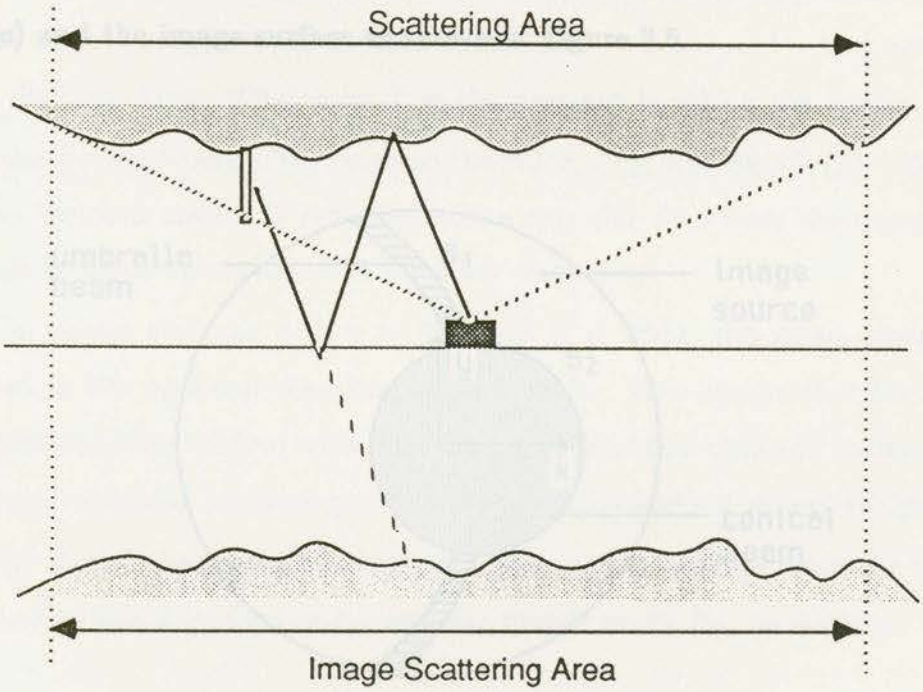

Figure 3.4: Application of image principle to rough sea surface

Part of the incident power P_i upon the surface is reflected in the specular direction while the remaining power P_s is diffusely scattered in all directions

as given by [61]:

$$P_s = (1 - \overline{\varrho^2})P_i = (1 - \overline{\varrho^2})\alpha P_t$$

where P_t is transmitted power

α is transmission loss from the projector to the surface

and $\overline{\varrho^2}$ is the variance of the scattering coefficient ϱ.

Since the receiving array is directional, only a certain amount of scattered power will be admitted to the system. This amount can be calculated by considering an intersection of the receiving beam (conical or umbrella-type) and the image surface as shown in Figure 3.5.

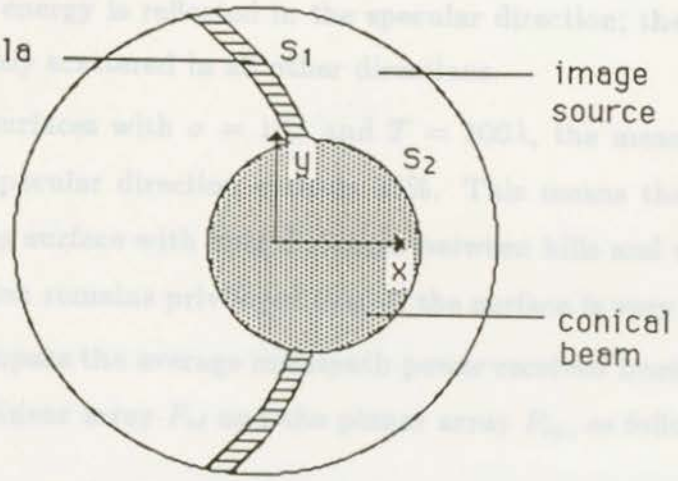

Figure 3.5: Intersection of the receiving beam and the image scattering surface

The total mean power received from the image surface is then obtained

$$P_r = \beta \cdot \int\int_{s_i} G(\phi, \theta, x, y, \phi_i, \theta_i) \; ds; \quad i = 1, 2 \tag{3.2}$$

where $G(\phi, \theta, x, y, \phi_i, \theta_i)$ is the intensity distribution function of the mean power scattered in the direction (ϕ, θ) from each source point (x, y) for a given incident angle (ϕ_i, θ_i), s_i is the shaded region as shown in Figure 3.5, and β is transmission loss along the surface-bottom-receiver path.

The intensity distribution function of the scattered field in various directions for a given angle of incidence has been discussed in [62]. For a slight surface roughness (standard deviation $\sigma = 0.1\lambda$) and a long correlation distance ($T = 200\lambda$) here T is the distance in which the spatial auto correlation coefficient $C(t)$ drops to the value e^{-1}), only 46.8% ($\overline{\varrho^2} = 0.468$) of the incident energy is reflected in the specular direction; the remaining energy is diffusely scattered in all other directions.

For rough surfaces with $\sigma = 10\lambda$ and $T = 200\lambda$, the mean power reflected in the specular direction exceeds 37%. This means that for large T (gently rolling surface with long distances between hills and valleys) the specular direction remains privileged even if the surface is very rough.

We now compare the average multipath power received from the image surface by the linear array $P_{r\ell}$ and the planar array P_{rp}, as follows:

$$\frac{P_{r\ell}}{P_{rp}} = \frac{\int\int_{s1} G(\phi, \theta, x, y, \phi_i, \theta_i) ds}{\int\int_{s2} G(\phi, \theta, x, y, \phi_i, \theta_i) ds} \tag{3.3}$$

For simplicity we assume that the intensity distribution function $G(\cdot)$ is uniform on the image surface, and therefore

$$\frac{P_{r\ell}}{P_{rp}} = \frac{S_1}{S_2}$$

$$= \frac{2\tan(\frac{\theta_{r\ell}}{2})}{\theta_{rp}^2}\sin 2\theta_0 \cdot$$

$$\tan^{-1}\left(\frac{\sqrt{10\tan^2\theta_0\tan^2(\frac{\gamma_t}{2}) - 9\tan^4\theta_o - \tan^4(\frac{\gamma_t}{2})}}{5\tan^2\theta_0 - \tan^2(\frac{\gamma_t}{2})}\right)$$

$$\simeq \frac{\theta_{r\ell}}{\theta_{rp}^2}\sin 2\theta_0 \tan^{-1}\left(\frac{\sqrt{10r - r^2 - 9}}{5 - r}\right) \tag{3.4}$$

where $\theta_{r\ell}$ and θ_{rp} are the beamwidths of the linear and planar array, respectively, θ_0 is the steering angle, γ_t is the beamwidth of transmitter, and

$$r = \frac{\tan^2(\frac{\gamma_t}{2})}{\tan^2\theta_0}. \tag{3.5}$$

The ratio $P_{r\ell}/P_{rp}$ changes only slightly when the number of elements N varies. Figure 3.6 shows the performance of two types of arrays: linear and planar with the same number of elements ($N = 1 \times 64$ and 8×8) separated by $\lambda/2$. We can see that at a steering angle $\theta_0 = 45°$ and for a transmitting beamwidth $\gamma_t = 100°$, the linear array gives a 7.4dB improvement over the planar array in rejecting the multipath.

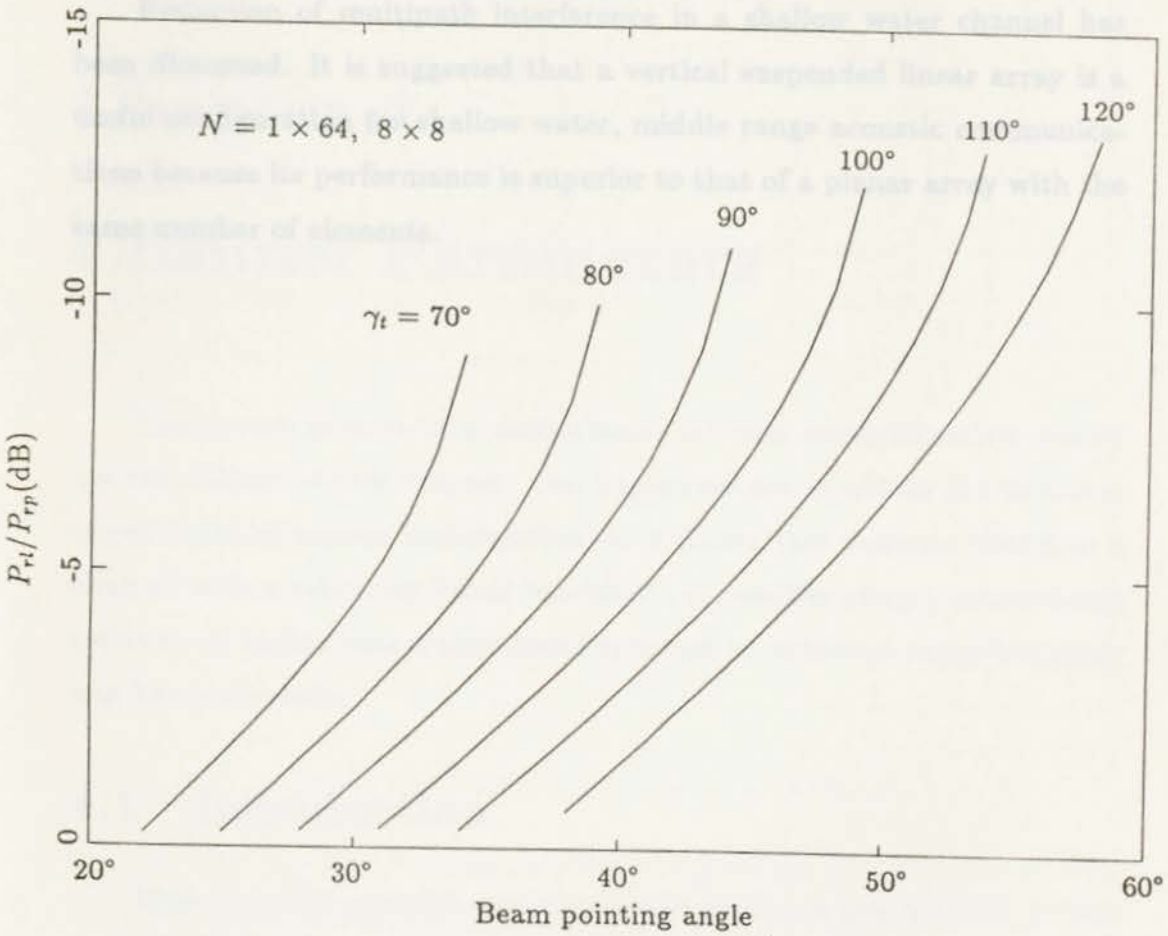

Figure 3.6: Comparison of multipath rejection for planar and linear arrays

3.5 Summary

Reduction of multipath interference in a shallow water channel has been discussed. It is suggested that a vertical suspended linear array is a useful configuration for shallow water, middle range acoustic communications because its performance is superior to that of a planar array with the same number of elements.

Chapter 4

Channel Parameters

The system aspects of a narrowbeam acoustic communication system are the subject of this chapter. Our objectives are to obtain the practical upper limits of system performance. It is shown that communication in a channel with a relatively broad bandwidth is possible using a narrowbeam receiver. A higher rate transmission rate can be achieved using frequency and beam diversity.

4.1 Introduction

High capacity acoustic communication links are required for diverse underwater operations [3,9,14,68]. In order to meet this demand, several experimental and commercial telemetry systems have been developed successfully [4,5,7,67,74]. Some of them are summarized in Table 4.1. The transmission rate varies greatly with carrier frequency, intended range, error rate required and type of propagation (direct or indirect path). For broadbeam systems the limiting factor arises from the presence of multipath. One possible method of multipath reduction is by using narrow

Manufacturer	Transmission Rate (bits/s)	Carrier (kHz)	Modulation Type	Range (km)
Honeywell Ltd.	40-160	15	MFSK	8
Oceano Ltd.	320	20	FSK	7
Acoustic Systems Ltd.	4800	25	DPSK	2
NOAA	75-1200	50	FSK	–
Thomson Ltd.	20,000	60	–	1
Herriot-Watt Univ.	120,000	600	–	0.1

Table 4.1: Representative acoustic systems

transmitting and receiving beams [63,69]. Alignment and tracking of these beams presents a separate problem which will be addressed later. This chapter is an attempt to establish an upper limit of performance of a narrow beam system assuming near ideal beam alignment and tracking. A transmission scenario considered is shown schematically in Figure 4.1.

A transmitter located at depth h transmits a signal along a conical beam towards a surface receiver. The transmitting beam is stationary and has beamwidth Ω_T, while the receiving beam with beamwidth $\Omega_R < \Omega_T$

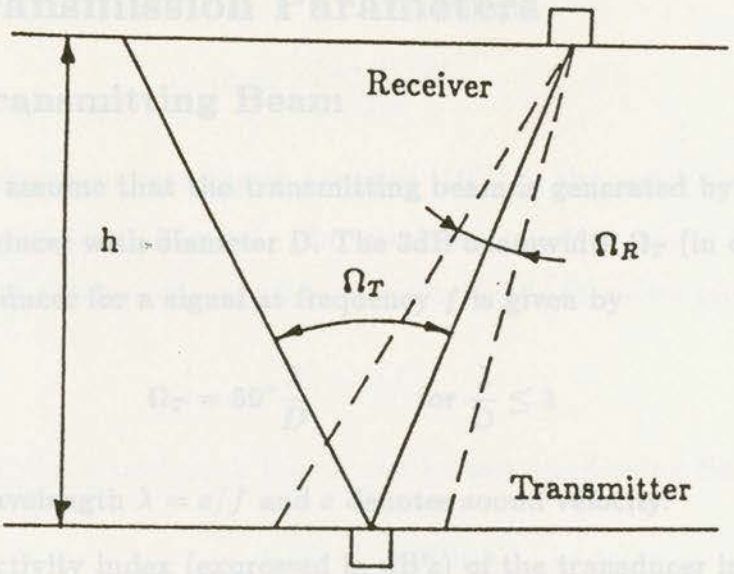

Figure 4.1: A transmission scenario

can be electronically steered towards the transmitter.

This scenario is applicable to situations when data accumulated from underwater bottom sensors has to be retrieved using an acoustic link. Often a large amount of accumulated data (in order of tens of megabytes) and limited retrieval time necessitates a very high speed transmission. The scenario described is also applicable to data (such as slow scan TV) transmitted from an untethered Remotely Operated Vehicle (ROV) which is followed by a surface ship.

4.2 Transmission Parameters

4.2.1 Transmitting Beam

We will assume that the transmitting beam is generated by a circular piston transducer with diameter D. The 3dB beamwidth Ω_T (in degrees) of such a transducer for a signal at frequency f is given by

$$\Omega_T = 59^\circ \frac{\lambda}{D} \qquad \text{for } \frac{\lambda}{\mathrm{D}} \leq 1 \tag{4.1}$$

where wavelength $\lambda = c/f$ and c denotes sound velocity.

The directivity index (expressed in dB's) of the transducer is given by

$$DI_T = 20 \log \frac{\pi \mathrm{D}}{\lambda} \tag{4.2}$$

Combining Eq.(4.1) and (4.2) we can write

$$DI_T = 45.4 - 20 \log \Omega_T \tag{4.3}$$

The transmitter source level SL expressed in dB re $1\mu Pa$ as measured 1m away from the transducer is related to total acoustic power radiated by the transducer W, such that

$$SL = 170.9 + DI_T + 10 \log W \tag{4.4}$$

4.2.2 Cavitation Threshold

The maximum acoustic intensity (acoustic power per unit area) which can be produced by a transducer is limited by the cavitation threshold I_c

given by

$$I_c = \frac{(P_{atm} + hg\rho)^2}{2\rho c} \tag{4.5}$$

where P_{atm} denotes atmospheric pressure ($10^5 \mathrm{P}_a$), the water density $\rho = (10^3 kg/m^3)$ and $g = 9.81 m/s^2$. The maximum acoustic power which can be radiated by the transducer without cavitation is therefore given by

$$W_c = AI_c \tag{4.6}$$

where area of the transducer's face A can be expressed using Eq.(4.1) as

$$A = \frac{\pi D^2}{4} = \pi(\frac{29.5c}{\Omega_T f})^2 \tag{4.7}$$

The cavitation threshold increases rapidly with depth (from $0.3\mathrm{W/cm}^2$ at the surface to $13\mathrm{W/cm}^2$ at depth $h = 100m$). It is also an increasing function of frequency. This effect is not accounted for in Eq.(4.5) which can therefore be considered as a lower bound for cavitation.

4.2.3 Transmission Losses

Transmission losses (in dB) can be expressed as

$$TL = 20 \log r + \alpha r + 3dB \tag{4.8}$$

where r is a slant range between transmitter and receiver as shown in Figure 4.1.

$$r = h/\cos(\Omega_T/2) \tag{4.9}$$

α is the absorption loss given by the following empirical formula [10]

$$\alpha = \left[\frac{2.34 \times 10^{-6} S f_r f^2}{f_r^2 + f^2} + \frac{3.38 \times 10^{-6} f^2}{f_r}\right] \times (1 - 65.4P) \times 8.73 \quad \text{dB/m} \tag{4.10}$$

where S is salinity in parts per thousand, f is frequency in kHz, P is pressure in P_a, and

$$f_r = 21.9 \times 10^{6-1520/(T+273)} \quad \text{kHz} \tag{4.11}$$

T is temperature in degrees centigrade.

An additional 3dB loss in Eq.(4.8) was added to reflect the fact that the system may operate on the edge of the transmitted beam.

4.2.4 System Noise

At higher frequencies ($f \geq 100kHz$) the dominant source of ambient noise is isotropic thermal noise with one-sided power spectral density in $\mu Pa^2/Hz$ given by

$$G_n(f) = 10^{-7.5} f^2 \tag{4.12}$$

where f is frequency in Hz.

In the following analysis we assume that the transmitted signal occupies a finite frequency band B, centered around a central frequency f_o. The noise in this band (in-band noise) can be obtained from the following integral:

$$\overline{n_B^2} = \int_{f_o - B/2}^{f_o + B/2} G_n(f) df = 0.33 \times 10^{-8} \left[(f_o + B/2)^3 - (f_o - B/2)^3\right] \tag{4.13}$$

In logarithmic (dB) scale, the in-band noise is given by

$$NB = 10 \log \overline{n_B^2} \tag{4.14}$$

Since the receiving hydrophone is directional, the total in-band, in-beam noise at the receiver becomes:

$$N = NB - DI_R \tag{4.15}$$

where DI_R is the directivity index of the receiver given by a formula similar to Eq.(4.3), that is

$$DI_R = 45.4 - 20 \log \Omega_R \tag{4.16}$$

where Ω_R denotes the receiving hydrophone beamwidth (in degrees).

4.2.5 Signal-to-Noise Ratio

It is evident from Eq.(4.3) and (4.16) that both the transmitting and the receiving directivity indexes (as well as the beamwidths) depend on frequency. On the other hand, the transmitted signal will occupy a finite frequency band. To resolve this difficulty we will tactically assume a narrowband system such that $B << f_o$. From a practical point of view, the narrowband system is more efficient and easier to implement than a broadband one. The directivity indices can be calculated at the central frequency f_o and assumed constant within the bandwidth B. For a narrowband system we can write

$$B = f_o/Q \tag{4.17}$$

where the quality factor $Q \geq 10$. Since it is desired that the bandwidth B is as large as possible, we subsequently assume $Q = 10$.

The quality of this transmission channel depends on the signal-to-noise ratio. The signal level at the receiver S can be obtained from Eq.(4.4) and Eq.(4.8), namely

$$S = SL - TL \tag{4.18}$$

The signal-to-noise ratio SNR (in dB) is simply

$$SNR = S - N \tag{4.19}$$

where the noise N is given by Eq.(4.15).

Depending on the type of transmission, and required error rate, an acceptable SNR can vary between 5 and 30dB or more.

4.3 Summary

In the calculation of absorption losses given by Eq.(4.10) the following parameters were assumed: $S = 33ppt, T = 4°C$ and $P = 10^5 P_a$. Figures 4.2 through 4.5 show the maximum central frequency f_o where a desired signal-to-noise ratio SNR is obtained as a function of depth h. Figure 4.2 shows f_o vs h for different values of receiving beamwidths and other parameters as indicated. For the assumed parameters, the cavitation level as given by Eq.(4.5) was never exceeded. As we can see from the diagram Figure 4.3, at a depth 500m (representative to continental shelf) the maximum carrier frequency is 400 kHz with $W = 1$ watt, $\Omega_T = 45°$ and $\Omega_R = 10°$. This implies that for a $Q = 10$, the available transmission bandwidth B is 40

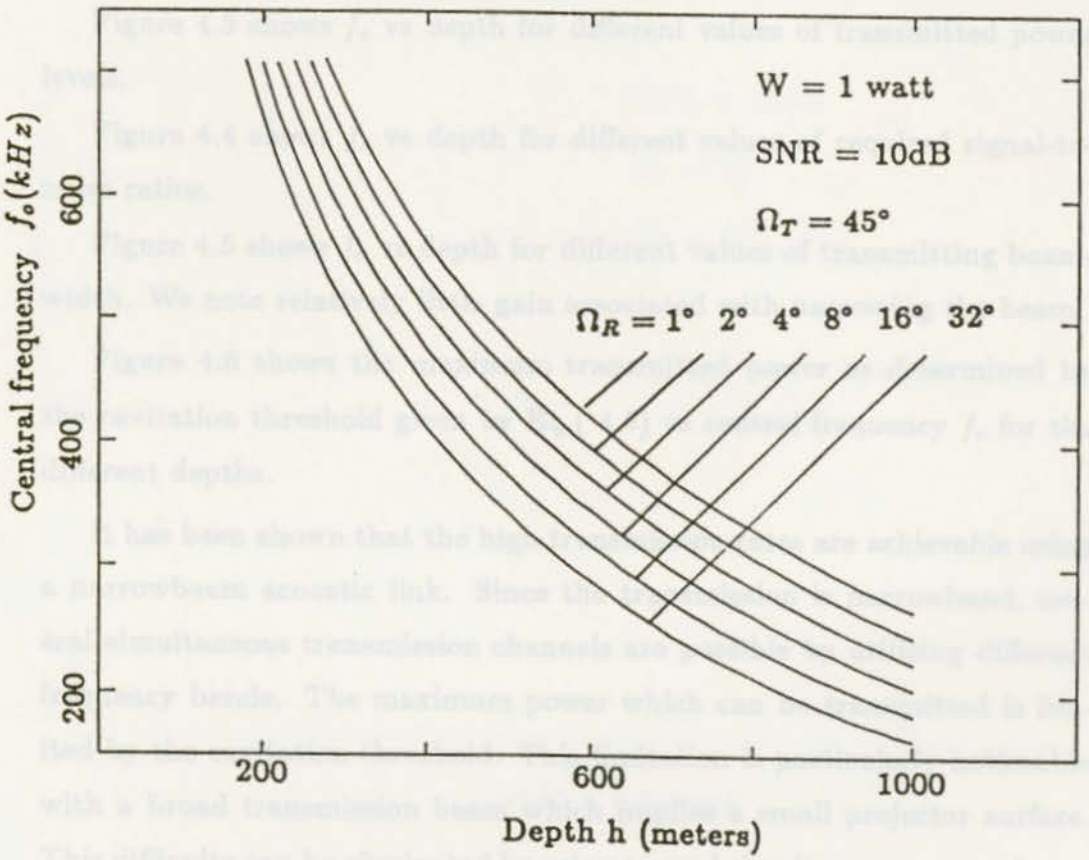

Figure 4.2: Central frequency versus depth for different receiving beamwidths

kHz with a 10dB total signal-to-noise ratio. This bandwidth can be utilized for transmission of analog (like slow-scan TV) or digital data at rates of approximately 2-4 bits per Hz of the available bandwidth.

Figure 4.3 shows f_o vs depth for different values of transmitted power levels.

Figure 4.4 shows f_o vs depth for different values of required signal-to-noise ratios.

Figure 4.5 shows f_o vs depth for different values of transmitting beamwidth. We note relatively little gain associated with narrowing the beam.

Figure 4.6 shows the maximum transmitted power as determined by the cavitation threshold given by Eq.(4.5) vs central frequency f_o for the different depths.

It has been shown that the high transmission rates are achievable using a narrowbeam acoustic link. Since the transmission is narrowband, several simultaneous transmission channels are possible by utilizing different frequency bands. The maximum power which can be transmitted is limited by the cavitation threshold. This limitation is particularly noticeable with a broad transmission beam which implies a small projector surface. This difficulty can be eliminated by using several simultaneous narrowbeam transmitters suitable oriented such as to form a broadbeam coverage.

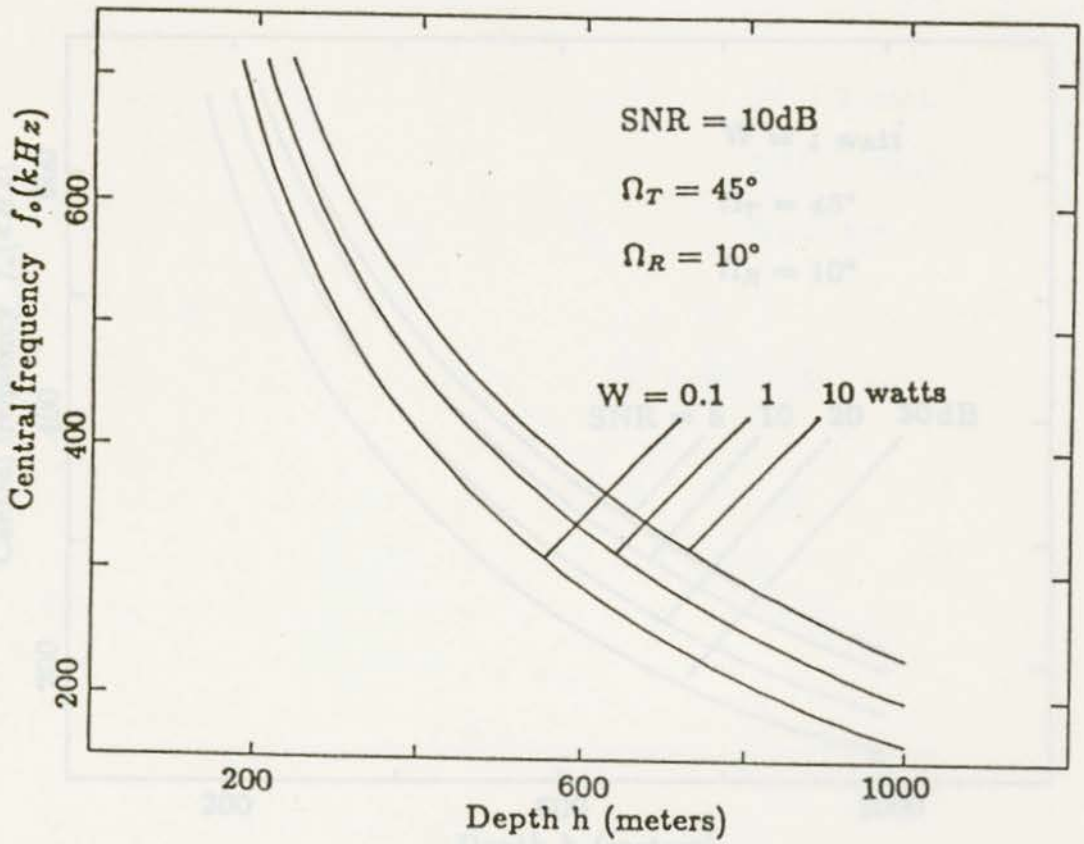

Figure 4.3: Central frequency vs depth for different transmitted powers

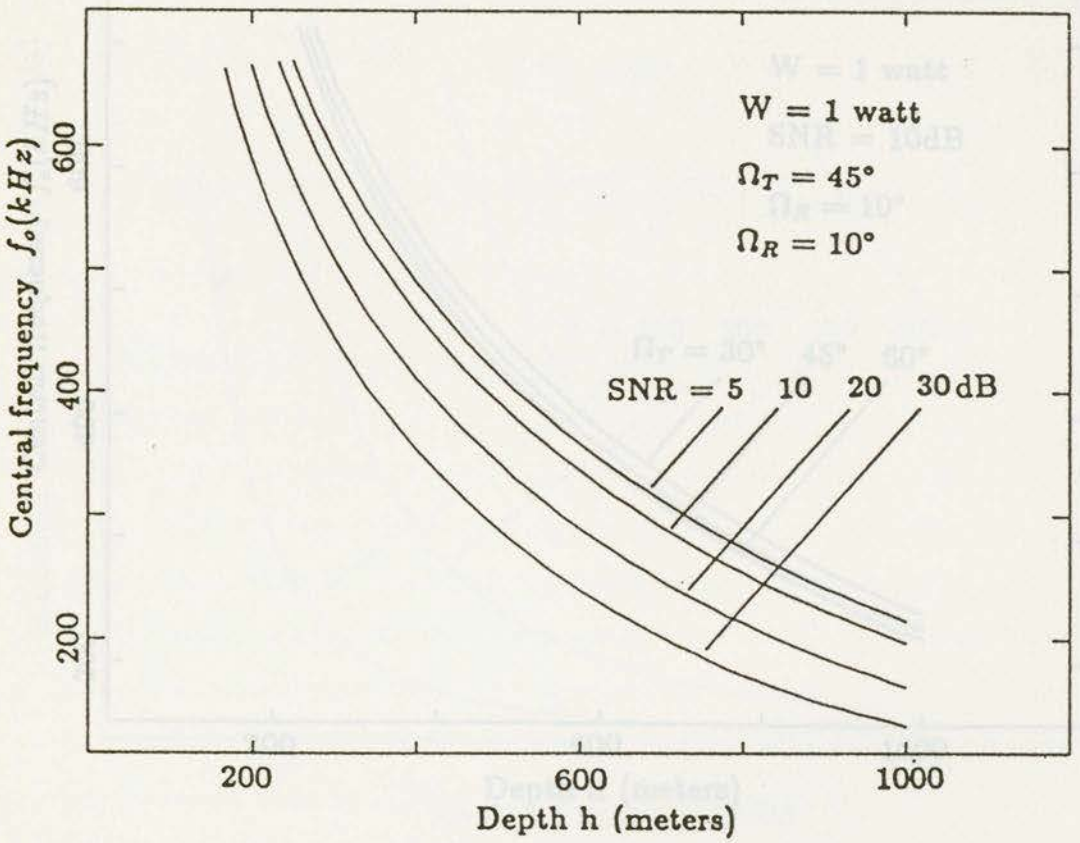

Figure 4.4: Central frequency vs depth for different signal-to-noise ratios

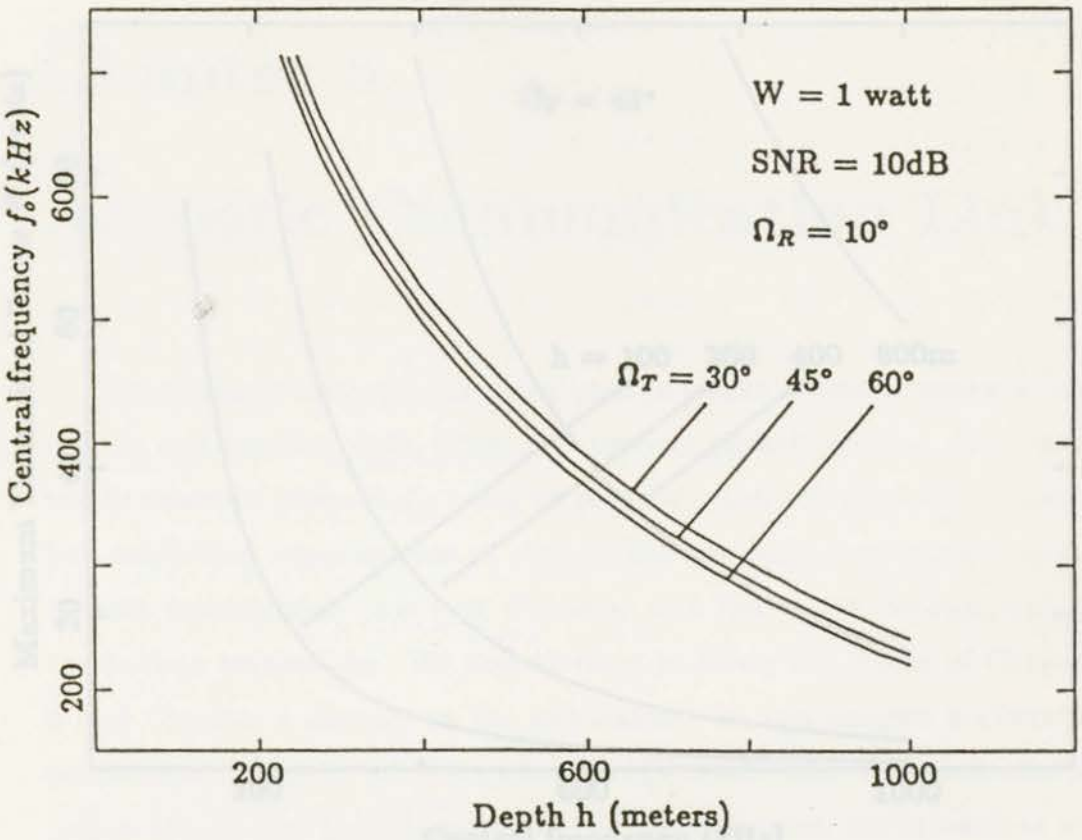

Figure 4.5: Central frequency vs depth for different transmitting beamwidths

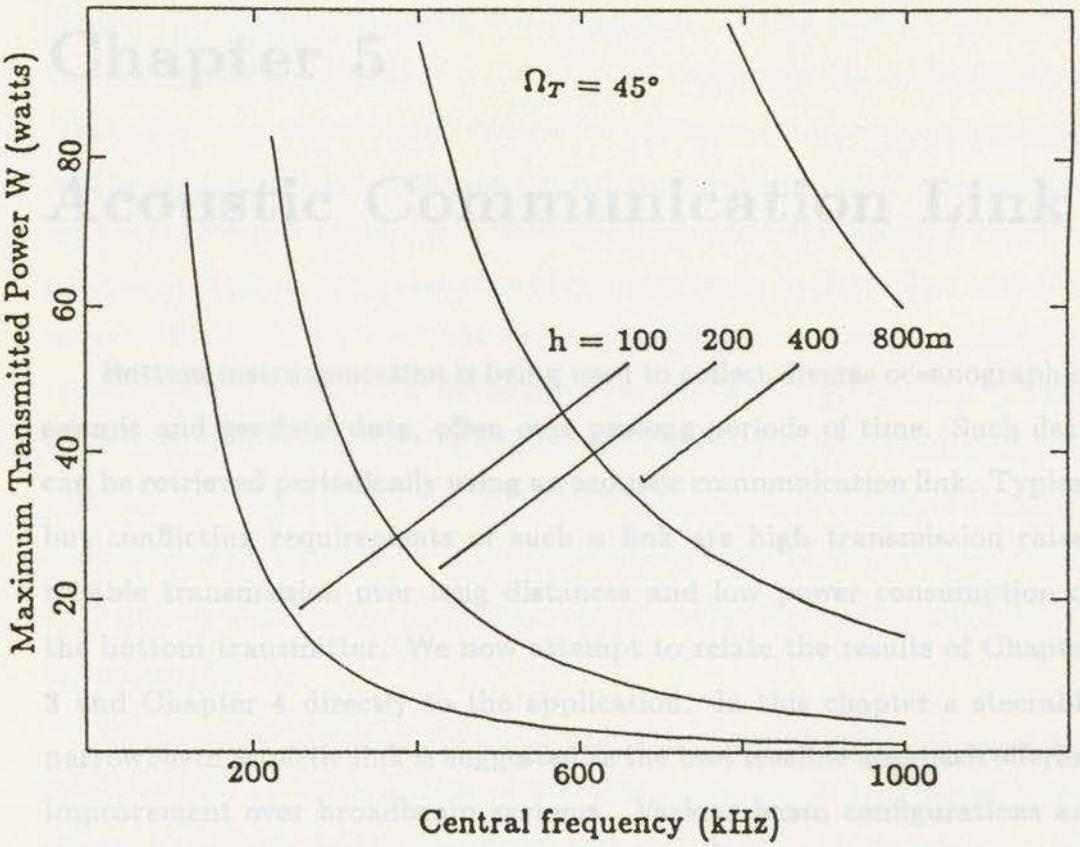

Figure 4.6: Maximum transmitted power vsersu frequency for different depths

Chapter 5

Acoustic Communication Link

Bottom instrumentation is being used to collect diverse oceanographic, seismic and geodetic data, often over prolong periods of time. Such data can be retrieved periodically using an acoustic communication link. Typical but conflicting requirements of such a link are high transmission rates, reliable transmission over long distances and low power consumption of the bottom transmitter. We now attempt to relate the results of Chapter 3 and Chapter 4 directly to the application. In this chapter a steerable narrowbeam acoustic link is suggested as the best feasible approach offering improvement over broadbeam systems. Various beam configurations are considered and compared in terms of their ability to reject ambient noise and multipath interference. A vertically suspended linear receiving array is postulated as the best solution to multipath suppression and beam tracking.

5.1 Introduction

Bottom instrumentation is sometimes deployed for prolonged periods of time to collect diverse oceanographic, seismic and geodetic data. Such

data can be temporarily stored in a suitable memory bank and retrieved when the instrument is recovered.

Another possible scenario involves an acoustic link established between bottom instrumentation and a surface platform. Using such a link the data can be retrieved without the necessity of recovering the instrument. A large amount of accumulated data, often on the order of several megabytes, has to be transmitted within a limited retrieval time. This necessitates high transmission rates. It is also desirable that the acoustic link can provide reliable transmission over long distances in both shallow and deep waters without an excessive transmitted power. These generally conflicting requirements are achieved differently depending on application. Several experimental and commercial digital underwater acoustic communication systems have been developed for diverse purposes [3]. Some of them are summarized in Table 4.1. The transmission rates of the systems shown vary greatly with carrier frequency, range and type of propagation (direct or indirect path).

The presence of multipath signals caused by surface and bottom reflections, as well as by refraction of acoustic waves, limits high speed transmission, particularly in broadbeam systems. Multipath signals generally arrive from different angular directions, and therefore they can be suppressed if properly aligned narrow transmitting/receiving beams are used. With multipath power reduced to a negligible level, the system performance is limited by ambient noise which, at higher frequencies (above approximately 100 kHz), is dominated by thermal noise [2]. Reduction of ambient noise admitted to the system is possible by the narrowing of the transmit-

ting/receiving beams. Proper alignment and tracking of such beams are required for a reliable data transmission link.

5.2 General Assumptions

In order to adopt a proper design philosophy, certain general assumptions regarding a transmission scenario and system functions are made as follows:

(a) The acoustic link is to be established between a surface (or near surface) unit and an underwater unit. The surface unit is typically deployed from a ship, helicopter or from an ice-based station. A receiving array is lowered to a certain depth to avoid effects of possible *shadow zones* caused by the refraction of acoustic waves. The underwater unit is moored on or near ocean bottom and is powered from its own batteries. The surface unit can be relatively more complex than the underwater unit.

(b) It is assumed that a higher data rate is required from the underwater unit to the surface unit (up-link) while the down-link data rate can be much lower. For this reason, we will refer to the surface unit as a *receiver* and the underwater unit as a *transmitter*. Three basic beam configurations depicted in Figure 3.2 a), b) and c) are considered. Shown in Figure 3.2 a) are narrow search-light type beams for both transmitter and receiver [46]. Both beams are produced by steerable multi-element arrays. Although this configuration offers the best rejection of ambient noise, a relatively complex scheme is required to

steer and to track the beams. Additional difficulties arise from the fact that the steerable transmitting beam must be able to handle the necessary transmission power. This necessitates a number of power amplifiers driving each element of the transmitting array.

The configuration shown in Figure 3.2 b) uses a relatively broad conical fixed transmitting beam while the steerable receiving beam is narrow [63]. The beam alignment for this configuration is less complicated. It will be demonstrated that the system performance is not critically dependent on a transmitting beamwidth.

Shown in Figure 3.2 c) is a steerable umbrella-type receiving beam, produced by a vertically suspended linear array. Beam alignment and tracking for this configuration is particularly simple. Subsequently it will be assumed that a fixed, relatively broad conical transmitting beam and steerable narrow (search light or umbrella-type) receiving beams are utilized.

A general functional block diagram of the receiver is shown in Figure 5.1. The narrowband up-link signal is incident upon the receiving array. The output signals from the receiving array elements are used to estimate the angles of arrival of the direct-path signal as well as the interfering multipath. Based on these estimates a beam is formed and electronically steered in the direction of the strongest signal (typically the direct-path signal). The beamformed signal is then demodulated to yield the desired data. Doppler shift information can be extracted from the signal and can be utilized to improve the estimate of the angles of arrival. The system can be used for the transmission of both digital or analog data. Subsequently, we

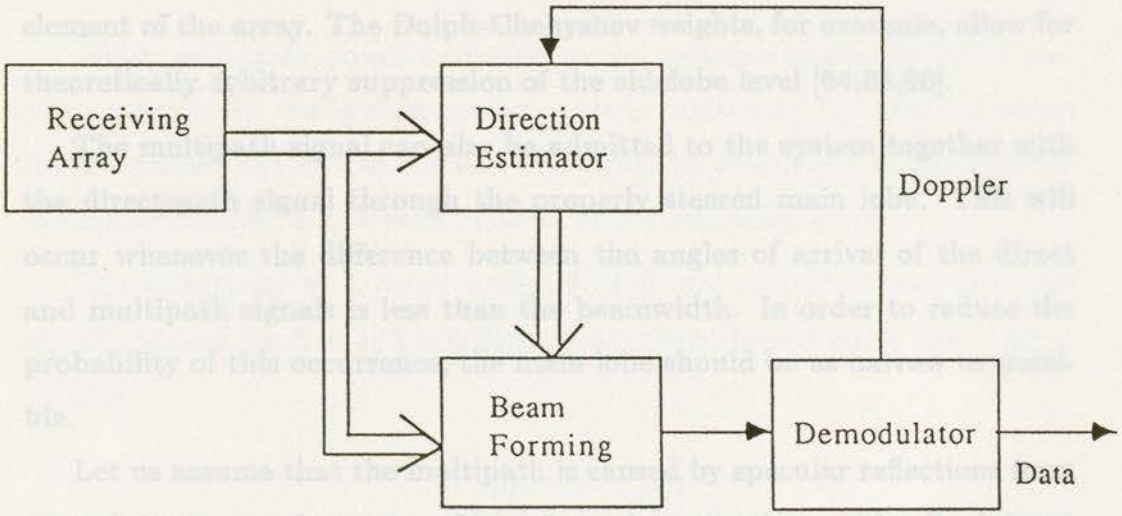

Figure 5.1: Functional block diagram of the receiver

will consider in some detail system performance and various aspects of system implementation. In particular we will compare the performance of a system utilizing a search type receiving beam as formed by a square planar steerable array with that utilizing an umbrella-type beam as formed by a linear array.

5.3 System Performance

5.3.1 Multipath Suppression

The multipath signals can be admitted to the receiver through the main lobe beam or through the sidelobes of the radiation pattern. Sidelobe

levels can be controlled by proper weighting coefficients applied to each element of the array. The Dolph-Chebyshev weights, for example, allow for theoretically arbitrary suppression of the sidelobe level [64,65,66].

The multipath signal can also be admitted to the system together with the direct-path signal through the properly steered main lobe. This will occur whenever the difference between the angles of arrival of the direct and multipath signals is less than the beamwidth. In order to reduce the probability of this occurrence, the main lobe should be as narrow as possible.

Let us assume that the multipath is caused by specular reflections from smooth bottom and ocean surfaces. In such a situation, angles Ω_P (planar array) and Ω_L (linear array) indicated in Figure 3.2 b) and 3.2 c) provide a measure of array ability to reject multipath signals which might otherwise be admitted through the main lobe — the smaller the angle, the better ability to reject multipath.

Shown in Figure 3.3 is the ratio Ω_P/Ω_L vs. the pointing angle (off vertical) for steered arrays employing the same number of elements N separated by a half wavelength. A 3dB beamwidth has been assumed for calculations. It can be seen that the linear array has a greater capacity of multipath suppression than the planar array for practically all ranges of pointing angles and array sizes. The above findings also apply in the case of rough scattering surfaces as discussed in Chapter 3 [75].

5.3.2 Ambient Noise Suppression

With multipath power admitted to the system suppressed below ambient noise level, the system performance is limited by the ambient noise. In the presence of isotropic noise, the signal-to-noise ratio at the receiver is directly related to the directivity D of the receiving array.

The directivity of a linear array of N (even) nondirectional elements equally spaced by $\Delta = \lambda/2$ is independent of the steered angle and is given by [71]

$$D = 2\left(\sum_{n=1}^{N/2} a_n\right)^2 \Big/ \sum_{n=1}^{N/2} a_n^2 \tag{5.1}$$

For an array with an odd number of elements, a modified formula applies

$$D = \left(a_o + 2\sum_{n=1}^{(N-1)/2} a_n\right)^2 \Big/ \left(a_0^2 + 2\sum_{n=1}^{(N-1)/2} a_n^2\right) \tag{5.2}$$

In Eq.(5.1) and (5.2), weighting coefficients $\{a_i\}$ are used for beam shading.

Since generally a beam broadens when steered, one would expect that the directivity should depend on steering angle. However, in the case of a linear array, reduction of directivity due to beam broadening is compensated by the decrease in the solid angle embraced by the beam.

Figure 5.2 shows the directivity index $DI = 10\log D$ of Dolph-Chebyshev arrays with different sidelobe suppression levels vs. array size. For comparison, the directivity index of a uniformly weighted array is also

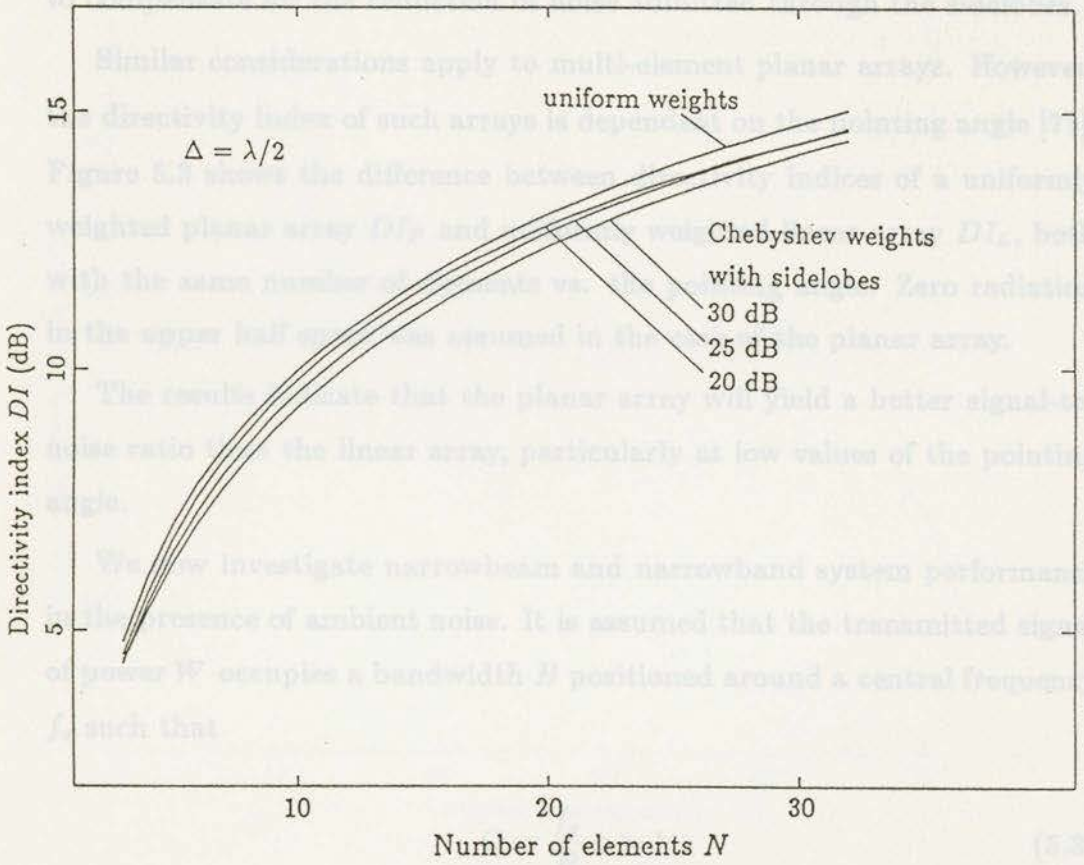

Figure 5.2: Directivity indexes of Dolph-Chebyshev arrays

shown. We observe only a small difference in DI for different sidelobe suppressions. This is due to the broadening of the main beam which tends to compensate for the reduction of noise admitted through the sidelobes.

Similar considerations apply to multi-element planar arrays. However, the directivity index of such arrays is dependent on the pointing angle [71]. Figure 5.3 shows the difference between directivity indices of a uniformly weighted planar array DI_P and uniformly weighted linear array DI_L, both with the same number of elements vs. the pointing angle. Zero radiation in the upper half space was assumed in the case of the planar array.

The results indicate that the planar array will yield a better signal-to-noise ratio than the linear array, particularly at low values of the pointing angle.

We now investigate narrowbeam and narrowband system performance in the presence of ambient noise. It is assumed that the transmitted signal of power W occupies a bandwidth B positioned around a central frequency f_o such that

$$Q = \frac{f_o}{B} >> 1 \tag{5.3}$$

For frequencies above 100kHz omnidirectional thermal noise dominates other sources of ambient noise [2] and this only type of noise will be considered here. A transmitted signal is subject to spherical and absorption losses which increase with the central frequency and the transmission distance. For a given transmission distance h, there is a corresponding central frequency f_0 which yields a required signal-to-noise ratio SNR at the receiver. Shown in Figure 5.4 is the central frequency plotted vs. transmission dis-

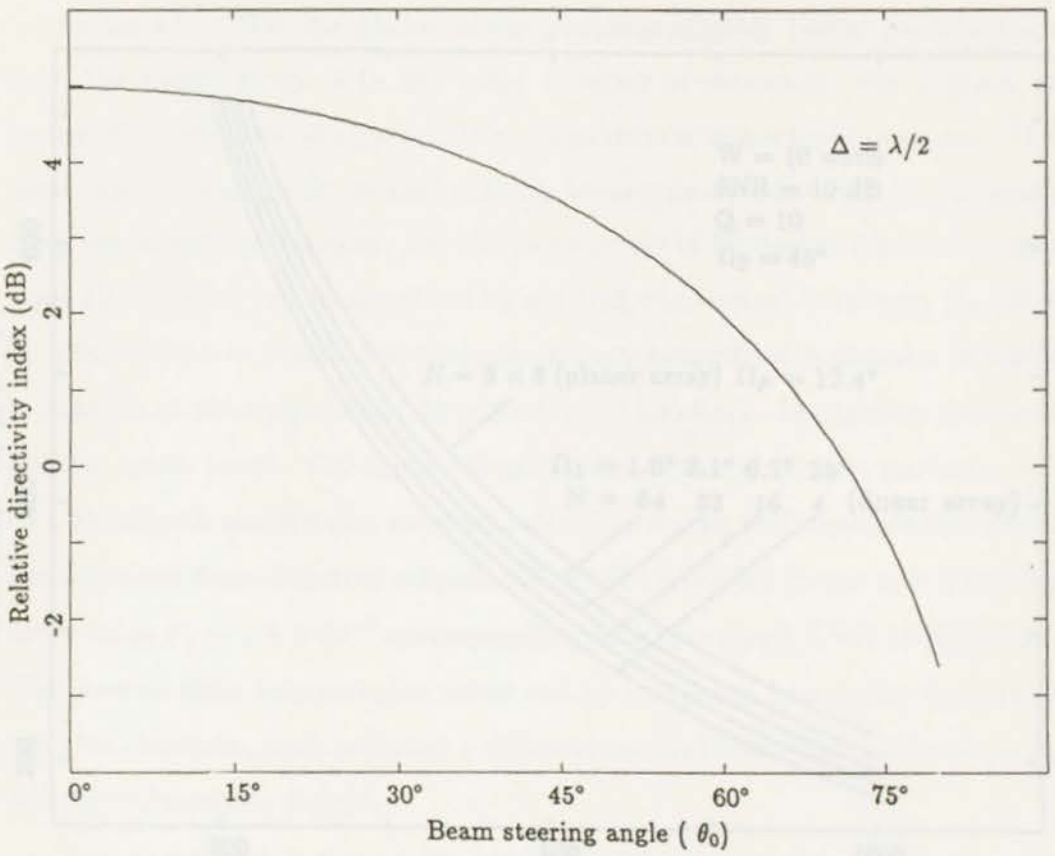

Figure 5.3: Difference between directivity indices of planar and linear arrays

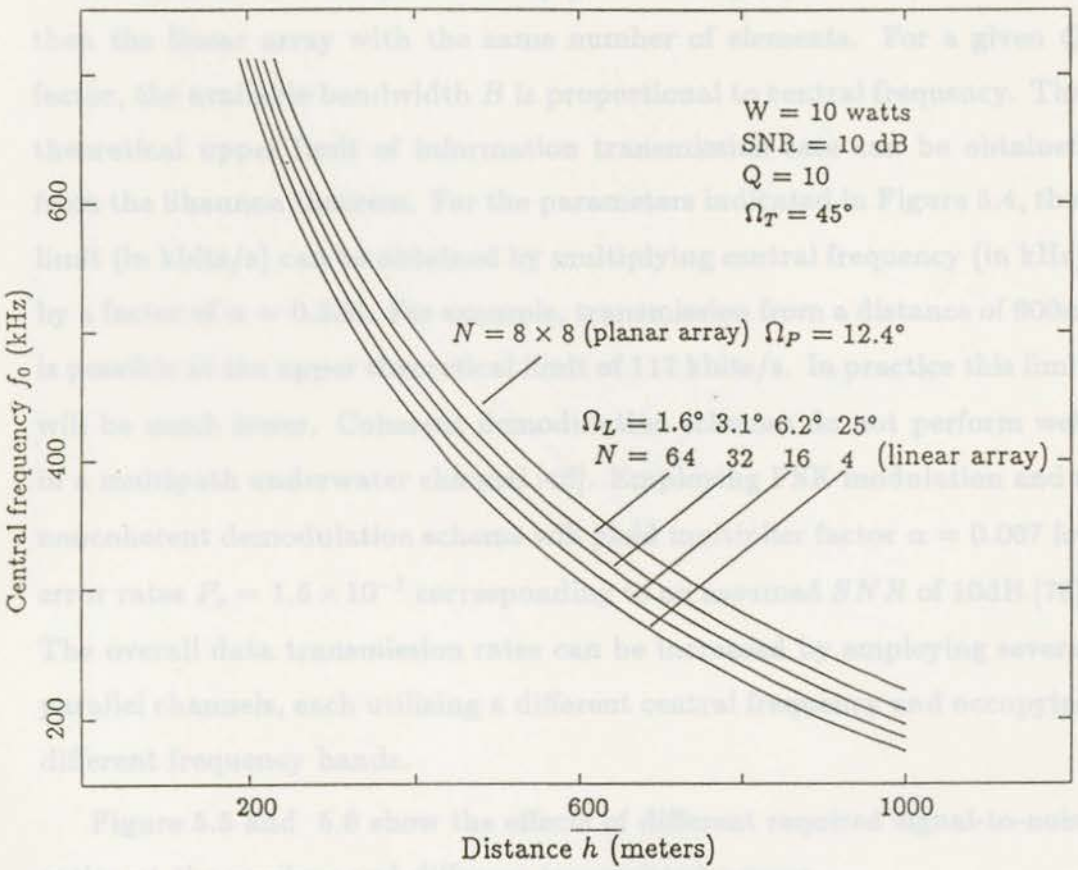

Figure 5.4: Maximum central frequency vs. distance for different arrays

tance for linear and planar arrays of different sizes and the assumed values of transmission parameters.

As noted earlier the planar array provides slightly better performance then the linear array with the same number of elements. For a given Q factor, the available bandwidth B is proportional to central frequency. The theoretical upper limit of information transmission rate can be obtained from the Shannon theorem. For the parameters indicated in Figure 5.4, this limit (in kbits/s) can be obtained by multiplying central frequency (in kHz) by a factor of $\alpha = 0.336$. For example, transmission from a distance of 600m is possible at the upper theoretical limit of 117 kbits/s. In practice this limit will be much lower. Coherent demodulation schemes do not perform well in a multipath underwater channel [46]. Employing FSK modulation and a noncoherent demodulation scheme will yield multiplier factor $\alpha = 0.067$ for error rates $P_e = 1.5 \times 10^{-7}$ corresponding to an assumed SNR of 10dB [76]. The overall data transmission rates can be increased by employing several parallel channels, each utilizing a different central frequency and occupying different frequency bands.

Figure 5.5 and 5.6 show the effects of different required signal-to-noise ratios at the receiver and different transmitted powers.

In Figure 5.7 the effects of different transmitting beamwidths are presented. It is worthwhile to note that central frequency is not critically dependent on transmitting beamwidth. For this reason, a relatively broad transmission beam is suggested as shown in Figure 3.2 c).

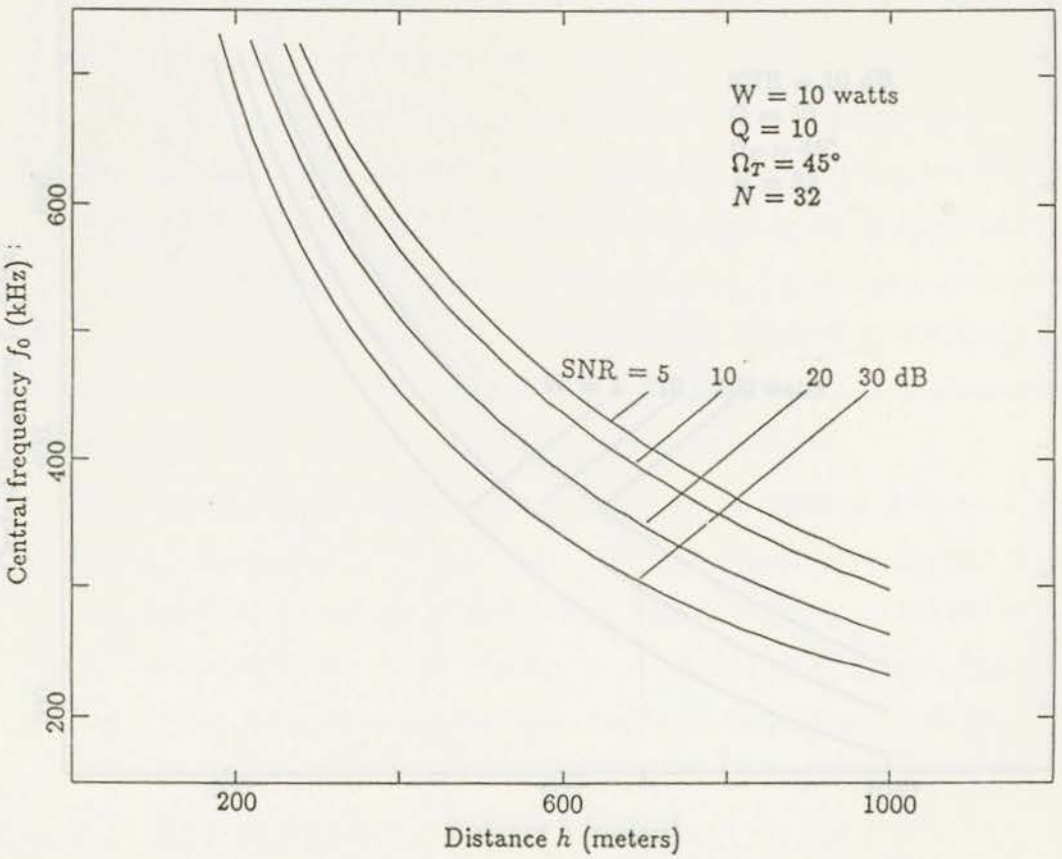

Figure 5.5: Maximum central frequency vs. distance for different signal-to-noise ratios

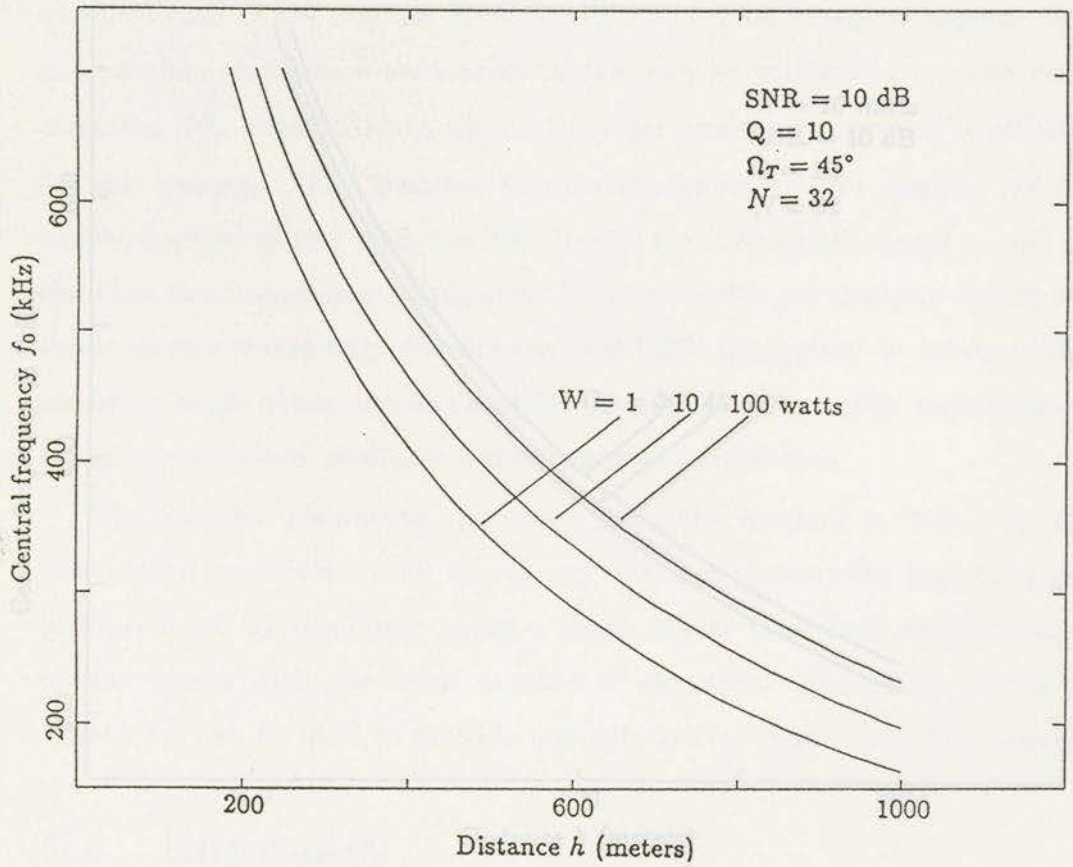

Figure 5.6: Maximum central frequency vs. distance for different transmitted powers

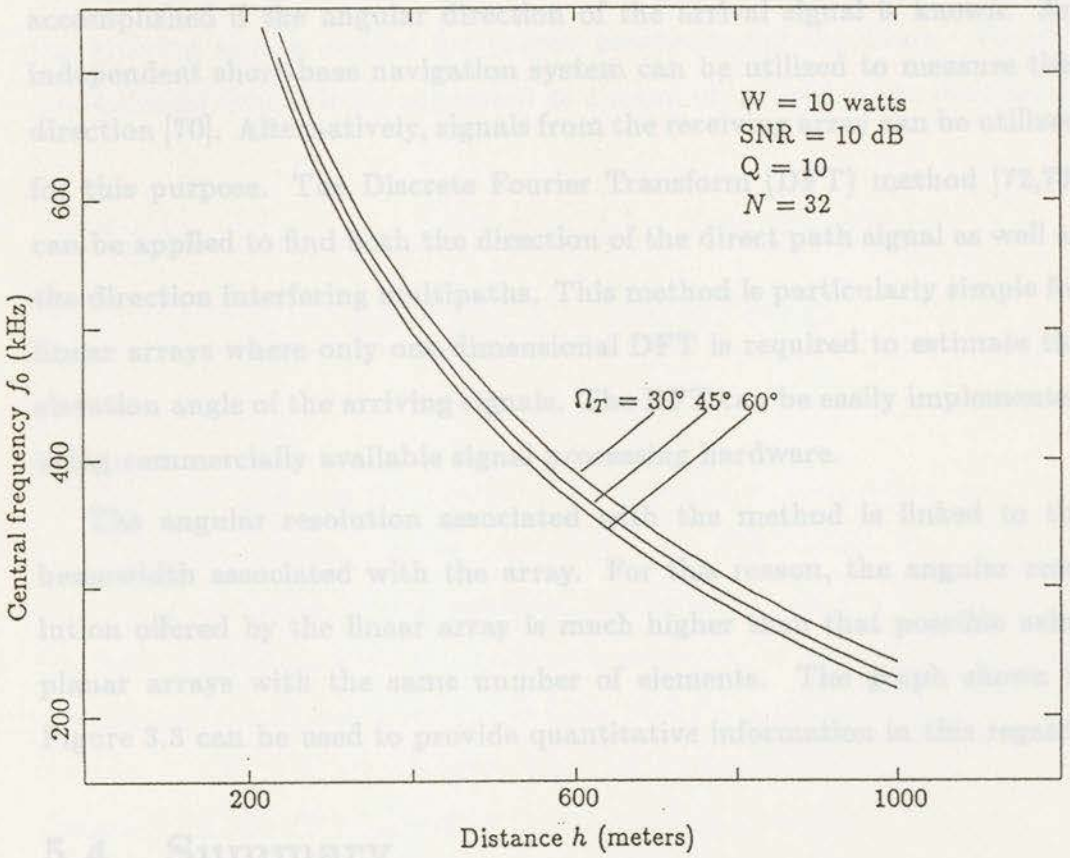

Figure 5.7: Maximum central frequency vs. distance for different transmitting beamwidths

5.3.3 Direction Finding

Steering of the narrow receiving beam towards the transmitter can be accomplished if the angular direction of the arrival signal is known. An independent short-base navigation system can be utilized to measure this direction [70]. Alternatively, signals from the receiving array can be utilized for this purpose. The Discrete Fourier Transform (DFT) method [72,73] can be applied to find both the direction of the direct path signal as well as the direction interfering multipaths. This method is particularly simple for linear arrays where only one-dimensional DFT is required to estimate the elevation angle of the arriving signals. The DFT can be easily implemented using commercially available signal processing hardware.

The angular resolution associated with the method is linked to the beamwidth associated with the array. For this reason, the angular resolution offered by the linear array is much higher than that possible using planar arrays with the same number of elements. The graph shown in Figure 3.3 can be used to provide quantitative information in this regard.

5.4 Summary

A high capacity acoustic communication link suitable for transmitting data from bottom instrumentation to the surface receiver is feasible using a fixed, broad transmitting beam and a steerable, narrow receiving beam. A vertically suspended linear array is suggested to generate an umbrella-type narrow beam which offers superior performance in rejecting multipath interference. Because of a high directivity index associated with such an

array, a longer transmission range is possible in comparison with broad-beam systems with the same transmitted powers. The receiving array can be conveniently utilized to estimate the angular direction (elevation) at the arriving signals needed for proper positioning of the beam. Parallel transmission channels are suggested as a mean of increasing the data rates.

Chapter 6

High Rate Digital Acoustic Communication System

This chapter presents the design and performance description of a High Rate Digital Acoustic Communication System (HRDACS). The system is to be used to transmit broadband signal in shallow water environment. An incoherent data transmission system is employed to overcome multipath. Multibeam transmission technique and the FFT algorithm are applied to achieve a high data transmission rate. Noncoherent binary FSK (BFSK) detected by the FFT algorithm has number of advantages. In summary, we may state the following: 1. The Doppler shift of the received signals are effectively removed by adjusting the sampling instants in the frequency domain. 2. The multiband signals are detected simultaneously in one FFT operation cycle. 3. The channel cross talk interferences can be easily reduced by weighting samples in time domain.

In this chapter, a High Rate Digital Acoustic Communication System (HRDACS) is proposed. The system is to be used to transmit broad band

signal , such as slow-san TV in shallow water environment. To a achieve high data rate, a multibeam transmission technique and the FFT algorithm are used. The system design and performance description of HRDACS is presented.

6.1 System Design

A functional block diagram of the receiver is shown in Figure 6.1. The up-link signal is received by a receiving array. The output signals from the receiving array elements are used to estimate the angles of arrival of the direct-path signal as well as the interfering multipath. Based on these estimates a beam pattern can be suitably modified to reject some of the multipath signals. A signal received by such a beam is then demodulated to yield the desired data. Doppler shift information can be utilized to improve the estimate of the angle of arrival.

The HRDACS is an incoherent binary shift keying (BFSK) system. It accepts digital input, performs a selected coding operation, and modulates the coded word onto a set of sinusoids. The selected sinusoids are transmitted for a duration T_b , which determines the data transmission rate.

At the receiver, the data is demodulated using the FFT algorithm. The FFT outputs are supplied to the root squarer and then sampled at $f = f_i$ in the frequency domain. A decision regarding data transmitted is made by comparison of their sampled values.

The HRDACS is designed for incoherent data transmission over a fading channel. Such channel may be considered as composed of many signal scatterers, each of which contributes a delayed and Doppler shifted signal

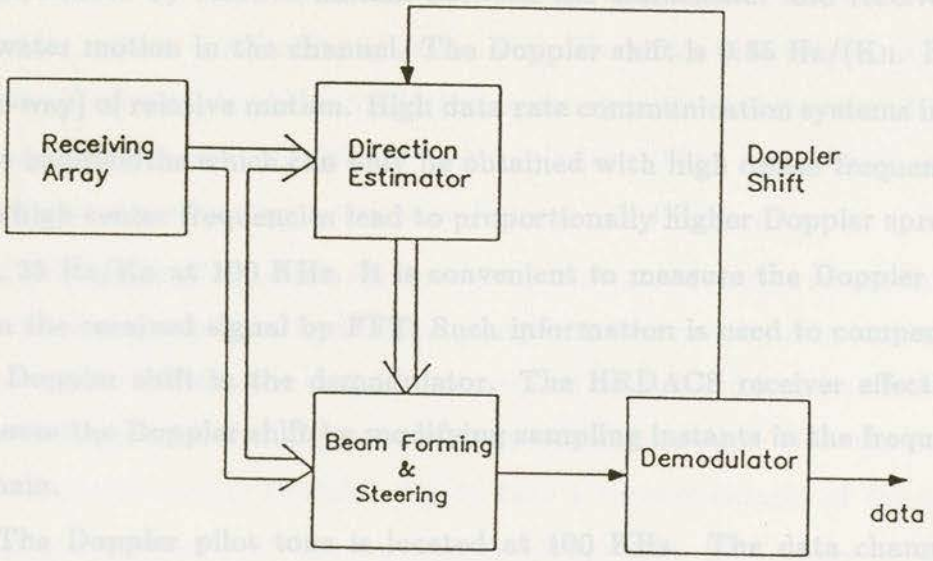

Figure 6.1: Functional block diagram of the receiver

replica to the received waveform. In shallow water environment, scattering is due to the sea surface and sea bottom. It can be shown that by applying sidelobe suppression, the dominant scattered wave is the second multipath which is the sea bottom reflecting wave scattered from sea surface [75].

The delay τ between direct path and the second multipath is dependent of the steering angle of receiving beam and the depth of ocean. If such multipath prove to be a problem they can be "blanked" (i.e, suppressed), just as interfering spikes are blanked by noise-blanking circuits in radio communications receivers. This blanking process will decrease the data transmission rate by half, and the maximum transmitted data block length equals τ .

Another constraint in acoustic communication is Doppler spreading which is introduced by relative motion between the transmitter and receiver or by water motion in the channel. The Doppler shift is 0.35 Hz/(Kn. KHz) (one-way) of relative motion. High data rate communication systems imply wide bandwidths which can only be obtained with high center frequencies. The high center frequencies lead to proportionally higher Doppler spreads, e.g., 35 Hz/Kn at 100 KHz. It is convenient to measure the Doppler shift from the received signal by FFT. Such information is used to compensate the Doppler shift in the demodulator. The HRDACS receiver effectively removes the Doppler shift by modifying sampling instants in the frequency domain.

The Doppler pilot tone is located at 100 KHz. The data channel is demodulated by a FFT started from the Doppler pilot tone. The sampling and detection are implemented in software, and easily changed. The system throughput is enhanced by software and hardware provisions for several FFT's to execute in parallel.

Ambient noise influences the signal-to-noise ratio which ultimately constrains the data transmission rate versus reliability trade off. Ambient noise has been found to have a Gaussian amplitude distribution at moderate depths [2]. Based on this fact, we assume the channel has a white additive Gaussian noise.

6.2 Broadband Consideration

A more significant constraint on an acoustic communication system is the narrow transmission bandwidth of the projector. The quality factor Q

of the projector generally ranges from 10 to 100 for a realistic operating frequency. A 50 KHz bandwidth transmission requires carrier frequency of 500 KHz, which is difficulty to realize [77]. Therefore the number of independent channels should be used, that is, the individual narrow bandwidth beam should be transmitted by each projector. Thus a technique called Multiband Acoustic Communication System (MACS) is adopted.

The concept of MACS is illustrated by the block diagram shown in Figure 6.2. The input broadband message signal is first restricted in bandwidth by a low-pass filter, the outputs are applied to a decommutator which is usually implemented using electronic switching circuity. The function of the decommutator is twofold: (1) to take a narrow sample of the input message at a rate $1/T_s$ that is slightly higher than $2W$, where W is the cutoff frequency of the lowpass input filter, and (2) sequentially interleave these samples to N individual channels. Indeed, this latter function is the essence of the time-division demultiplexing (TDDM) operation. Following the decommutation process, the multiplexed signals are applied to N pulse modulators. It is clear that the use of time-division demultiplexing introduces a bandwidth compression factor N, because the scheme expends samples from N into 1 at each time slot.

At the receiving end of the system, the multiband signal is received by a broadband array. The received signals are then applied to N individual pulse demodulators which perform the reverse operation of the pulse modulation. For BFSK incoherent data transmission, a FFT demodulator is used instead of N individual pulse demodulators, which perform the reverse operation in the frequency domain. A possible frequency allocation

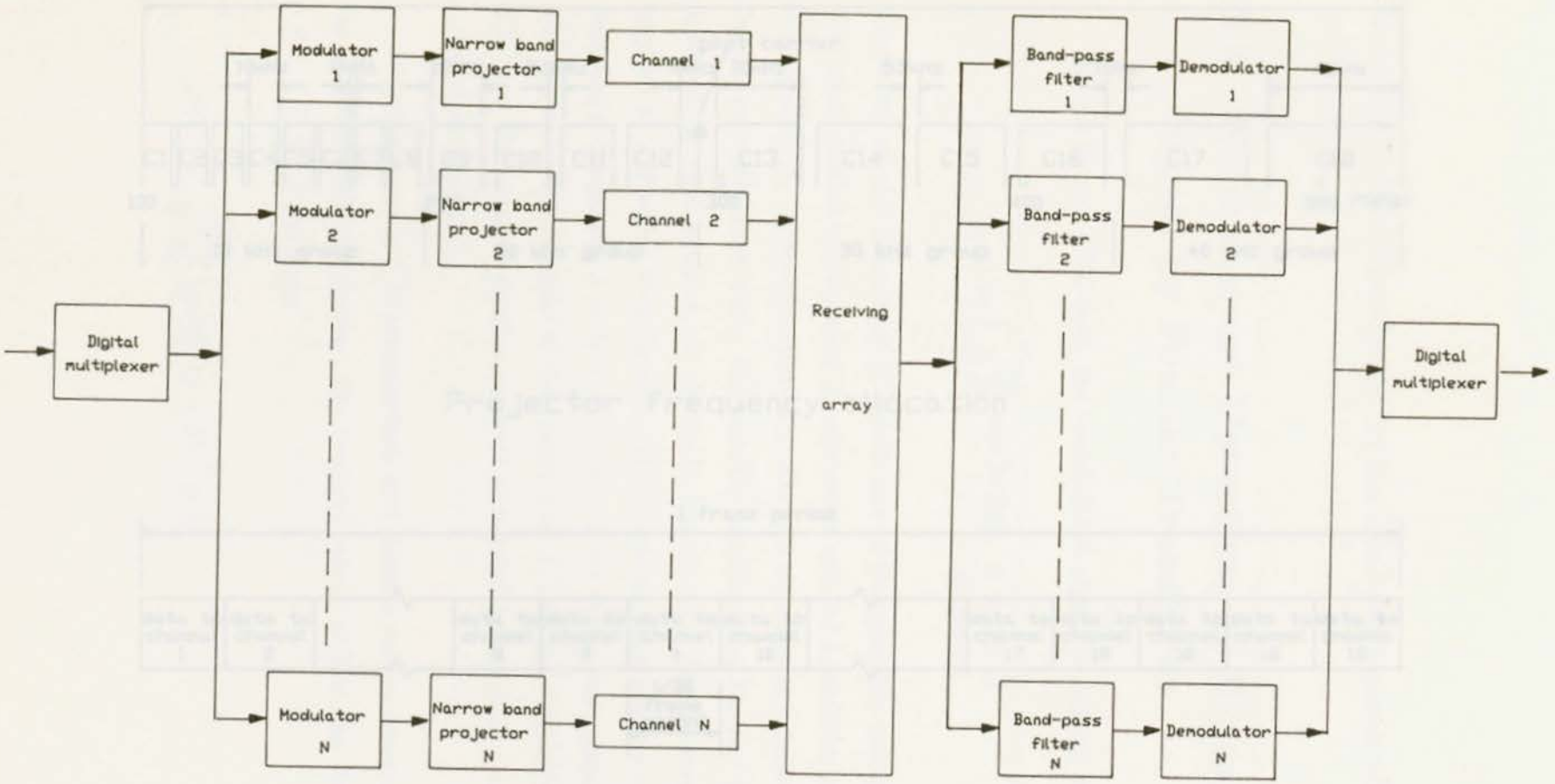

Figure 6.2: Block diagram of multiband acoustic communication system

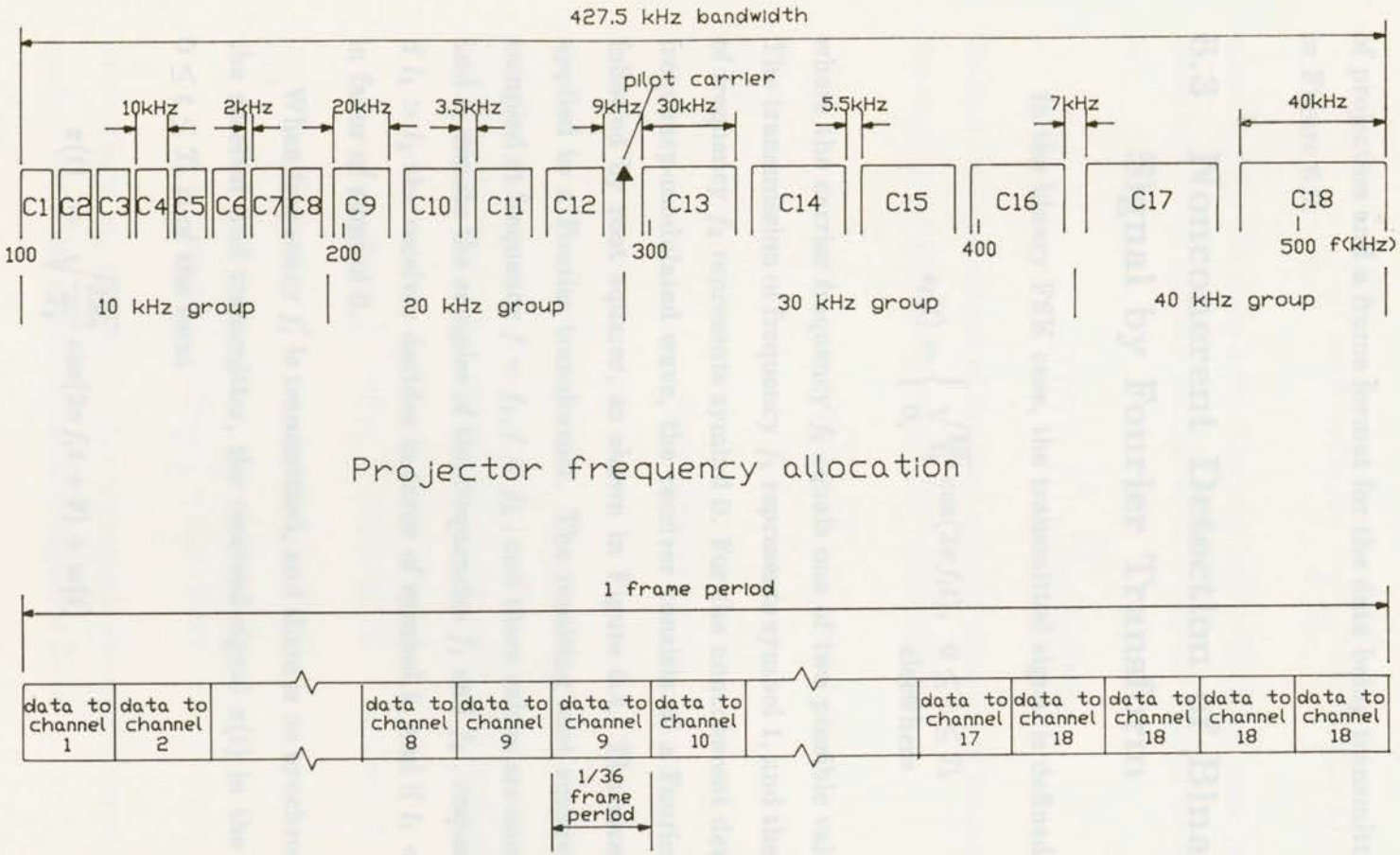

Figure 6.3: Frequency allocation and data format

of projectors and a frame format for the data being transmitted are shown in Figure 6.3.

6.3 Noncoherent Detection of Binary FSK Signal by Fourier Transform

In the binary FSK case, the transmitted signal is defined by [76]

$$s_i(t) = \begin{cases} \sqrt{\frac{2E_b}{T_b}}\cos(2\pi f_i t), & 0 \le t \le T_b \\ 0, & \text{elsewhere} \end{cases} \tag{6.1}$$

where the carrier frequency f_i equals one of two possible values f_1 and f_2 The transmission of frequency f_1 represents symbol 1, and the transmission of frequency f_2 represents symbol 0. For the noncoherent detection of this frequency-modulated wave, the receiver consists of a Fourier transformer followed by root squarer, as shown in Figure 6.4. The received signal is applied to a Fourier transformer. The resulting root squarer outputs are sampled at frequency $f = f_1, f = f_2$, and there values are compared. Let l_1 and l_2 denote the samples of the frequencies f_1 and f_2 , respectively. Then, if $l_1 > l_2$ the receiver decides in favor of symbol 1, and if $l_1 < l_2$ it decides in favor of symbol 0.

When frequency f_i' is transmitted, and there is no synchronism between the receiver and transmitter, the received signal $x(t)$ in the time interval $0 \le t \le T_b$ is of the form

$$x(t) = \sqrt{\frac{2E_b}{T_b}}\cos(2\pi f_i t + \theta) + w(t)$$

$$= \sqrt{\frac{2E_b}{T_b}}\cos\theta\cos(2\pi f_i t) - \sqrt{\frac{2E_b}{T_b}}\sin\theta\sin(2\pi f_i t) + w(t) \quad (6.2)$$

where $w(t)$ is the sample function of a white Gaussian noise process of zero mean and power spectral density $N_0/2$. With the Fourier transform defined as

$$X(f) = \int_{-\infty}^{\infty} \sqrt{\frac{2}{T_b}} x(t) e^{j2\pi ft} dt \quad (6.3)$$

we find that the output of the root squarer sampled at frequency $f = f_i$ in the receiver of Figure 6.4 equals (see Appendix A)

$$l_i = \sqrt{x_{ci}^2 + x_{si}^2} \qquad i = 1, 2 \quad (6.4)$$

where

$$x_{ci} = \sqrt{E_b}\cos\theta + w_{ci} \quad (6.5)$$

and

$$x_{si} = -\sqrt{E_b}\sin\theta + w_{si} \quad (6.6)$$

The w_{ci} and $w_{si}, i = 1, 2$ are related to the noise $w(t)$ as follows:

$$w_{ci} = \int_0^{T_b} w(t)\sqrt{\frac{2}{T_b}}\cos(2\pi f_i t)dt \qquad i = 1, 2 \quad (6.7)$$

and

$$w_{si} = \int_0^{T_b} w(t)\sqrt{\frac{2}{T_b}}\sin(2\pi f_i t)dt \qquad i = 1, 2 \quad (6.8)$$

Accordingly, w_{ci} and $w_{si}, i = 1, 2$ are sample values of independent Gaussian random variables of zero mean and variance $N_0/2$.

The above results are the same as the receiver which consists of a pair of matched filters followed by an envelope detector, shown in [76]. Therefore, we find that the average probability of symbol error for the noncoherent binary FSK detected by Fourier transform is given by

$$P_e = \frac{1}{2}\exp(-\frac{E_b}{2N_0}) \tag{6.9}$$

6.4 Implementation of Fourier Transform by Discrete Fourier Transform

When Discrete Fourier Transform (DFF) is applied to implement Fourier transform, integrating noise is produced in the receiver by approximating the continuous integration to a uniform step summation. We assume the step size is not infinitly small(i.e, finite samples), so that the orthonormal characteristics of basis function does not hold as integration is replaced by DFT summation.

Consider a DFT operation defined as

$$X(K) = \frac{T_b}{N}\sqrt{\frac{2}{T_b}}\sum_{n=0}^{N-1} x(n)e^{\frac{j2\pi Kn}{N}} \tag{6.10}$$

Therefore

$$\begin{aligned} X(f_i) &= \int_0^{T_b} x(t)\sqrt{\frac{2}{T_b}}e^{j2\pi f_i t}dt \\ &\approx \frac{T_b}{N}\sqrt{\frac{2}{T_b}}\sum_{n=0}^{N-1} x(n)e^{\frac{j2\pi K_i n}{N}} \end{aligned}$$

$$= \frac{\sqrt{2T_b}}{N}[\sum_{n=0}^{N-1} x(n)\cos(\frac{j2\pi K_i n}{N})$$

$$+[\sum_{n=0}^{N-1} x(n)\sin(\frac{j2\pi K_i n}{N})] \tag{6.11}$$

where $K_i = f_i T_b$

The orthonormal condition of the basis function becomes

$$\int_0^{T_b} \phi_i(t)\phi_j(t)dt \approx \sum_{n=0}^{N-1} \frac{T_b}{N}\phi_i(n)\phi_j(n)$$

$$= \begin{cases} 1 \pm \sigma^+_{cij}, & i = j \\ \sigma^+_{bij} \pm \sigma^-_{bij}, & i \neq j \end{cases} \tag{6.12}$$

where

$$\sigma^{\pm}_{bij} = \sigma^{\pm}_{bij}(N, k_i \pm K_j) \tag{6.13}$$

and the subscript $b \in \{s, c\}$ for abbreviation of sin and cosine basis functions, respectively. Note that k_i is a continuous value and K_j is an integer (bin number of DFT). For example, σ^-_{cij} and σ^-_{sij} are of the form

$$\sigma^-_{cij} = \frac{\sin(\frac{N}{2}\alpha)}{N\sin(\frac{\alpha}{2})}\cos(\frac{N-1}{2}\alpha) \tag{6.14}$$

and

$$\sigma^-_{sij} = \frac{\sin(\frac{N}{2}\alpha)}{N\sin(\frac{\alpha}{2})}\sin(\frac{N-1}{2}\alpha) \tag{6.15}$$

where

$$\alpha = \frac{2\pi(k_i - K_j)}{N} \tag{6.16}$$

The upper bound of σ_{cij}^{-} versus α with $N = 64$ is shown in Figure 6.5.

With the DFT having the form shown in Eq.(6.10), we find that the output of root squarer sampled at $f = f_i$ equals

$$l_i = \sqrt{x_{ci}^2 + x_{si}^2} \qquad i = 1, 2 \tag{6.17}$$

where

$$x_{ci} = \sqrt{E_b}\cos\theta(\sigma_{cij}^{+} + \sigma_{cij}^{-}) - \sqrt{E_b}\sin\theta(\sigma_{sij}^{+} + \sigma_{sij}^{-}) + w_{ci} \tag{6.18}$$

and

$$x_{ci} = \sqrt{E_b}\cos\theta(\sigma_{sij}^{+} + \sigma_{sij}^{-}) - \sqrt{E_b}\sin\theta(-\sigma_{cij}^{+} + \sigma_{cij}^{-}) + w_{si} \tag{6.19}$$

It can be shown(see Appendix B) that w_{ci} and $w_{si}, i = 1, 2$, are sample values of independent Gaussian random variables of zero mean and variance $N_0/2(1 \pm \sigma_{cij}^{+})$.

The error term $\sigma_{bij}^{\pm}$ becomes maximum at $\alpha = 0$. It decreases rapidly when $|\alpha| > 2\pi/N$ (i.e. $|k_i - K_j| > 1$). The condition also illustrates the minimum tone spacing in the frequency domain. In order to suppress the sidelobe, we can apply the window technique rather than a uniform shading. Figure 6.6 and Figure 6.7 show the channel cross talk of two tones due to the sidelobe with uniform and Dolph-Chebyshev shading, respectively. It can be seen that we can ignore all the σ_{bij}^{+} terms (including σ_{sij}^{-} , if K_j does not close to k_i) in Eq.(6.18) and(6.19) since

$$\sigma_{bij}^{+} = 0.01 \ll 1 \qquad \text{(40dB sidelobe suppression)} \tag{6.20}$$

On the other hand, the term σ_{sij}^{-} is vanished when K_j approaches to k_i since

$$\begin{aligned} \sigma_{sij}^{-} &= \lim_{\alpha \to 0} \frac{\sin(\frac{N}{2}\alpha)}{N \sin(\frac{\alpha}{2})} \sin(\frac{N-1}{2}\alpha) \\ &= 0 \end{aligned} \tag{6.21}$$

Similarly, we find that the average probability of symbol error for the noncoherent BFSK detected by DFT equals

$$P_e = \frac{1}{2} \exp(-\frac{E_b(\sigma_{cij}^{-})^2}{2N_0}) \tag{6.22}$$

The degradation factor $(\sigma_{cij}^{-})^2$ varies with the frequency f_i of the received signal which was shifted by Doppler effect. The maximum value of $|k_i - K_j|$ which corresponds to the minimum value of σ_{cij}^{-} is equal to $1/2$. The error performance increases with a decreasing of $|K_j - k_i|$. Therefore, a process called zero padding is employed which will improve the degradation significantly. If we pad N zero samples, then the maximum value of $|k_i - K_j|$ approximates to $1/4$. Thus we obtain the upper bound of the average probability of symbol error P_e , which is shown in Figure 6.8.

The lower bound is indicated by Eq.(6.9) as $k_i \to K_j$ and $N \to \infty$ which is identical with noncoherent binary FSK detected by a matched filter. The gap between the lower and upper bounds is described by Eq.(6.14) which is plotted as a function of N in Figure 6.9.

6.5 Summary

A high data transmission rate acoustic communication system can be relatively easily implemented using multibeam transmission technique and a broad band receiving array. A noncoherent BFSK data transmission scheme is employed and a FFT algorithm is suggested to implement for both direction finding and demodulation. The system can be used to derive information from sea bottom in shallow water environment.

Noncoherent binary FSK detected by FFT algorithm has a number of advantages. In summary, we may state the following:

1. The Doppler shift of the received signals are effectively removed by adjusting the sampling instants in the frequency domain.

2. The multiband signals are detected simultaneously in one FFT operation cycle.

3. The channel cross talk interferences can be easily reduced by weighting samples in time domain.

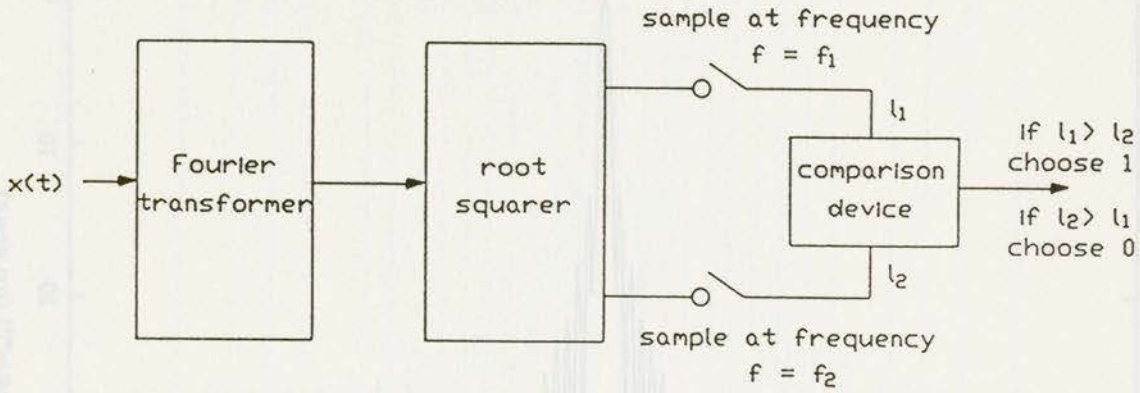

Figure 6.4: Noncoherent receiver for the detection of binary FSK signals by Fourier transform

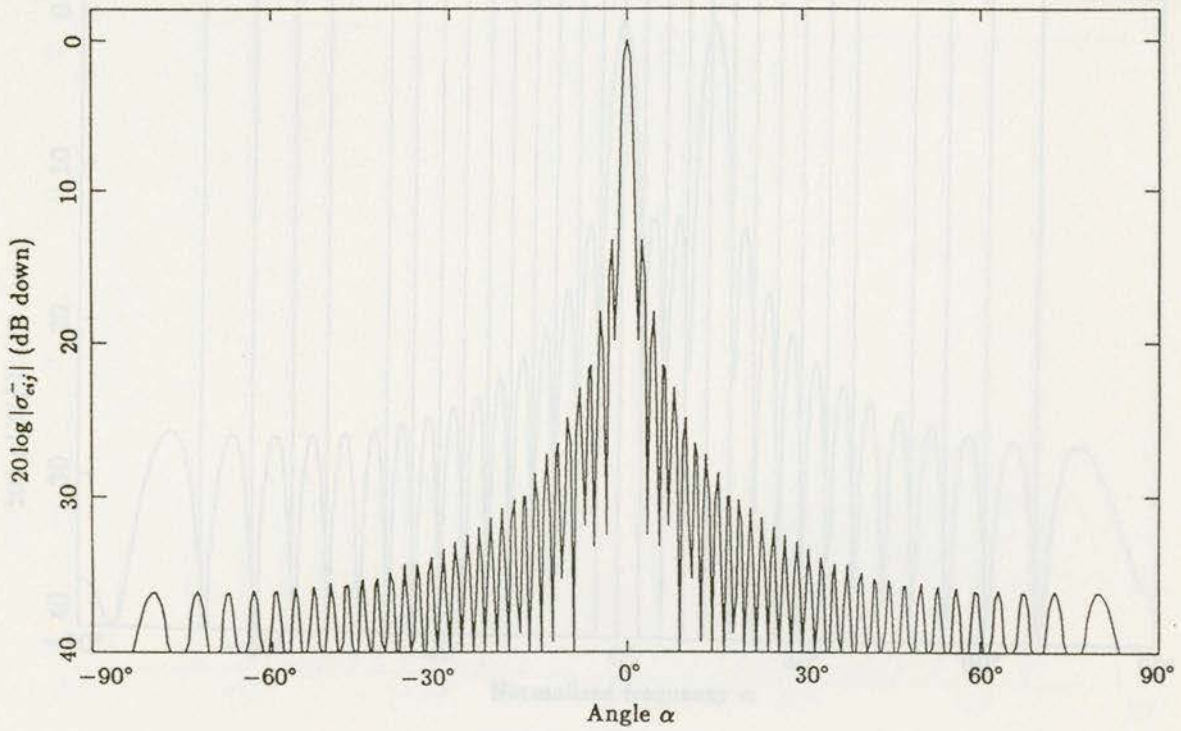

Figure 6.5: Upper bound of $\sigma_{\bar{c}ij}^{-}$ versus α with $N = 64$

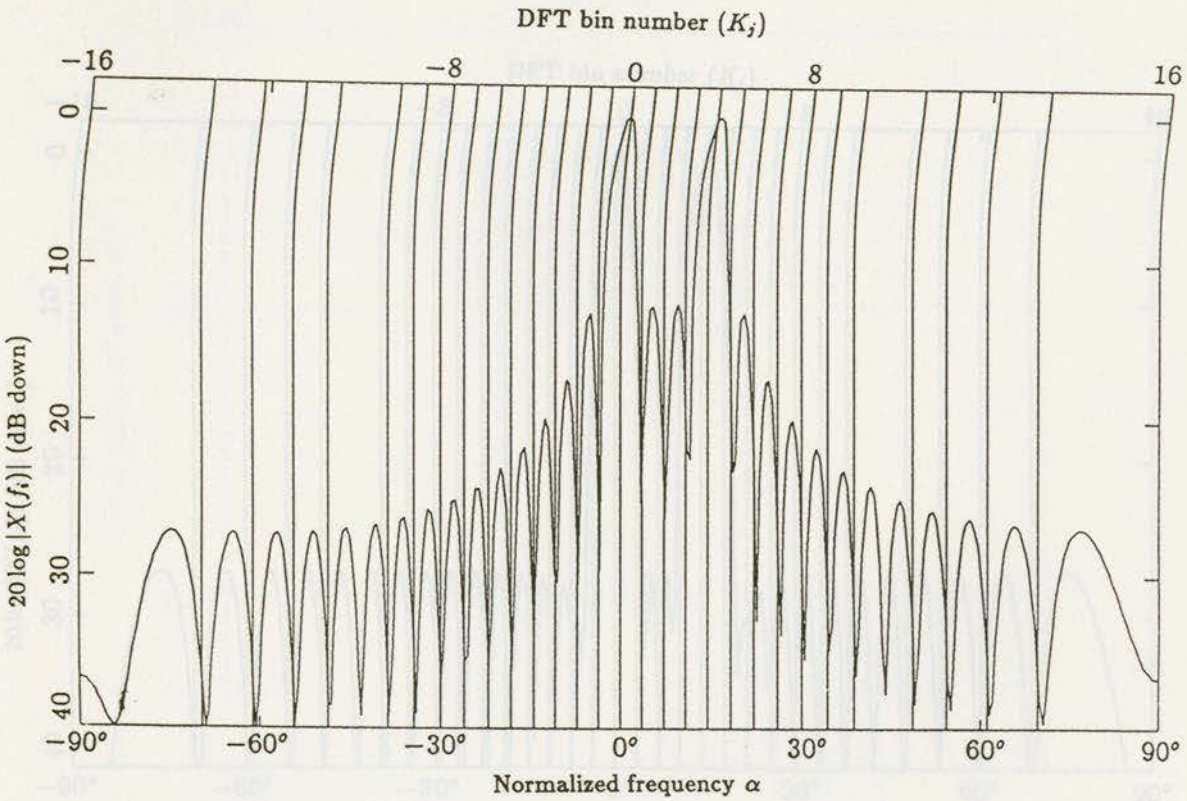

Figure 6.6: Channel cross talk interference of uniform shading

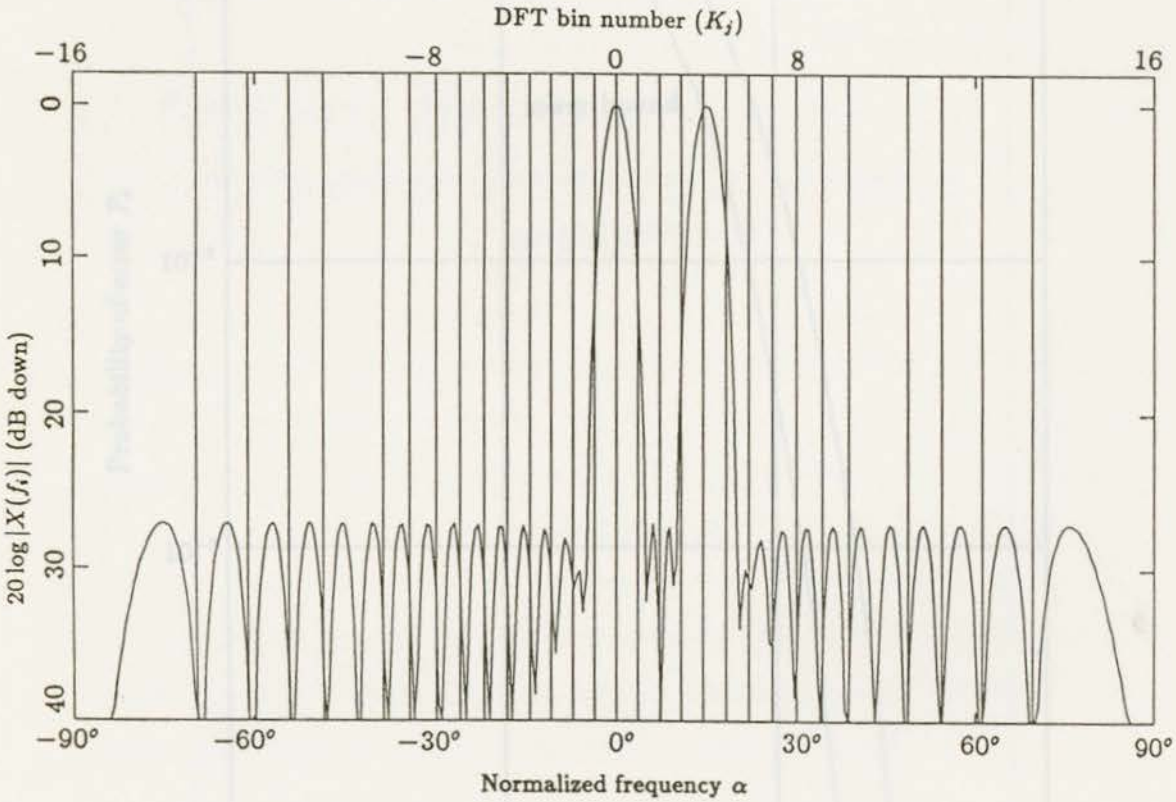

Figure 6.7: Channel cross talk interference of Dolph-Chebyshev shading

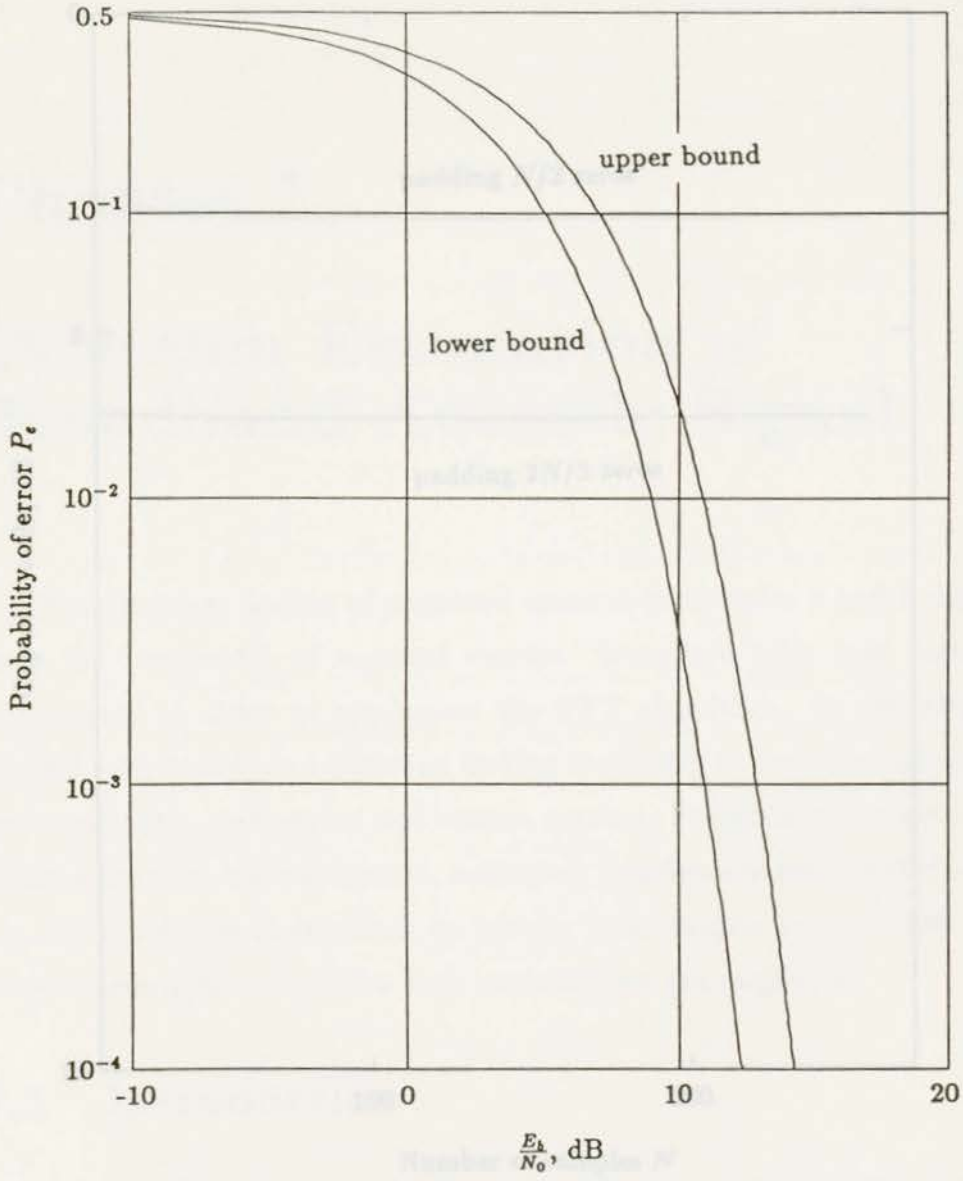

Figure 6.8: Noise performance of a noncoherent BFSK system detected by FFT

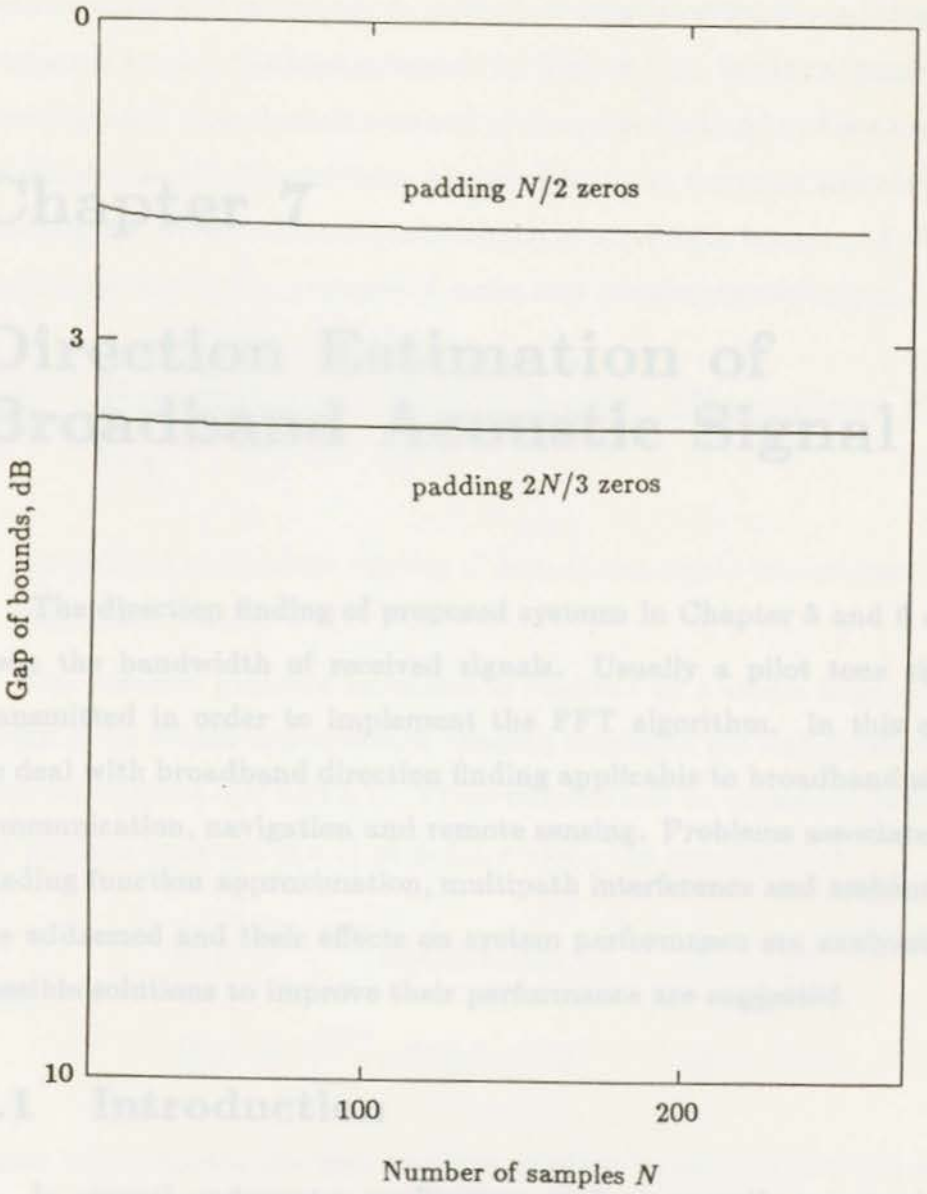

Figure 6.9: Comparison of the gap between lower and upper bound of different number of samples

Chapter 7

Direction Estimation of Broadband Acoustic Signal

The direction finding of proposed systems in Chapter 5 and 6 depend upon the bandwidth of received signals. Usually a pilot tone signal is transmitted in order to implement the FFT algorithm. In this chapter we deal with broadband direction finding applicable to broadband acoustic communication, navigation and remote sensing. Problems associated with shading function approximation, multipath interference and ambient noise are addressed and their effects on system performance are analysed. The possible solutions to improve their performance are suggested.

7.1 Introduction

In several underwater applications such as acoustic communication, navigation and remote sensing it is necessary to find the angular direction of an incident waveform [10,72,77]. For narrowband acoustic signals the direction of signal arrival can be determined by sequential or parallel

beamforming and scanning. A method of paralleled beam scanning in the frequency domain has been proposed by Rudnik [73]. For broadband continuous signals a time-domain method of direction finding has been suggested by Henderson [78,79] and later extended to finite duration signals [80]. In this chapter we will discuss performance of a realistic broadband direction finding system in the presence of noise and interfering multipath.

7.2 Principle of Broadband Direction Finding

A method of direction finding of broadband signal was proposed by T. L. Henderson [79,80].

The acoustic pressure waveform is received by a single linear array of length L on which two aperture shading functions are impressed to form separate outputs $a(t)$ and $b(t)$. These outputs can be expressed in terms of the acoustic pressure $p(x,t)$ at point x along the array axis as

$$a(t) = \int_{-\infty}^{+\infty} w(x)p(x,t)dx, \qquad |x| \leq L/2 \tag{7.1}$$

$$b(t) = \int_{-\infty}^{+\infty} w'(x)p(x,t)dx, \qquad |x| \leq L/2 \tag{7.2}$$

where $w(x)$ denotes the first aperture shading function, and $w'(x)$ denotes the second shading function, which is specified to be the derivative of the first. As has been established in [79] and [80], the use of aperture shading functions that are matched in this particular way makes it possible to determine the direction of an incident plane wave of arbitrary spectrum,

without any spectral decomposition or multibeam scanning.

The principle of direction finding is quite simple. If the pressure field on the array axis is produced by a plane wave coming from a distant acoustic source whose direction cosine relative to the positive end of the x axis is denoted as u, (i.e., $u = \cos\theta$) then $p(x,t)$ may be replaced by $p(t + ux/c)$ where $p(t)$ denotes the acoustic pressure at the coordinate origin(i.e., at $x = 0$) and c denotes the speed of sound in the water. With this substitution Eq.(7.2) can be differentiated to yield

$$\begin{aligned} \frac{d}{dt}[a(t)] &= \int_{-\infty}^{+\infty} w(x)\left\{\frac{d}{dt}[p(t+ux/c)]\right\}dx \\ &= cu^{-1}\int_{-\infty}^{+\infty} w(x)\left\{\frac{d}{dx}[p(t+ux/c)]\right\}dx \end{aligned} \tag{7.3}$$

Integrating by parts one obtains, since $w(x)$ goes to zero outside of a finite interval,

$$\frac{d}{dt}[a(t)] = -cu^{-1}b(t) \tag{7.4}$$

where

$$b(t) = \int_{-\infty}^{+\infty} w'(x)p(t+ux/c)dx \tag{7.5}$$

The special relationship between the two aperture shading functions thus yields the following important result: regardless of the spectral content of the incident wave, $b(t)$ is a perfect replica of the derivative of $a(t)$, except for a multiplicative term $-uc^{-1}$, where c is a know constant and u is the

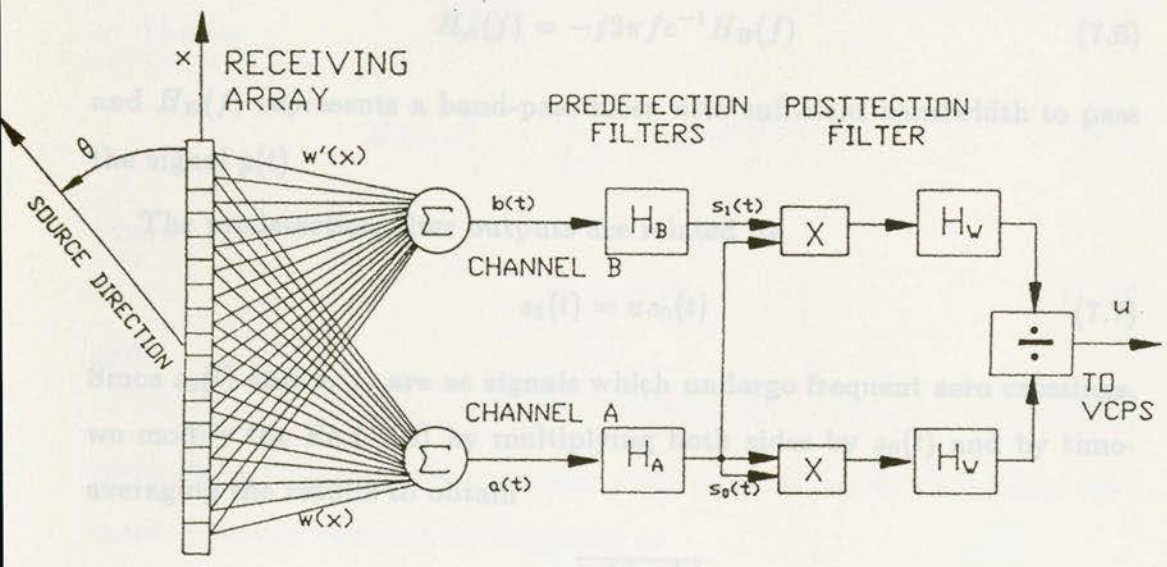

Figure 7.1: A broadband direction finder

direction cosine of the source. The transmitter's direction can thus be inferred from a comparison of $b(t)$ and derivative of $a(t)$, or a comparison of $a(t)$ and the integral of $b(t)$.

For practical purposes an arbitrary shading function can be approximated by using a segmented linear array and by summing up signals from each segment with appropriate weights. The broadband direction finder shown in Figure 7.1 applies to such an array. The approximation error is neglected here and will be discussed later.

The two predetection filters H_A and H_B are applied to suppress noise outside the signal band, and to perform time derivative operation. The

frequency responses of these filters are therefore given by

$$H_A(f) = -j2\pi f c^{-1} H_B(f) \tag{7.6}$$

and $H_B(f)$ represents a band-pass filter with sufficient bandwidth to pass the signal $p(t)$.

The predetection filter outputs are related by

$$s_1(t) = u s_0(t) \tag{7.7}$$

Since $s_0(t)$ and $s_1(t)$ are ac signals which undergo frequent zero crossings, we modify the Eq.(7.6) by multiplying both sides by $s_0(t)$ and by time-averaging the results to obtain

$$u = \frac{\overline{s_1(t)s_0(t)}}{\overline{s_0(t)s_0(t)}} \tag{7.8}$$

The averaging can be performed by low-pass filters H_W as shown in Figure 7.1.

7.3 Approximation in Implementing Shading Functions

As indicated in Figure 7.1, the continuous shading functions $w(x)$ and $w'(x)$ can be implemented using a stepwise approximation. The errors associated with the approximation of $w(x)$ and its derivative are manageable, and have been studied [80], but the analysis was restricted to harmonic waves only(i.e., single frequency). In this section, we shall derive a formulation which can be applied to broadband signals.

Let us define a complex beam response function $D_i(u,\omega)$, which is the system transfer function for input harmonic waves arriving from direction u. That is

$$D_i(u,\omega) = \int_{-\infty}^{+\infty} w_i(x) e^{j\omega(t-ux/c)} dx \tag{7.9}$$

where

$$w_0 = w(x) \tag{7.10}$$

and

$$w_1 = w'(x) \tag{7.11}$$

Using these transform functions the array outputs due to an incident harmonic pressure wave can be expressed as

$$s_i(t) = \mathrm{Re}[D_i(u,\omega) A e^{j\omega t}], \qquad i = 0,1 \tag{7.12}$$

A simple shading function is a triangle weighting given by

$$w(x) = 1 - |2x/L|, \qquad \text{for} |x| < L/2 \tag{7.13}$$

and it's stair-case approximation is given by

$$\hat{w}_0(x) = \hat{w}(x) = 1 - \frac{1}{N}\left(\frac{1}{2} + \left|\frac{2Nx}{L}\right|_{\text{int}}\right) \tag{7.14}$$

where $|x|_{\text{int}}$ denotes the integer part of $|x|$, and L is the aperture length. The corresponding $\hat{w}'(x)$ has unit magnitude along the entire aperture, but with a sign reversal at the center, i.e.,

$$\hat{w}_1(x) = \hat{w}'(x) = \mathrm{sgn}(x), \qquad \text{for} |x| < L/2 \tag{7.15}$$

The beam response functions can be obtained by carrying out the integrations indicated by Eqs. (7.2) and (7.2) using stair-case approximations $\hat{w}(x)$ and $\hat{w}'(x)$, respectively, to obtain

$$\hat{D}_0(u,\omega) = \frac{4c}{NL\omega u}\frac{\sin^2(L\omega u/4c)}{\tan(L\omega u/4Nc)} \tag{7.16}$$

and

$$\hat{D}_1(u,\omega) = \left(\frac{4c}{L\omega}\right)^2 \frac{\sin^2(L\omega u/4c)}{u} \tag{7.17}$$

As before the ratio of $\hat{s_1}(t)/\hat{s_0}(t)$ can be used as an estimate $\hat{u}$ of the cosine direction u, that is

$$\begin{aligned}
\hat{u} &= \frac{\hat{s_1}(t)}{\hat{s_0}(t)} \\
&= \frac{\overline{\hat{s_1}(t)\hat{s_0}(t)}}{\overline{\hat{s_0}(t)\hat{s_0}(t)}} \\
&= \frac{\hat{D}_1(u,\omega)}{\hat{D}_0(u,\omega)} \\
&= \frac{4Nc}{L\omega}\tan\left(\frac{L\omega u}{4Nc}\right) \\
&= u + \frac{u}{3}\left(\frac{L\omega u}{4Nc}\right)^2 + \ldots
\end{aligned} \tag{7.18}$$

We note that in the case of stair-case approximation for array weighting function, the direction estimation $\hat{u}$ becomes frequency dependent.

A direction error Δu is defined as

$$\Delta u = |u - \hat{u}| = \left|\frac{u}{3}\left(\frac{L\omega u}{4Nc}\right)^2 + \ldots\right| \tag{7.19}$$

Alternately Eq. (7.18) can be solved for u to yield the exact result if the wave frequency is known, that is

$$u = \frac{4Nc}{L\omega} \tan^{-1} \frac{\hat{u} L\omega}{4Nc} \tag{7.20}$$

The above analysis can be generalized to accommodate finite duration signals $p(t)$. The Fourier transform $P(\omega)$ of such signal can be assumed to be zero outside some region $(\omega_{\min}, \omega_{\max})$ in the frequency domain. For such signals Eqs. (7.18) and (7.19) become (see Appendix C for details)

$$\begin{aligned} \hat{u} &= \frac{\hat{s_1}(t)}{\hat{s_0}(t)} \\ &= \frac{\int_{-\infty}^{+\infty} P(\omega) D_1(u,\omega) e^{j\omega t} d\omega}{\int_{-\infty}^{+\infty} P(\omega) D_0(u,\omega) e^{j\omega t} d\omega} \\ &= u + \frac{u}{3} \left(\frac{L\omega_i u}{4Nc} \right)^2 + \dots \end{aligned} \tag{7.21}$$

and

$$\Delta u = \left| \frac{u}{3} \left(\frac{L\omega_i u}{4Nc} \right)^2 + \dots \right| \tag{7.22}$$

where ω_i is a certain frequency such that $\omega_i \subseteq [\omega_{\min}, \omega_{\max}]$.

The maximum error occurs therefore for $\omega_i = \omega_{\max}$, and its magnitude can be reduced to an arbitrary value by proper selection of L/N ratio. For example, for $L/N = \lambda$, the direction error is less than 5.1% when the arrival angle is at 60°. The maximum direction errors versus array parameters and arrival angle are plotted in Figure 7.2 and 7.3.

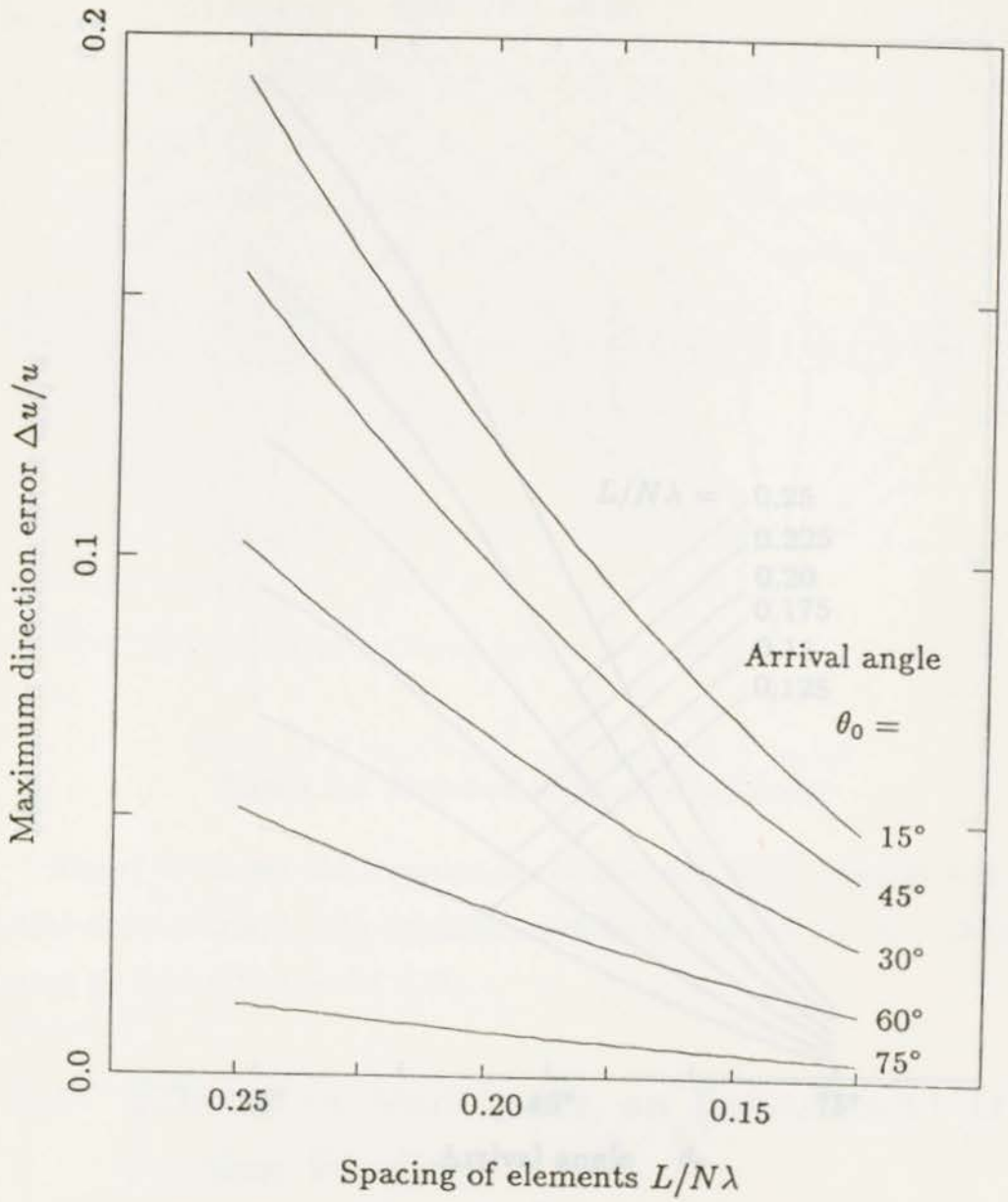

Figure 7.2: Maximum direction error versus spacing of elements for different arrival angles

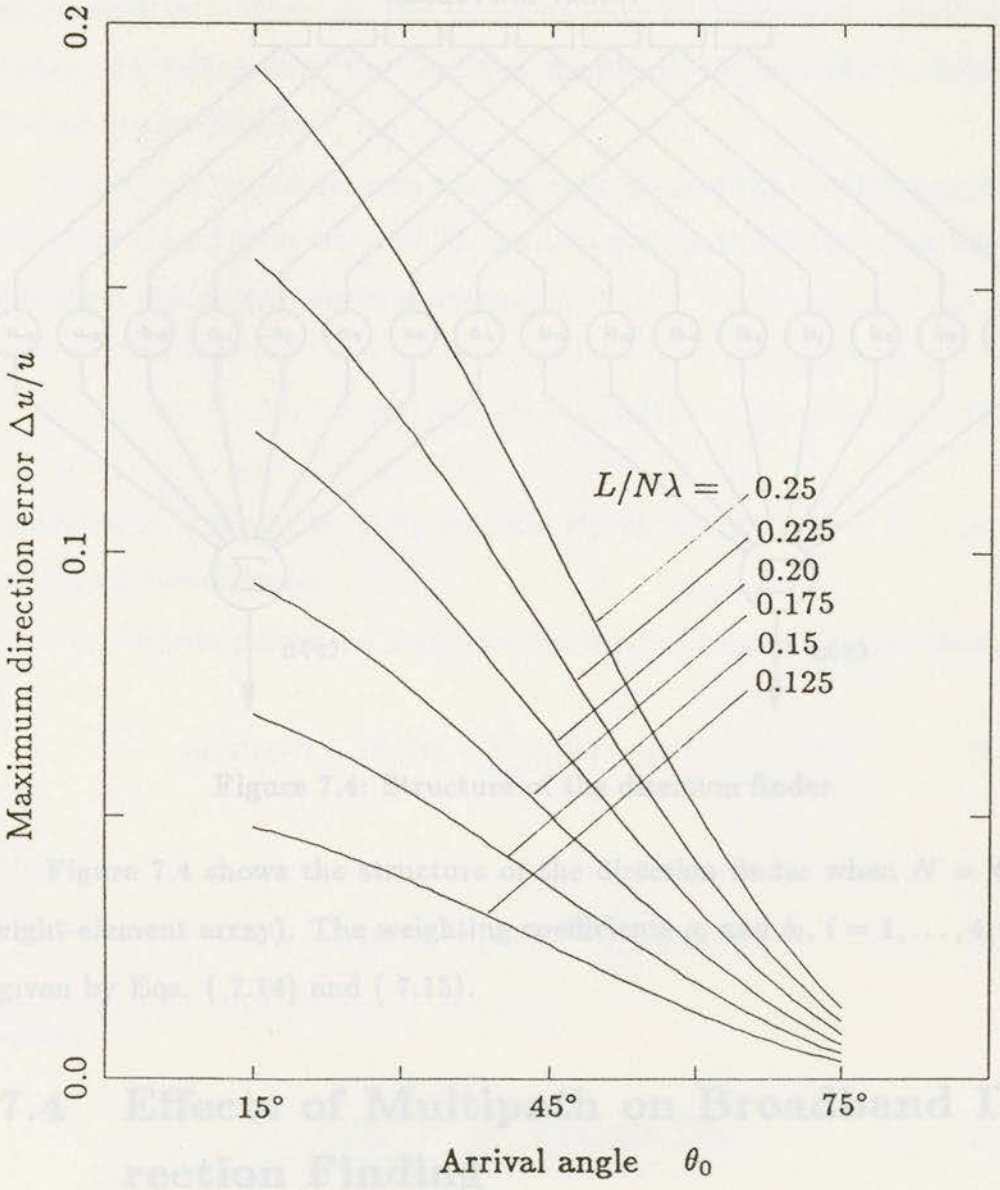

Figure 7.3: Maximum direction error versus arrival angle for different array parameters

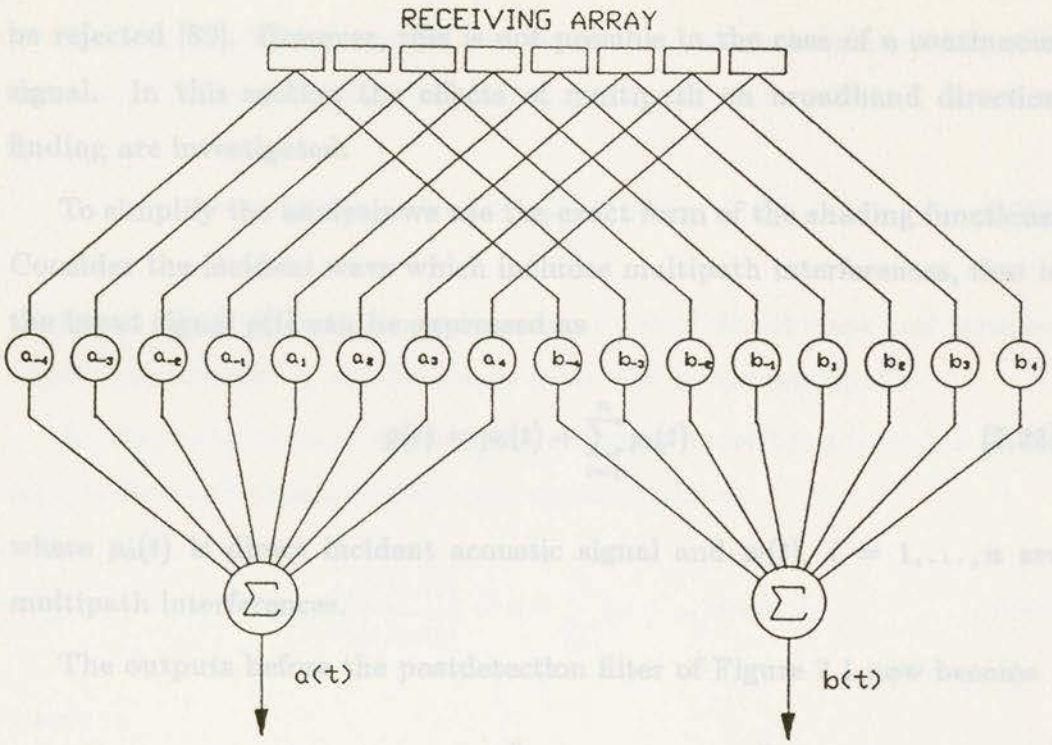

Figure 7.4: Structure of the direction finder

Figure 7.4 shows the structure of the direction finder when $N = 4$ (a eight-element array). The weighting coefficients a_i and b_i, $i = 1, \ldots, 4$, are given by Eqs. (7.14) and (7.15).

7.4 Effects of Multipath on Broadband Direction Finding

The direction finding method described is sensitive to the presence of interfering signals coming from different directions, in particular multipath. In wide-band monopulse sonar application, the later arriving multipath can

be rejected [80]. However, this is not possible in the case of a continuous signal. In this section the effects of multipath on broadband direction finding are investigated.

To simplify the analysis we use the exact form of the shading functions. Consider the incident wave which includes multipath interferences, that is the input signal $p(t)$ can be expressed as

$$p(t) = p_0(t) + \sum_{i=1}^{n} p_i(t) \tag{7.23}$$

where $p_0(t)$ is direct incident acoustic signal and $p_i(t)$, $i = 1, \ldots, n$ are multipath interferences.

The outputs before the postdetection filter of Figure 7.1 now become

$$s_1(t)s_0(t) = [s_{10}(t) + \sum_{i=1}^{n} s_{1i}(t)][s_{00}(t) + \sum_{i=1}^{n} s_{0i}(t)] \tag{7.24}$$

and

$$s_0(t)s_0(t) = [s_{00}(t) + \sum_{i=1}^{n} s_{0i}(t)]^2 \tag{7.25}$$

where

$$s_{0i}(t) = \int_{-\infty}^{\infty} w'(x)p_i(x,t)dx \tag{7.26}$$

$$s_{1i}(t) = u_i s_{0i}(t) \tag{7.27}$$

and u and u_i are the incident direction cosine of direct wave and multipath interferences, respectively.

To simplify the results, we assume that a harmonic plane wave with frequency f is transmitted. The input signal $p(t)$ becomes

$$p(t) = A_0 \cos \omega t + \sum_{i=1}^{n} A_i \cos(\omega t + \phi_i) \tag{7.28}$$

where $\omega = 2\pi f$, A_0 and A_i are the magnitude of direct wave and interferences, respectively, ϕ_i are the phase delay due to the multipath.

By assuming triangle shading, the output of broadband direction finder can be obtained approximately (see Appendix D) as

$$\hat{u}_0 = \frac{\overline{s_1(t)s_0(t)}}{\overline{s_0(t)s_0(t)}} = u + \sum_{i=1}^{n} (u - u_i) e_i \cos \phi_i \tag{7.29}$$

where

$$\begin{aligned} e_i &= \frac{s_{0i}}{s_{00}} \\ &= \frac{A_i}{A_0} \frac{\sin^2(\frac{\omega u_i L}{4c})}{\sin^2(\frac{\omega u L}{4c})} \end{aligned} \tag{7.30}$$

The maximum direction error is given by

$$\Delta u = |u - \hat{u}_0| \leq \sum_{i=1}^{n} |(u - u_i)| e_i \tag{7.31}$$

The maximum direction error versus relative multipath intensity is shown in Figure 7.5. Two multipath signals of equal amplitudes but different arrival angles were assumed.

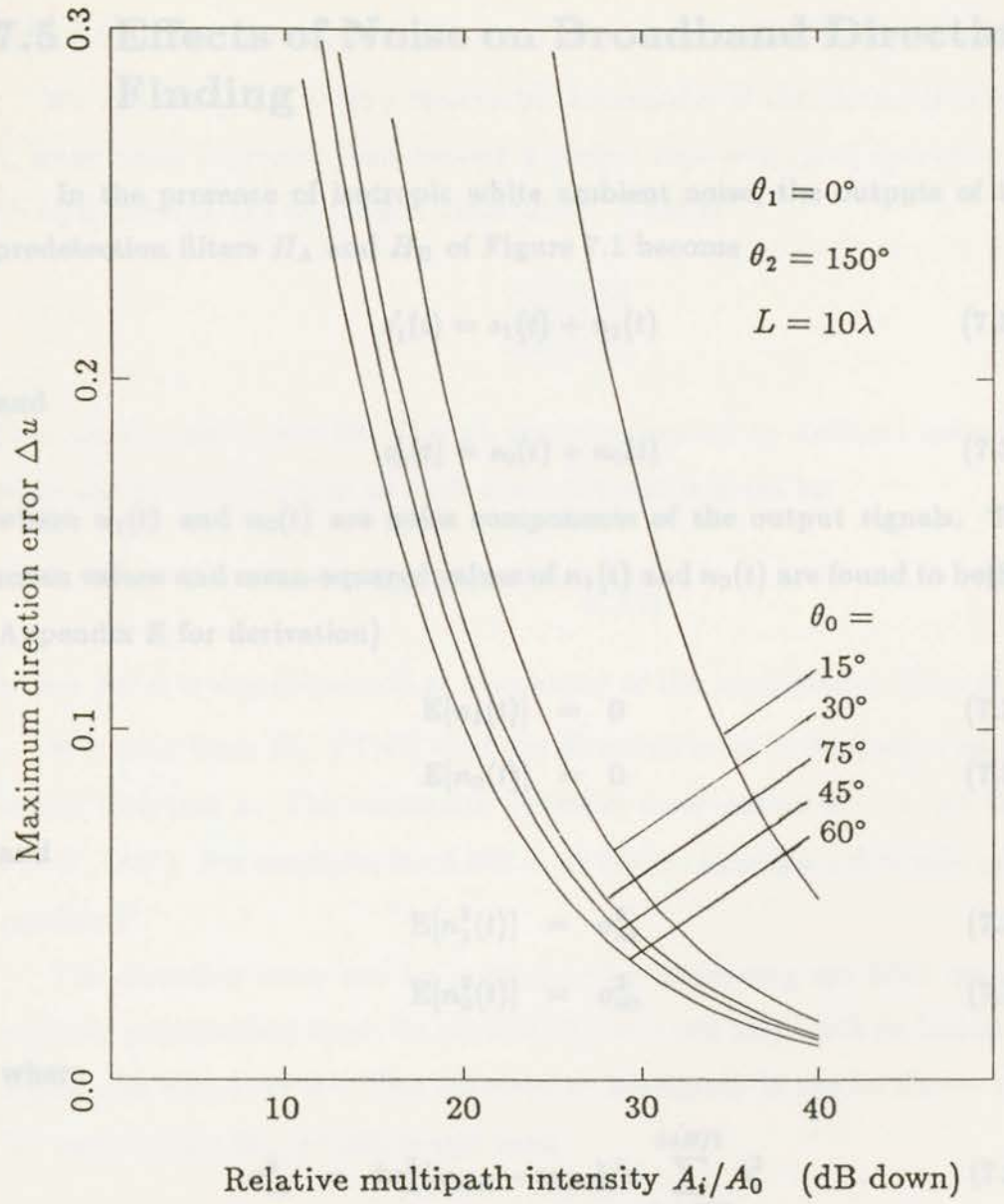

Figure 7.5: Maximum direction error versus multipath intensity for different arrival angles of the direct path

7.5 Effects of Noise on Broadband Direction Finding

In the presence of isotropic white ambient noise, the outputs of the predetection filters H_A and H_B of Figure 7.1 become

$$s_1'(t) = s_1(t) + n_1(t) \tag{7.32}$$

and

$$s_0'(t) = s_0(t) + n_0(t) \tag{7.33}$$

where $n_1(t)$ and $n_0(t)$ are noise components of the output signals. The mean values and mean-squared values of $n_1(t)$ and $n_0(t)$ are found to be(See Appendix E for derivation)

$$\mathrm{E}[n_1(t)] = 0 \tag{7.34}$$

$$\mathrm{E}[n_0(t)] = 0 \tag{7.35}$$

and

$$\mathrm{E}[n_1^2(t)] = \sigma_{n1}^2 \tag{7.36}$$

$$\mathrm{E}[n_0^2(t)] = \sigma_{n0}^2 \tag{7.37}$$

where

$$\sigma_{n1}^2 = 2\sigma_n^2(\omega_{\max} - \omega_{\min})/\pi \sum_{i=-N/2}^{i=N/2} b_i^2 \tag{7.38}$$

$$\sigma_{n0}^2 = 2\sigma_n^2(\omega_{\max}^3 - \omega_{\min}^3)/(3\pi) \sum_{i=-N/2}^{i=N/2} a_i^2 \tag{7.39}$$

(7.40)

and σ_n^2 denotes noise power in the band $(\omega_{\min}, \omega_{\max})$ at each array element.

We apply Eq. (7.8) as a reasonable estimate $\hat{u}$ of the cosine direction u, when noise is present, and assume a perfect time averaging operation to be equivalent to the statistical expectation. That is

$$\hat{u} = \frac{\overline{s_1'(t)s_0'(t)}}{\overline{s_0'(t)s_0'(t)}} \tag{7.41}$$

It is shown (see Appendix F) that the error caused by ambient noise for large signal-to-noise ratio at each array element is given by

$$\Delta u = u - \hat{u} = \frac{u}{SNR} \tag{7.42}$$

where SNR is signal-to-ratio at the output of the predetection filter H_A.

It is clear from Eq. (7.42) that the direction error is dependent on the cosine direction u. The maximum direction error occurs at $u = \pm 1$ (i.e., $\theta = 0°, 180°$). For example, for $SNR = 20$ dB the maximum direction error reaches 8°.

The direction error can be minimized by improving the SNR using a suitable predetection filter. In particular, for white noise and an impulsive signal, the best filter is a filter matched to the signal. It can be shown that for such a filter Eq. (7.42) is still valid.

7.6 Summary

It has been shown that the error of the direction of arrival estimate due to approximation of shading functions for bandlimited signals can be

reduced to an acceptable value by proper selection of array parameters. The broadband direction finding is sensitive to the presence of multipath and noise particularly in broadside directions and therefore can be used only in low multipath situations and restricted geometries. The match filter is suggested as a predetection filter rather than a bandpass filter proposed in [80].

Chapter 8

Summary of Results and Recommendations

The primary goal of this thesis has been to demonstrate that high rates digital acoustic communication in the shallow water environments is possible. In the thesis the theoretical work serves to develop the realistic acoustic communication systems which operate in such environment.

Methods of reduction of multipath interference in a shallow water channel are discussed. It is found that a vertically suspended linear array is a useful configuration for middle range acoustic communications and its performance is superior to that of a planar array with the same number of elements.

The system aspects of a narrowbeam acoustic communication system are presented. The practical upper limit of system performance has been obtained. It has been shown that a communication channel with a relatively broad bandwidth is possible using a narrowbeam receiver. A higher transmission rate can be achieved using frequency and beam diversity.

Based on these results, the high data rate acoustic communication sys-

tem using VLSI technique has been proposed. It has been shown that an acoustic communication link suitable for transmitting data from bottom instrumentation to the surface receiver is feasible using a fixed, broad transmitting beam and a steerable, narrow receiving beam. A vertically suspended linear array is suggested to generate an umbrella-type narrow beam which offers superior performance in rejecting multipath interference. Such an array can be conveniently utilized to estimate the angular direction (elevation) of the arriving signals needed for proper positioning of the beam. The proposed acoustic communication system can be relatively easily implemented using a multi-transmitted-beam and a broad band receiving array. A noncoherent BFSK data transmission scheme is postulated and a FFT algorithm is suggested to implement both direction finding and demodulation algorithms.

A method of broadband direction finding applicable to broadband acoustic communication, navigation and remote sensing is proposed. Problems associated with shading function approximation, multipath interference and ambient noise are addressed and their effects on system performance are analysed. The possible solutions to improve the performance are suggested.

The analysis of error probability in Chapter 6 is based on the assumption of additive white noise, while the effects of multipath are not considered. The further investigation should include the effects of multipath on error retes.

The implementation of broadband direction finder discussed in Chapter 7 is a linear array approach. The approximation error increases with the broadening of signal bandwidth. A continuous aperture utilizing piezoelectric polymetric films will be considered to implement a error free broadband

direction finder in future studies.

References

[1] *Notebook of Leonardo da Vinci*, Edward MacCurdy, ed., New York: George Braziller, 1954.

[2] R. J. Urick, *Principles of Underwater Sound for Engineering*, New York: McGraw-Hill, Edition 3, 1983.

[3] J. A. Adam, *Probing Beneath the Sea*, IEEE Spectrum, April 1985, pp. 55-64.

[4] Anonymous, Oceanographic Instrumentation Review, Underwater System Design, May/June 1985, p. 35.

[5] Anonymous, Sonarlink, Model SP 650, Specification, 1984.

[6] D. E. Ryerson, and G. C. Hauser, *A High-Data-Rate Wide-Angle Underwater Acoustic Telemetry System*, Sandia Report, SAND 84-0994, July 1984.

[7] G. R. Mackelburg, S. J. Watson and A. Gordon, *Bentic 4800 bit/s Acoustic Telemetry*, OCEANS '81 Conference, Boston, MA, Sept. 1981, pp. 48-53.

[8] D. Howse and A. Zielinski, "Multipath modeling for acoustic communication," *MTS-IEEE Conf., Oceans '82*, Washington, Sept. 1982, pp. 217-222.

[9] A. Zielinski and M. Caldera, "Digital acoustic communication in multipath underwater channel," *Oceans '85*, San Diego, CA, 1985, pp. 1296-1301.

[10] A. Zielinski, and L. Wu, "A High Rate Underwater Acoustic Communication system", *Pacific Congress on Marine Technology PACON'88*, Honolulu, Hawaii, pp. OTS4/1-7.

[11] Zielinski, A. and L. Wu, "Data Retrieval From Bottom Instrumentation Using Acoustic Link", *MTS & IEEE/OES Workshop on Instrumentation and Measurements in the Polar Regions*, Monterey, January 1988, pp. 283-294.

[12] V. C. Anderson, "Acoustic Communication is Better than None", *IEEE Spectrum*, October 1970, pp. 63-68.

[13] A. H. Quazi and W. L. Conrad, "Underwater Acoustic Communications", *IEEE Commun. Magazine*, Vol. 20, No. 2, March 1982, pp. 24-30.

[14] A. B. Baggeroer, "Acoustic Telemetry - An Overview", *IEEE J. Oceanic Eng.*, Vol. OE-9, No. 4, Oct. 1984, pp. 229-235.

[15] R. Coates and P. A. Willison, "Underwater Acoustic Communications: A Review and Bibliography", *Proc. Inst. Acoustics*, Vol. 9, Part 4, Dec. 1987, pp. 54-62.

[16] H. Weinberg, "Generic Sonar Model", NUSC Technical Document 5971C, 1981.

[17] H. Weinberg, "Generic Sonar Model", *MTS-IEEE Conf., Oceans '82*, Washington, Sept. 1982, pp. 201-205.

[18] D. R. Hummels, "The Capacity of a Model for the Underwater Acoustic Channel", *IEEE Trans. Sonics and Ultrasonics*, Vol. SU-19, 1972, pp. 350-353.

[19] H. M. Kwon and T. G. Birdsall, "Channel Capacity in Bits per Joule", *IEEE J. Oceanic Eng.*, Vol. OE-11, No. 1, Jan. 1986, pp. 97-99.

[20] R. O. Rowlands and F. G. Quinn, "Transmission Rate Limits in Underwater Acoustic Telemetry", in *Underwater Acoustics, Vol II.* (ed. Albers), New York: Plenum Press, pp. 393-408.

[21] E. P. Gulin, "Amplitude and Phase Fluctuations of a Sound Wave Reflected from a Statistically Uneven Surface", *Sov. Phys.-Acous.*, Vol. 8, No. 2, Oct.-Dec. 1962, pp. 135-140.

[22] E. P. Gulin, "Amplitude and Phase Fluctuations of a Sound Wave Reflected from a Sinusoidal Surface", *Sov. Phys.-Acous.*, Vol. 8, No. 3, Jan.-Mar. 1963, pp. 223-227.

[23] E. P. Gulin and K. I. Malyshev, "Statistical Characteristics of Sound Signals Reflected from the Undulating Sea Surface", *Sov. Phys.-Acous.*, Vol. 8, No. 3, Jan.-Mar. 1963, pp. 228-239.

[24] E. P. Gulin, "The Correlation of Amplitude and Phase Fluctuations in Sound Waves Reflected from a Statistically Rough Surface", *Sov. Phys.-Acous.*, Vol. 8, No. 4, Apr.-June. 1963, pp. 335-339.

[25] E. P. Gulin and K. I. Malyshev, "Experiments in the Spatial Correlation of the Amplitude and Phase Fluctuations of Acoustic Signals Reflected from a Rough Ocean Surface", *Sov. Phys.-Acous.*, Vol. 10, No. 4, Apr.-June. 1965, pp. 365-368.

[26] E. P. Gulin and K. I. Malyshev, "Spatial Correlation of Amplitude and Phase Fluctuations of a Continuous Tone Signals with Reflection from Ocean Surface Waves", *Sov. Phys.-Acous.*, Vol. 11, No. 4, Apr.-June. 1966, pp. 428-430.

[27] E. P. Gulin and K. I. Malyshev, "Some Results of an Investigation of the Frequency Correlation of Amplitude Fluctuations in Sound Signals", *Sov. Phys.-Acous.*, Vol. 12, No. 1, July-Sept. 1966, pp. 87-88.

[28] W. Jobst and L. Dominijanni, "Measurements on the Temporal, Signal and Frequency Stability of an Underwater Acoustic Channel", *J. Acous. Soc. Am.*, Vol. 65, No. 1. Jan. 1979, pp. 62-69.

[29] R. L. Veenkant, "Investigation of the Propagation Stability of a Doubly Spread Underwater Acoustic Channel", *IEEE Trans. Acoustics, Speech and Signal Processing*, Vol. ASSP-25, No. 2, April 1977, pp. 109-116.

[30] R. M. Dunbar, "Electric, Magnetic and Acoustic Noise Generated Underwater During Offshore Piling Operations", *Proc. Inst. Acoustics*,

Vol. 9, Dec. 1987.

[31] R. J. Urick, *Ambient Noise in the Sea*, Peninsula Publishing, 1986.

[32] Per O. Fjell, "Use of the Cepstrum Method for Arrival Times Extraction of Overlapping Signals due to Multipath Conditions in Shallow Water", *J. Acous. Soc. Am.*, Vol. 59, No. 1. Jan. 1976, pp. 209-211.

[33] J. C. Hassab, "Time Delay Processing Near the Ocean Surface", *J. Sound and Vib.*, Vol. 35, No. 4, 1974, pp. 489-501.

[34] J. C. Hassab and R. Boucher, "Analysis of Signal Extraction, Echo Detection and Removal by Complex Cepstrum in the Presence of Distortion", *J. Sound and Vib.*, Vol. 40, No. 3, 1975, pp. 321-335.

[35] G. R. Legters, N. L. Weinberg and J. G. Clarke, "Long-Range Atlantic Acoustic Multipath Identification", *J. Acous. Soc. Am.*, Vol. 73, No. 5. 1983, pp. 1571-1580.

[36] J. Northrop and R. C. Shockley, "Long-Range Pacific Multipath Identification", *J. Acous. Soc. Am.*, Vol. 75, No. 6, 1984, pp. 1760-1765.

[37] J. L. Galloway, J. S. Collins and M. R. Balderson, " Auto Aligning System for Narrow Beam Acoustic Telemetry", *Proc. IEEE Oceans '85 Conf.*, San Diego, Calif., Nov. 1985, pp. 490-493.

[38] R. E. Williams and H. F. Battestin, "Coherent Recombination of Acoustic Multipath Signals Propagated in the Deep Ocean", *J. Acous. Soc. Am.*, Vol. 50, No. 6(Part 1), 1971, pp. 1433-1442.

[39] A. Vine, "Present and Prospective Needs of Submersibles for Underwater telecommunication", in *Present and Future Civil Uses of Underwater Sound*, NAS Book, 1970.

[40] W. Dow, "A Telemetering hydrophone", *Deep-Sea Res.*, Vol. 7, 1960, pp. 142-147.

[41] P. Hearn, "Underwater Acoustic Telemetry", *IEEE Trans. Commun. Technol.*, Vol. CT-14, Dec. 1966, pp. 839-843.

[42] C. S. Miller and C. E. Bohman, "An Experiment in High Rate Underwater Telemetry", in *Proc. Ocean '72*, 1972.

[43] D. Garrod, "Applications of MFSK Acoustic Communication systems", *Proc. IEEE Oceans '81 Conf.*, 1981, pp. 67-71.

[44] F. C. Jarvis, "Description of a Secure, Reliable Acoustic System for Use in Offshore Oil BOP or Wellhead Operations", *IEEE J. Oceanic Eng.*, Vol. OE-9, No. 4, Oct. 1984, pp. 253-258.

[45] A. B. Baggeroer, D. Keolsch, K. von der Heydt, and J. Catipovic, "DATS—A Digital Acoustic Telemetry System", *Proc. IEEE Oceans '81 Conf.*, 1981, pp. 56-66.

[46] J. Catipovic, A. B. Baggeroer, K. von der Heydt and D. Keolsch, "Design and Performance Analysis of a Digital Telemetry System for the Short Range Ubderwater Channel", *IEEE J. Oceanic Eng.*, Vol. OE-9, No. 4, Oct. 1984, pp. 242-252.

[47] P. O. Kearmey and C. A. Laufer, "SONARLINK—A Deep Ocean, High Data Rate, Adaptive-Telemetry System", *Proc. IEEE Oceans '84 Conf.*, 1984, pp. 49-54.

[48] R. S. Andrews and L. F. Turner, " On the Performances of Underwater Data Transmission using Amplitude Shift Keying techniques", *IEEE J. sonics Ultrason.*, Vol. SU-23, No. 1, June 1976, pp. 64-71.

[49] R. S. Andrews and L. F. Turner, "Investigations of Amplitude Fluctuations of High Frequency, Short Duration Sound Pulses Propagated under Short Range, Shallow Water Conditions", *J. Acous. Soc. Am.*, Vol. 58, No. 2, Aug. 1975, pp. 331-335.

[50] J. E. Pieper, J. A. Proakis, R. R. Reed and J. K. Wolf, "Design of Efficient Coding and Modulation for a Rayleigh Fading Channel", *IEEE Trans. Inform. Theory*, Vol. IT-24, No. 4, July 1978, pp. 457-468.

[51] A. Venetsanpoulos, "Signal Design for Active Signaling under Various SNR's at Receiver Input", *IEEE Trans. Commun. Technol.*, Vol. CT-19, No. 10, Oct. 1971, pp. 646-659.

[52] A. Zielinski and L. Barbow, "Swept Carrier Acoustic Underwater Communications", *Proc. IEEE Oceans '78 Conf.*, 1978, pp. 60-65.

[53] W. I. Gluth and C. E. Schnud, "Analysis of an Underwater DPSK Telemetry Equipment", *J. Acous. Soc. Am.*, Vol. 64, Supp. No. 1, 1978, p. S119.

[54] S. D. Mogera, "Small Submersible Acoustic Communications System Design", *Proc. IEEE Oceans '78 Conf.*, 1978, pp. 66-71.

[55] T. Birdsall, "Acoustic Telemetry For Ocean Acoustic Tomography", *IEEE J. Oceanic Eng.*, Vol. OE-9, No. 4, Oct. 1984, pp. 237-241.

[56] J. Makhoul, "Linear Prediction Theory: A Tutorial Review", *Proc. IEEE*, Vol. 63, No. 4, Apr. 1975, pp. 561-581.

[57] W. K. Pratt, *Digital Image Processing*, New York: Wiley, 1978.

[58] C. S. Clay and H. Medwin, *Acoustical Oceanography: Principles and Applications*, New York: Wiley, 1977.

[59] R. S. Kennedy, *Fading Dispersive Communication Channel*, New York: Wiley, 1969.

[60] H. L. Van Tress, *Detection, Estimation and Modulation Theory, Part III*, New York: Wiley, 1971.

[61] Osborne-Hoffman, Inc., "Advanced Underwater Telemetry and Voice Sinks for Inland and Coastal Waters research", Final Project Rep., NSF Award DAR 8009716, Feb. 1981.

[62] P. Berkmann and A. Spizzichino, *The Scattering of Electromagnetic Waves from Rough Surface*, New York: Macmillan, 1963, pp. 137-146.

[63] J. S. Collins and K. H. V. Booth, " Simulation of Multipath Channels Terminated by Narrow Beam Non-parametric Transducers", *Fourth International Symposium on Unmanned Untethered Submersible Technology*, June 1985, pp. 124-139.

[64] C. L. Dolph, "A Current Distribution of Broadside Arrays which Optimizes the Relationship between Beamwidth and Side Lobe Levels", *Proc. I.R.E.*, June 1946, pp. 335-348; May 1947, pp. 489-492.

[65] R. J. Stegen, "Excitation Coefficients and Beamwidth of Tschebyscheff Arrays", *Proc. I.R.E.*1, pp. 1671-1674, Nov. 1953.

[66] A. Zielinski, "Matrix Formulation for Dolph-Chebyshev Beamforming", *Proc. of IEEE*, Vol. 74, No. 12, Dec. 1986, pp. 1799-1800.

[67] Anonymous, *Honeywell Acoustic Telemetry System MT-300*, Specifications.

[68] A. Zielinski, "Acoustic Telemetry and Communication", *Pacific Congress on Marine Technology, PACON 86*, Honolulu, HI, Mar. 1986, pp. OST4/31-35,

[69] W. L. Konrad, "Application of the Parametric Source to Wideband Undersea Communication", *Acoustic Communications Workshop*, Washington, D.C., Aug. 1982, Section B3, 13 pages.

[70] C. D. Porta Eck and C. Fang, "High Speed Digital Acoustic Telemetry", *Fifth Int. Symp. on Unmanned Untethered Submersible Technology*, University of New Hampshire, June 22-24, 1987, pp. 348-362.

[71] R. E. Elliot *The Theory of Antenna Arrays*, Vol. 2 of Microwave Scanning Antennas, ed. R. C. Hansen, New York: Academic Press, 1966, pp. 23-45.

[72] M. Okino and Y. Higashi, "Measurement of Seabed Topography by Multibeam Sonar Using CFFT", *IEEE J. Oceanic Eng.*, Vol. OE-11, No. 4, Oct. 1986, pp. 474-479.

[73] P. Rudnik, "Digital beamforming in the frequency domain", *J. Acoust. Soc. Amer.*, Vol. 4b, No. 5, 1969, pp. 1089-1090.

[74] D. E. Ryerson and G. C. Hauser, "A High-Data-Rate Wide-Angle Underwater Acoustic Telemetry System", *Sandia Report*, SAND 84-0994, July 1984.

[75] L. Wu and A. Zielinski, "Multipath Rejection Using Narrowbeam Acoustic Link", *OCEAN '88, MTS-IEEE Conf.*, Baltimore.

[76] S. Haykin, *Digital Communications*, New York: John Wiley, 1988.

[77] A. Zielinski and L. Wu, "A narrow-beam acoustic communication", *IV Symp. on Underwater Acoustics*, Poland, May 1987, pp. 331-338.

[78] T. L. Henderson, "Fractional beamwidth resolution with a paired beamformer," in *Proc. IEEE EASCON '82 Conf.*, Washington, DC, Sept. 1982, pp. 251-252.

[79] T. L. Henderson, "Matched beam theory for unambiguous broadband direction finding," *J. Acoust. Soc. Amer.*, vol. 78, pp. 563-574, 1985.

[80] T. L. Henderson, "Wide-band monopluse sonor: processor performance in the remote profilong application," *IEEE Jour. of Oceanic Engineering*, vol. OE-12, pp. 182-197, 1987.

Appendix A

Derivation of Noise Components

The outputs of arrays before the predetection filters are

$$\begin{aligned} b'(t) &= \sum_{i=-N/2}^{i=N/2} b_i[p(t) + n_i(t)] \\ &= \sum_{i=-N/2}^{i=N/2} b_i p(t) + \sum_{i=-N/2}^{i=N/2} b_i n_i(t)] \\ &= b(t) + n_b(t) \end{aligned} \tag{A.1}$$

and

$$\begin{aligned} a'(t) &= \sum_{i=-N/2}^{i=N/2} a_i[p(t) + n_i(t)] \\ &= \sum_{i=-N/2}^{i=N/2} a_i p(t) + \sum_{i=-N/2}^{i=N/2} a_i n_i(t)] \\ &= a(t) + n_a(t) \end{aligned} \tag{A.2}$$

where a_i and b_i are weighting coefficients, and $n_i(t)$ is ambient noise at ith element. The ambient noise n_i is assumed to be zero mean, independent from each other, and with the mean-squared value of σ_n^2 in the bandwidth $(\omega_{\min}, \omega_{\max})$. Then we calculate

$$\begin{aligned} \mathrm{E}[n_b(t)] &= \sum_{i=-N/2}^{i=N/2} b_i \mathrm{E}[n_i(t)] \\ &= 0 \end{aligned} \tag{A.3}$$

and

$$\begin{aligned} \mathrm{E}[n_b^2(t)] &= \sum_{i=-N/2}^{i=N/2} \sum_{i=-N/2}^{j=N/2} b_i b_j \mathrm{E}[n_i(t) n_j(t)] \\ &= \sum_{i=-N/2}^{i=N/2} b_i^2 \mathrm{E}[n_i^2(t)] \\ &= \sigma_n^2 \sum_{i=-N/2}^{i=N/2} b_i^2 \end{aligned} \tag{A.4}$$

A similar development shows that

$$\mathrm{E}[n_a(t)] = 0 \tag{A.5}$$

and

$$\mathrm{E}[n_a^2(t)] = \sigma_n^2 \sum_{i=-N/2}^{i=N/2} a_i^2 \tag{A.6}$$

We may readily find the mean value of the predetection filters' noise outputs $n_1(t)$ and $n_0(t)$. These are

$$\begin{aligned} \mathrm{E}[n_1(t)] &= \mathrm{E}[n_b(t)] \int_{-\infty}^{\infty} h_b(\xi) d\xi \\ &= 0 \end{aligned} \tag{A.7}$$

and

$$\begin{aligned} \mathrm{E}[n_0(t)] &= \mathrm{E}[n_a(t)] \int_{-\infty}^{\infty} h_a(\xi) d\xi \\ &= 0 \end{aligned} \tag{A.8}$$

where $h_a(\xi)$ and $h_b(\xi)$ are impulse responses of the predetection filters H_A and H_B, respectively.

The mean-squared values of $n_1(t)$ and $n_0(t)$ are given by

$$\begin{aligned} \mathrm{E}[n_1^2(t)] &= \mathrm{E}[n_b^2(t)] \int_{-\infty}^{\infty} |H_B(f)|^2 df \\ &= 2\sigma_n^2(\omega_{\max} - \omega_{\min})/\pi \sum_{i=-N/2}^{i=N/2} b_i^2 \end{aligned} \tag{A.9}$$

and

$$\begin{aligned} \mathrm{E}[n_0^2(t)] &= \mathrm{E}[n_a^2(t)] \int_{-\infty}^{\infty} |H_A(f)|^2 df \\ &= 2\sigma_n^2(\omega_{\max}^3 - \omega_{\min}^3)/(3\pi) \sum_{i=-N/2}^{i=N/2} a_i^2 \end{aligned} \tag{A.10}$$

here we assume that the frequency response of predetection filter $H_A(f)$ is

given by

$$H_A(f) = \begin{cases} 1 & f_{\min} \leq |f| \leq f_{\max} \\ 0 & \text{otherwise} \end{cases} \tag{A.11}$$

and $H_B(f)$ is defined by Eq. (7.6).

The cross-correlation function $R_{10}(\tau)$ of $n_1(t)$ and $n_0(t)$ is obtained by

$$\begin{aligned} R_{10}(\tau) &= R_{11}(\tau) * h_a(\tau) \\ &= \frac{1}{2\pi} \int_{-\infty}^{\infty} S_{11}(\omega) H_A(\omega) e^{j\omega\tau} d\omega \end{aligned} \tag{A.12}$$

As a special case for $\tau = 0$, Eq. (A.12) becomes

$$\begin{aligned} \mathrm{E}[n_1(t) n_0(t)] &= R_{10}(0) \\ &= \frac{1}{2\pi} \int_{-\infty}^{\infty} S_{11}(\omega) H_A(\omega) d\omega \\ &= 0 \end{aligned} \tag{A.13}$$

Appendix B

Direction Error Due to Ambient Noise

$$
\begin{aligned}
\hat{u} &= \frac{\overline{s_1'(t)s_0'(t)}}{\overline{s_0'(t)s_0'(t)}} \\
&= \frac{\overline{s_1(t)s_0(t)} + \overline{s_0(t)}\mathrm{E}[n_1(t)] + \overline{s_1(t)}\mathrm{E}[n_0(t)] + \mathrm{E}[n_1(t)n_0(t)]}{\overline{s_0(t)s_0(t)} + 2\overline{s_0(t)}\mathrm{E}[n_0(t)] + \mathrm{E}[n_0^2(t)]} \\
&= \frac{\overline{s_1(t)s_0(t)}}{\overline{s_0(t)s_0(t)} + \mathrm{E}[n_0^2(t)]} \\
&= \frac{\overline{s_1(t)s_0(t)}}{\overline{s_0(t)s_0(t)}}\left(1 + \frac{\mathrm{E}[n_0^2(t)]}{\overline{s_0(t)s_0(t)}}\right)^{-1} \\
&= u(1 + \frac{1}{SNR})^{-1} \qquad \text{(B.1)}
\end{aligned}
$$

where SNR is signal-to-ratio at the output of the prodetection filter.

Expanding $(1 + 1/SNR)^{-1}$ in series and neglecting higher order terms,

we obtain approximately

$$\hat{u} = u - \frac{u}{SNR} \tag{B.2}$$

Therefore, we can write

$$\Delta u = u - \hat{u} = \frac{u}{SNR} \tag{B.3}$$

Appendix C

Output of Root Squarer

The Fourier transform of received signal $x(t)$ is of the form

$$\begin{aligned} X(f) &= \int_{-\infty}^{\infty} \sqrt{\frac{2}{T_b}} x(t) e^{j2\pi ft} dt \\ &= \int_0^{T_b} x(t) \sqrt{\frac{2}{T_b}} \cos(2\pi ft) dt + j \int_0^{T_b} x(t) \sqrt{\frac{2}{T_b}} \sin(2\pi ft) dt \end{aligned} \quad \text{(C.1)}$$

The sample values of $X(f)$ at $f = f_i$ is given by

$$\begin{aligned} X(f_i) &= \int_0^{T_b} x(t) \sqrt{\frac{2}{T_b}} \cos(2\pi f_i t) dt + j \int_0^{T_b} x(t) \sqrt{\frac{2}{T_b}} \sin(2\pi f_i t) dt \\ &= \sqrt{E_b} \cos\theta + w_{ci} + j(-\sqrt{E_b} \sin\theta + w_{si}) \end{aligned} \quad \text{(C.2)}$$

where w_{ci} and $w_{si}, i = 1, 2$ are related to the noise $w(t)$ as follows:

$$w_{ci} = \int_0^{T_b} w(t) \sqrt{\frac{2}{T_b}} \cos(2\pi f_i t) dt \qquad i = 1, 2 \quad \text{(C.3)}$$

and

$$w_{si} = \int_0^{T_b} w(t)\sqrt{\frac{2}{T_b}}\sin(2\pi f_i t)dt \qquad i = 1,2 \tag{C.4}$$

The output of the root squarer sampled at frequency $f = f_i$ in the receiver of Fig. 2 is then obtained

$$\begin{aligned} l_i &= \sqrt{|X(f_i)|^2} \\ &= \sqrt{x_{ci}^2 + x_{si}^2} \qquad i = 1,2 \end{aligned} \tag{C.5}$$

where

$$x_{ci} = \sqrt{E_b}\cos\theta + w_{ci} \tag{C.6}$$

and

$$x_{si} = -\sqrt{E_b}\sin\theta + w_{si} \tag{C.7}$$

Appendix D

Means and Variances of w_{ci} and w_{si}

The mean values of w_{ci} and $w_{si}, i = 1, 2$ are given by

$$\begin{aligned} \mathrm{E}[w_{ci}] &= \mathrm{E}[\sum_{n=0}^{N-1} w(n)\sqrt{\frac{2}{T_b}}\cos(\frac{2\pi K_j n}{N}) \cdot \frac{T_b}{N}] \\ &= 0 \end{aligned} \tag{D.1}$$

and

$$\begin{aligned} \mathrm{E}[w_{si}] &= \mathrm{E}[\sum_{n=0}^{N-1} w(n)\sqrt{\frac{2}{T_b}}\sin(\frac{2\pi K_j n}{N}) \cdot \frac{T_b}{N}] \\ &= 0 \end{aligned} \tag{D.2}$$

The variance of w_{ci} and w_{si}, $i = 1, 2$ are obtained as follows:

$$\begin{aligned} \mathrm{Var}[w_{ci}] &= \mathrm{E}[\sum_{n=0}^{N-1} w(n)\frac{\sqrt{2T_b}}{N}\cos(\frac{2\pi K_j n}{N}) \sum_{m=0}^{N-1} w(m)\frac{\sqrt{2T_b}}{N}\cos(\frac{2\pi K_j m}{N})] \\ &= \sum_{n=0}^{N-1} \frac{N_0}{2}\delta(n-m)\frac{\sqrt{2T_b}}{N}\cos(\frac{2\pi K_j n}{N}) \sum_{m=0}^{N-1} \frac{\sqrt{2T_b}}{N}\cos(\frac{2\pi K_j m}{N}) \end{aligned}$$

$$
\begin{aligned}
&= \frac{N_0}{2}\sum_{n=0}^{N-1}\frac{2}{T_b}\cos^2\left(\frac{2\pi K_j n}{N}\right)\cdot\frac{T_b}{N} \\
&= \frac{N_0}{2}\sum_{n=0}^{N-1}\left[1+\cos\left(\frac{4\pi k_j n}{N}\right)\right]\cdot\frac{1}{N} \\
&= \frac{N_0}{2}(1+\sigma^{+}_{cjj}) \qquad \text{(D.3)}
\end{aligned}
$$

and

$$
\begin{aligned}
\mathrm{Var}[w_{si}] &= \mathrm{E}\left[\sum_{n=0}^{N-1} w(n)\frac{\sqrt{2T_b}}{N}\sin\left(\frac{2\pi K_j n}{N}\right)\sum_{m=0}^{N-1} w(m)\frac{\sqrt{2T_b}}{N}\sin\left(\frac{2\pi K_j m}{N}\right)\right] \\
&= \sum_{n=0}^{N-1}\frac{N_0}{2}\delta(n-m)\frac{\sqrt{2T_b}}{N}\sin\left(\frac{2\pi K_j n}{N}\right)\sum_{m=0}^{N-1}\frac{\sqrt{2T_b}}{N}\sin\left(\frac{2\pi K_j m}{N}\right) \\
&= \frac{N_0}{2}\sum_{n=0}^{N-1}\frac{2}{T_b}\sin^2\left(\frac{2\pi K_j n}{N}\right)\cdot\frac{T_b}{N} \\
&= \frac{N_0}{2}\sum_{n=0}^{N-1}\left[1-\cos\left(\frac{4\pi k_j n}{N}\right)\right]\cdot\frac{1}{N} \\
&= \frac{N_0}{2}(1-\sigma^{+}_{cjj}) \qquad \text{(D.4)}
\end{aligned}
$$

Appendix E

Output of Broadband Direction Finder

The Eq.(7.16) can be written in the following forms.

$$\begin{aligned} s_1(t) &= \int_{-\infty}^{+\infty} P(\omega) D_1(u,\omega) e^{j\omega t} d\omega \\ &= \frac{4}{L} \int_{-\infty}^{+\infty} G(\omega,t) \frac{c}{\omega} d\omega \end{aligned} \tag{E.1}$$

and

$$\begin{aligned} s_0(t) &= \int_{-\infty}^{+\infty} P(\omega) D_0(u,\omega) e^{j\omega t} d\omega \\ &= \frac{1}{N} \int_{-\infty}^{+\infty} G(\omega,t) \cot(L\omega u/4Nc) d\omega \end{aligned} \tag{E.2}$$

where

$$G(\omega,t) = \frac{4}{Lu} P(\omega) \frac{c}{\omega} \sin^2(L\omega u/4c) e^{j\omega t} \tag{E.3}$$

By applying mean value theorem of the integration, one can obtain

$$s_1(t) = \frac{4}{L} G(\omega_j, t) \frac{c}{\omega_j} (\omega_{max} - \omega_{min}) \tag{E.4}$$

and

$$s_0(t) = \frac{1}{N} G(\omega_i, t) \cot(L\omega u / 4Nc)(\omega_{max} - \omega_{min}) \tag{E.5}$$

where $\omega_i, \omega_j \subseteq [\omega_{\min}, \omega_{\max}]$.

Expanding $s_1(t)$ as a series around point ω_i, we have

$$\begin{aligned} s_1(t) &= \frac{4}{L} G(\omega_j, t) \frac{c}{\omega_j} (\omega_{max} - \omega_{min}) \\ &= (\omega_{max} - \omega_{min}) \frac{4}{L} \left\{ G(\omega_i, t) \frac{c}{\omega_i} + \right. \\ &\quad \left. \frac{d}{d\omega} \left[G(\omega, t) \frac{c}{\omega} \right]_{\omega=\omega_i} (\omega_j - \omega_i) + \dots \right. \end{aligned} \tag{E.6}$$

Assume that the spectrum of signal is flat within $(\omega_{\min}, \omega_{\max})$, we find

$$\frac{d}{d\omega} \left[G(\omega, t) \frac{c}{\omega} \right]_{\omega=\omega_i} (\omega_j - \omega_i) \approx 0 \tag{E.7}$$

and therefore

$$\begin{aligned} \frac{s_1(t)}{s_0(t)} &= \frac{4N}{L} \frac{c}{\omega_i} \tan\left(\frac{L\omega_i u}{4Nc} \right) \\ &= u + \frac{u}{3} \left(\frac{L\omega_i u}{4Nc} \right)^2 + \dots \end{aligned} \tag{E.8}$$

Appendix F

Output of Direction Finder When Multipath Exists

The ratio function $s_1(t)/s_0(t)$ can be rewritten as

$$\frac{s_1(t)}{s_0(t)}\frac{s_0(t)}{s_0(t)} = \frac{[s_{10}(t)+\sum_{i=1}^{n} s_{1i}(t)]}{[s_{00}(t)+\sum_{i=1}^{n} s_{0i}(t)]}\frac{[s_{00}(t)+\sum_{i=1}^{n} s_{0i}(t)]}{[s_{00}(t)+\sum_{i=1}^{n} s_{0i}(t)]} \quad \text{(F.1)}$$

where

$$\begin{aligned} s_{0i}(t) &= \int_{-\infty}^{+\infty} w'(x)p_i(x,t)dx \\ &= -4A_i \sin(\omega t+\phi_i)\sin^2(\omega u_i L/4) \end{aligned} \quad \text{(F.2)}$$

and

$$\begin{aligned} s_{1i}(t) &= u_i s_{0i}(t) \\ &= -4u_i A_i \sin(\omega t+\phi_i)\sin^2(\omega u_i L/4) \end{aligned} \quad \text{(F.3)}$$

The outputs of postdirection filters H_A and H_B shown in Figure 7.1 are

$$\overline{s_{0i}(t)s_{1j}(t)} = -16u_i A_i A_j \cos(\phi_i-\phi_j)\sin^2(\omega u_i L/4)\sin^2(\omega u_j L/4) \quad \text{(F.4)}$$

and

$$\overline{s_{0i}(t)s_{0j}(t)} = -16A_iA_j\cos(\phi_i-\phi_j)\sin^2(\omega u_iL/4)\sin^2(\omega u_jL/4) \qquad \text{(F.5)}$$

Let us consider the case $u \neq 0$. Neglecting the higher order terms, we have the following approximation

$$\begin{aligned}\frac{\overline{s_1(t)s_0(t)}}{\overline{s_0(t)s_0(t)}} &= \frac{u+\sum_{i=1}^n u_ih_i+\sum_{i=1}^n uh_i+\sum_{i=1}^n\sum_{j=1}^n uu_ih_ih_j}{1+2\sum_{i=1}^n h_i+\sum_{i=1}^n\sum_{j=1}^n h_ih_j} \\ &\approx u+\sum_{i=1}^n(u-u_i)e_i\cos(\phi_i)+\ldots \qquad \text{(F.6)}\end{aligned}$$

where

$$\begin{aligned}e_i &= \frac{s_{0i}}{s_{00}} \\ &= \frac{A_i}{A_0}\frac{\sin^2(\omega u_iL/4c)}{\sin^2(\omega uL/4c)} \qquad \text{(F.7)}\end{aligned}$$

and

$$h_i = e_i\cos(\phi_i) \qquad \text{(F.8)}$$

VITA

Surname: **WU** Given Names: **LIXUE**

Place of Birth: Shanghai, China Date of Birth: January 13, 1949

Educational Institutions Attended, with Dates of Entering and Leaving:

UNIVERSITY OF VICTORIA, B.C. 1987 to 1989

EAST CHINA NORMAL UNIVERSITY, CHINA. 1978 to 1982

Degrees, Diplomas, Etc., Awarded, with Dates and Names of Institutions:

B.Sc. 1986 East China Normal University.

Honours and Awards:

B.C. Advanced Systems Foundation Scholarship, 1989.

University of Victoria Fellowship, 1988 to 1989.

Advanced Technology Premium of Shanghai Provicial Government, 1984.

Publications and Book Translations:

1. Zielinski, A. and L. Wu, "Acoustic Positioning Using Multielement Array", accepted for *OCEAN '89, MTS-IEEE Conf.*, Seattle, Sep. 18-21, 1989.

2. Zielinski, A. and L. Wu, "Underwater Acoustic Positioning Using Surface Multipath", accepted for *IEEE Pacific Rim Conf. on Communications, Computers and Signal Processing*, Victoria, B.C. June 1989.

3. Zielinski, A. and L. Wu, "Acoustic Navigation in Multipath Conditions", accepted for *13th International Congress on Acoustics, Symposium on Sea Acoustics*, Dubrovnik, Sep. 4-6, 1989.

4. Zielinski, A. and L. Wu, "Underwater Acoustic Communication system", accepted for publication in *Marine Geodesy Journal.*

5. Zielinski, A. and L. Wu, "Direction Estimation of Broadband Acoustic Signal" *Canadian Conf. on Electrical and Computer Engineering*, Vancouver, Nov. 1988, pp. 61-65.

6. Wu, L. and A. Zielinski, "Multipath Rejection Using Narrowbeam Acoustic Link", *OCEAN '88, MTS-IEEE Conf.*, Baltimore, 1988, pp. 287-290.

7. Zielinski, A. and L. Wu, "A High Rate Underwater Acoustic Communication system", *Pacific Congress on Marine Technology PACON'88*, Honolulu, Hawaii, 1988, pp. OTS4/1-7.

8. Zielinski, A. and L. Wu, "Data Retrieval From Bottom Instrumentation Using Acoustic Link", *MTS & IEEE/OES Workshop on Instrumentation and Measurements in the Polar Regions*, Monterey, January 1988, pp. 283-294.

9. Zielinski, A. and L. Wu, "A Narrow-beam Acoustic Communication", *IV Symp. on Underwater Acoustics*, Poland, May 1987, pp. 331-338.

10. Stenton, D. E. and L. Wu, "Computer-based Introductory Electronics: Course Design", *Joint Coordinating Forum on International Cooperation in Canada-China Project on Computer Aided Learning*, Shanghai, May 1987,(24 typed pages).

11. Stenton, D. E. and L. Wu, "Computer-based Introductory Electronics: Problem Delivery", *Joint Coordinating Forum on International Cooperation in Canada-China Project on Computer Aided Learning*, Victoria, Jan. 1987,(21 typed pages).

12. Gu, L.,L. Wu and Y. Lin, "A Microcomputer Inquiry System of Satellite TV Stations," *CIC Conference on Image Transmission*, Gualing, Jan. 1986, pp. 139-141.

13. Wu, L. and L. Gu, "A Low Cost Microwave Amplifier," presented at *CIC Conference on Radio Communications*, China Institute of Communication, Shanghai, May 1985.

14. Gu, L. and L. Wu, "An Optimization of 12 GHz Satellite TV Receiver," in *1984 EDC Computer Application Dig.*, p. 121

15. Wu, L. and L. Gu, "L Band Low Noise Amplifier CAD," presented at *CIE Conference on Broadcasting*, China Institute of Electronics, Shanghai, Oct. 1983.

16. Zhou, X., S. Zhu and L. Wu, "A New Transmission Line: Finline," *Journal of Electronic Technology*, no. 9, pp. 21-23, 1982.

17. Gu, L. and L. Wu, *Satellite TV Receiver Design*, by Y. Konishi, NHK Press, 1978, *Shanghai, Elec. Infor. Network*, 1984 (translation from English).

18. Gu, L. and L. Wu, *An Introduction to Satellite Television*, by NHK Press, 1984, Shanghai, Science & Technology Press, (translation from Japanese and accepted for publication).

PARTIAL COPYRIGHT LICENSE

I hereby grant the right to lend my thesis to users of the University of Victoria Library, and to make single copies only for such users or in response to a request from the Library of any other university, or similar institution, on its behalf or for one of its users. I further agree that permission for extensive copying of this thesis for scholarly purposes may be granted by me or a member of the University designated by me. It is understood that copying or publication of this thesis for financial gain shall not be allowed without my written permission.

Title of Thesis:

Underwater Acoustic Communication

Lixue Wu

February 12, 1989

ISBN 0-315-50142-1